



Royal Netherlands
Meteorological Institute
*Ministry of Infrastructure
and Water Management*

An evaluation of the use of regional climate model data applied to extreme precipitation in the Meuse basin

L. van Voorst en H. van den Brink

De Bilt, 2024 | Technical report; TR 413

An evaluation of the use of regional climate model data applied to extreme precipitation in the Meuse basin

Leon van Voorst
Henk van den Brink





The EMfloodResilience project is being carried out within the context of Interreg V-A Euregio MeuseRhine and is 90% funded from the European Regional Development Fund.

Deliverable requirements

This section provides an overview of the location in this report in which the deliverable requirements can be found.

This report is an English report which contains at least the following content:

- Description of the synthetic datasets, statistical method and discharge model
 - A description of the raw synthetic dataset is provided in section 2.2.2. The approach from getting to the bias-corrected synthetic data and synthetic hydrological data is explained in section 2.3.1.
 - The statistical method that is used in this study to analyse extremes is provided in section 2.3.3.
 - A description of the discharge model used for the hydrological results of the combined effort of this study and the study by Couasnon et al. (2023) is provided in section 2.3.3.
- A table with estimated return values for 1, 10, 100 and 1000 year return periods for the Meuse basin and the tributaries
 - Section 3.1.6 provides an overview of the required return values for the Meuse basin and 15 of its tributaries for a daily and hourly time window. Results of larger time windows are presented in Appendix 6.5.
- Simulation of 80,000 years of daily weather with the weather generator based on the synthetic data
 - A brief overview of simulations with the weather generator based on the synthetic data for (more than) 80,000 in several tributaries of the Meuse basin is provided in section 3.1.5. Information on the other tributaries is provided in Appendix 6.4.
- A table with estimated return values for 10,000 and 100,000 year return periods for the Meuse basin and the tributaries
 - Section 3.1.6 also provides an overview of the 10,000 and 100,000 year return periods for the Meuse basin and 15 of its tributaries (based on the WG results). Results of larger time windows are also presented in Appendix 6.5.
- Review information from other meteorological institutes with the report or as separate document
 - The review information is provided as a separate document. Reviews were performed by:
 - Dr. Alex J. Cannon (Environment and Climate Change Canada)
 - Dr. Michael B. Butts (Danish Meteorological Institute)
 - Dr. Peter Krahe (Bundesanstalt für Gewässerkunde (BFG))

A summary of the report, both in English and in Dutch, will be provided in the following sections.



Summary

In July 2021, unprecedented extreme precipitation led to enormous summer discharges that were never observed before, causing disastrous flood events in parts of the Meuse basin and stressing the importance of adequate extreme estimates for flood resilience. Conventional techniques for extreme discharge estimation, such as statistical extrapolation or the GRADE Weather Generator, have clear limitations which are attributed to the restricted length of the observational input data. This study introduces an alternative approach, in which long synthetic meteorological data spanning more than 1000 years are employed in a hydrological model, generating a dataset from which large hydrological extremes can directly be derived. The main aim of this research is to evaluate the meteorological RACMO dataset for this specific purpose and to provide insight in the advantages of the synthetic RACMO dataset compared to observations, with focus on meteorology.

The climatology of RACMO precipitation means and extremes in the Meuse basin and its tributaries compare very well with observations, making the dataset useful for hydrological computations. Furthermore, the extensive length of the RACMO dataset reveals a range of extreme values that was previously unanalysed. This provides new insight into the tail of the distribution of annual precipitation extremes, particularly in the curvature of GEV distributions which is described by the shape parameter. This shape parameter has a large influence on the value of the high extremes estimated by a GEV distribution and can better be estimated with the use of the longer RACMO dataset.

The statistical uncertainty in the estimation of extreme precipitation is strongly reduced by the use of RACMO data: roughly a factor 4 for daily extremes and a factor 10 for hourly extremes. Further statistical analysis shows that the GEV shape parameter from observed precipitation is more robust with a long dataset. This is reflected by the spatial inconsistency of the shape parameter of observations and the more spatially consistent RACMO shape parameter. Furthermore, the shape parameter increases substantially by averaging over time and slightly when averaging in space.

There is a clear distinction between the GEV distributions of summer and winter precipitation extremes, suggesting the existence of a double population. Depending on the time step (and therefore the annual dominance of summer or winter events), such a double population may influence the GEV of annual maxima. The existence of a double population, particularly in summer precipitation, is well-known in literature and is said to be related to dewpoint temperature. The existence of a double population is difficult to obtain from observations, but can have an enormous impact on the return values of summer extremes, such as the event of July 2021. The translation of summer extremes of precipitation into extreme discharges depends on the rainfall-runoff response of the considered catchment and on its catchment characteristics.

Samenvatting

In juli 2021 was de Maas getuige van ongeëvenaarde tweedaagse neerslag met neerslagsommen die tot voorheen nog nooit gemeten waren. De enorme hoeveelheid water leidde tot catastrofale overstromingen in verschillende delen van het Maas stroomgebied en toonde aan dat een adequate schatting van zowel neerslag- als afvoerextremen essentieel is voor toekomstige weerbaarheid tegen dergelijke overstromingen. Conventionele technieken voor de schatting van extreme afvoeren, zoals statistische extrapolatie en de GRADE neerslaggenerator, hebben duidelijke beperkingen gerelateerd aan de beperkte lengte van de observatie datasets die gebruikt worden als input. In dit onderzoek wordt een alternatieve methode geïntroduceerd, waarin een hydrologisch model wordt gevoed met lange, synthetische meteorologische reeksen uit het RACMO klimaatmodel. Dit resulteert in lange hydrologische reeksen, waaruit hydrologische extremen kunnen worden bepaald. Het doel van deze studie is om het gebruik van de meteorologische RACMO dataset voor dit specifieke doeleinde te evalueren en om een inzicht te geven in de potentiële mogelijkheden van de RACMO dataset in vergelijking met observaties.

De klimatologie van RACMO neerslaggemiddelden en extremen in het stroomgebied van de Maas en haar zijrivieren komen goed overeen met observaties. De dataset is dus uitstekend bruikbaar voor de hydrologische computaties. Daarnaast, geeft de lange synthetische dataset meer inzicht in de diepe staart van extreme neerslagen en afvoeren dan voorheen mogelijk was. Met name de kromming van GEV distributies, omschreven door de vorm parameter, kan middels de lange synthetische datasets beter worden ingeschat. Deze vorm parameter is zeer belangrijk bij het schatten van grote extremen in een GEV distributie.

De statistische onzekerheid van extreme neerslag wordt sterk verminderd door het gebruik van de RACMO data: ongeveer een factor 4 voor dagelijkse extremen en een factor 10 voor uurlijkse extremen. Verdere statistische analyse toont aan dat de GEV vorm parameter een stuk robuuster is bij het gebruik van lange datasets dan de kortere lengte van observaties. Dit komt ook tot uiting in de ruimtelijke inconsistentie van de vorm parameter van observaties en de ruimtelijke consistentie van de RACMO vorm parameter. Daarnaast valt op dat de vorm parameter groter wordt naarmate gemiddeld wordt over een grotere tijdsperiode.

Er is een duidelijk onderscheid tussen de GEV distributies van zomer en winter neerslagextremen, wat het bestaan van een dubbele populatie doet vermoeden. Afhankelijk van de tijdstap kan een dergelijke dubbele populatie invloed hebben op de GEV van jaarlijkse maxima. Het bestaan van een dubbele populatie, met name in de zomer, is een bekend fenomeen in de literatuur en wordt vaak gerelateerd aan dauwpunt temperatuur. Verder is het bestaan van een dubbele populatie moeilijk te concluderen uit observatiedata, terwijl het een grote impact kan hebben op de herhaaltijden van zomerextremen, zoals bijvoorbeeld in juli 2021. De vertaling van zomer neerslagextremen in afvoerextremen hangt af van de hydrologische response van het beschouwde stroomgebied en daarom op de karakteristieken van dit stroomgebied.

List of Figures

Figure 1.1 a) Radar image of the accumulation of precipitation over 2 days in the extreme July 2021 event in the Geul tributary of the Meuse b) Overview of the Annual Average Discharge in 1) the Meuse river and 2) several tributaries of the Meuse river. Measurements in the main river branch date back to approximately 1910, whereas measurements in the tributaries date back to 1930 at the latest (Kwadijk et al., 2016).	10
Figure 1.2 a) Visualisation of the influence of arbitrary choice of extrapolation technique on the provided return period with 72 years of E-OBS data from the Vesdre catchment (a subcatchment in the Meuse basin). Note that precipitation amounts differ approximately 25 mm/day for a 100 year return value and 50 mm/day for a 1000 year return value b) Schematic representation of the resampling process. Reordering of the historical days allows multi-day values to take higher values than observed in the historical sequence. This does not hold for single-day values of the generated timeseries (Hegnauer et al., 2014).	11
Figure 1.3 a) Visualization of the annual extremes for both the observations and the WG result for multiple multi-day sums in the Meuse basin. Low multi-day precipitation extremes show probable underestimation. This is less pronounced for high multi-day precipitation extremes b) Overshoot of precipitation extremes due to inaccuracies in the WG resampling technique. The figure shows the WG result before and after addition of the July 2021 extreme.	13
Figure 2.1 Overview of the Meuse basin in with a) different precipitation totals in different regions of the basin and their HBV catchment numbers and b) the outline of the catchments generally used for visualization of the results in this study. Note that these catchments have different locations and sizes. Numbers of the catchments are 135 – St. Mihiel (green), 142 – Lesse (blue), 146 – Vesdre (purple), all numbered catchments – Borgharen (red).	17
Figure 2.2 Overview of the stations in the Meuse basin used to create the E-OBS product (Cornes et al., 2018)	18
Figure 2.3 Overview of the RACMO domain (Van Dorland et al., 2023).....	20
Figure 2.4 Three alternative approaches of using synthetic data being a) the original GRADE approach, b) the first alternative in which synthetic data are directly passed to the hydrological model, c) the second alternative in which synthetic RACMO data are used in	22
Figure 2.5 Schematic representation of the quantile mapping procedure for a bias correction	24
Figure 2.6 Schematic representation of the detrending procedure applied in this study.	25
Figure 2.7 Schematic representation of the wflow_sbm concept.....	26
Figure 3.1 Overview of the annual cycles of RACMO (original and corrected), E-OBS and GenRE, averaged over the catchment areas of the Vesdre, Lesse and the Meuse upstream of St. Mihiel and Borgharen. The annual cycle presents the average daily precipitation falling on a certain day of the year based on all years in the dataset and in each ensemble member.....	31
Figure 3.2 Annual cycles of daily average temperature and pet for the Meuse catchment upstream of Borgharen.	32
Figure 3.3 Overview of daily annual maximum precipitation of RACMO, E-OBS and GenRE, averaged over the catchment areas of the Vesdre, Lesse and the Meuse upstream of St. Mihiel and Borgharen.....	33
Figure 3.4 Overview of 5-daily annual maximum precipitation of RACMO, and E-OBS and GenRE, averaged over the catchment areas of the Vesdre, Lesse and the Meuse upstream of St. Mihiel and Borgharen.	34

Figure 3.5 Overview of hourly annual maximum precipitation of RACMO and GenRE, averaged over the catchment areas of the Vesdre, Lesse and the Meuse upstream of St. Mihiel and Borgharen.	35
Figure 3.6 Overview of 6-hourly annual maximum precipitation of RACMO and GenRE, averaged over the catchment areas of the Vesdre, Lesse and the Meuse upstream of St. Mihiel and Borgharen.	36
Figure 3.7 Overview of the daily precipitation cycle of RACMO (original and corrected) and GenRE, averaged over the catchment areas of the Vesdre, Lesse and the Meuse upstream of St. Mihiel and Borgharen.	37
Figure 3.8 Overview of the daily precipitation cycle in summer of RACMO (original and corrected) and GenRE, averaged over the catchment areas of the Vesdre, Lesse and the Meuse upstream of St. Mihiel and Borgharen.	37
Figure 3.9 Annual maximum precipitation for a 1-day precipitation sum for RACMO (with and without WG resampling) and E-OBS.....	38
Figure 3.10 Annual maximum precipitation for a 5-day precipitation sum for RACMO (with and without WG resampling) and E-OBS.....	39
Figure 3.11 Daily Annual maximum precipitation for all 16 RACMO members separately and the E-OBS dataset, including a confidence interval based the spread of the 16 RACMO members.....	41
Figure 3.12 Hourly Annual maximum precipitation for all 16 RACMO members separately and the GenRE dataset, including a confidence interval based the spread of the 16 RACMO members.....	42
Figure 3.13 6-Hourly Annual maximum precipitation for all 16 RACMO members separately and the GenRE dataset, including a confidence interval based the spread of the 16 RACMO members.....	43
Figure 3.14 Overview of the influence of the GEV-parameters on the extreme value plots (Gordon et al., 2015), with b) the influence of the location parameter, c) the influence of the scale parameter and d) the influence of the shape parameter.....	45
Figure 3.15 GEV distributions fitted to the daily annual extremes all separate RACMO member, the combined RACMO dataset and the E-OBS dataset.....	46
Figure 3.16 GEV distributions fitted to the hourly annual extremes of all separate RACMO member, the combined RACMO dataset and the E-OBS dataset.....	47
Figure 3.17 Spatial distribution of the shape parameter of the GEV distribution for the catchments in the Meuse basin based on E-OBS and RACMO.....	49
Figure 3.18 The influence of catchment size on the shape parameter for 4 different parameters, based on the RACMO dataset.....	49
Figure 3.19 1-day summer and winter annual extremes in different catchments of the Meuse basin.....	50
Figure 3.20 10-day summer and winter annual extremes in different catchments of the Meuse basin.....	51
Figure 3.21 1-hour summer and winter annual extremes in different catchments of the Meuse basin.....	52
Figure 3.22 Overview of the two maximum events in Borgharen (both summer events). There is a clear spatial spread between the two figures, which may lead to an entirely different hydrological response.....	53

Contents

Deliverable requirements	3
Summary	4
Samenvatting	5
List of Figures	6
1. Introduction	10
1.1. State of the art for the Netherlands	11
1.2. Problem statement	12
1.3. Synthetic observations.....	14
1.4. Research Goal	14
2. Methodology.....	16
2.1. Study area	16
2.2. Data.....	17
2.2.1. Observations	18
2.2.2. Synthetic data	19
2.3. Method	20
2.3.1. Approach.....	20
2.3.2. Hydrological model	25
2.3.3. Extreme value analysis.....	27
3. Results.....	30
3.1. Long synthetic timeseries for hydrological application	30
3.1.1. Annual cycle	30
3.1.2. Annual multi-day extremes.....	32
3.1.3. Annual sub-daily extremes.....	34
3.1.4. Daily cycle.....	36
3.1.5. Weather generator	38
3.1.6. Overview of RACMO return values	39
3.2. Ensemble members of the synthetic dataset	40
3.3. The GEV shape parameter	44
3.3.1. Daily GEV distributions.....	45
3.3.2. Hourly GEV distributions.....	47
3.3.3. Temporal and spatial spread of the shape parameter	48
3.4. Seasonal effects	49

4.	Conclusions, Discussion & Recommendations	54
4.1.	Conclusions	54
4.2.	Discussion.....	54
4.3.	Recommendations	57
5.	References	58
6.	Appendices.....	62
6.1.	Annual cycles.....	62
6.2.	Daily cycles.....	64
6.2.1.	Calendar year	64
6.2.2.	Summer half year.....	66
6.3.	Annual extremes	68
6.3.1.	Daily.....	68
6.3.2.	5-daily.....	70
6.3.3.	Hourly.....	72
6.4.	Weather generator	74
6.4.1.	Daily.....	74
6.4.2.	5-daily.....	76
6.5.	Return period tables	78
6.5.1.	2-day sum.....	78
6.5.2.	3-day sum.....	78
6.5.3.	5-day sum.....	79
6.6.	RACMO ensembles & confidence intervals	80
6.6.1.	Daily.....	80
6.6.2.	Hourly.....	82
6.6.3.	6-Hourly	84
6.7.	GEV distributions	86
6.7.1.	Daily.....	86
6.7.2.	5-daily.....	88
6.7.3.	Hourly.....	90
6.8.	Seasonal influence	92
6.8.1.	Daily.....	92
6.8.2.	10-daily.....	94
6.8.3.	Hourly.....	96

1. Introduction

Between 12 and 15 July 2021, unprecedented extreme precipitation occurred in and around the Meuse basin. As a consequence, the Meuse river registered summer discharges up to $3260 \text{ m}^3/\text{s}$ that were never observed before. On several locations in the Meuse basin, precipitation accumulated up to more than 250 mm within 2 days, as depicted in the radar image in Figure 1.1a. The events resulted in severe flooding of multiple tributaries of the Meuse basin and exceptionally high water levels in the main river branch. The total impact of the floods in and around the Meuse basin was immense. More than 200 casualties were reported and the total cost of the event is estimated to exceed 5 billion euros (Kreienkamp et al., 2021).

The disastrous flood events of July 2021 raised questions on the potential extremity of floods in the Meuse basin and stressed the importance of competent flood protection against fluvial floodings. Information on the frequency of occurrence of extreme hydrological events is essential for such adequate flood protection: Return periods¹ of extreme water levels are often used as an official guideline for flood protection. However, the return periods of interest are generally too high (e.g. 1000, 10.000 years in the Netherlands as set in Appendix II of Article 2.2(1) of the Water Act) to be directly determined from observations, which are at most available for only an order of 100 years as shown for the Meuse basin in Figure 1.1b (Kwadijk et al., 2016). Elongation of timeseries using a paleohydrological approach is possible (e.g. De Niel et al., 2017), but this does not provide a complete and stationary dataset due to the climate signal over such a long time period. Therefore, an alternative approach for derivation of adequate extreme estimates that correspond to these high return periods of interest is a prerequisite for good flood protection.

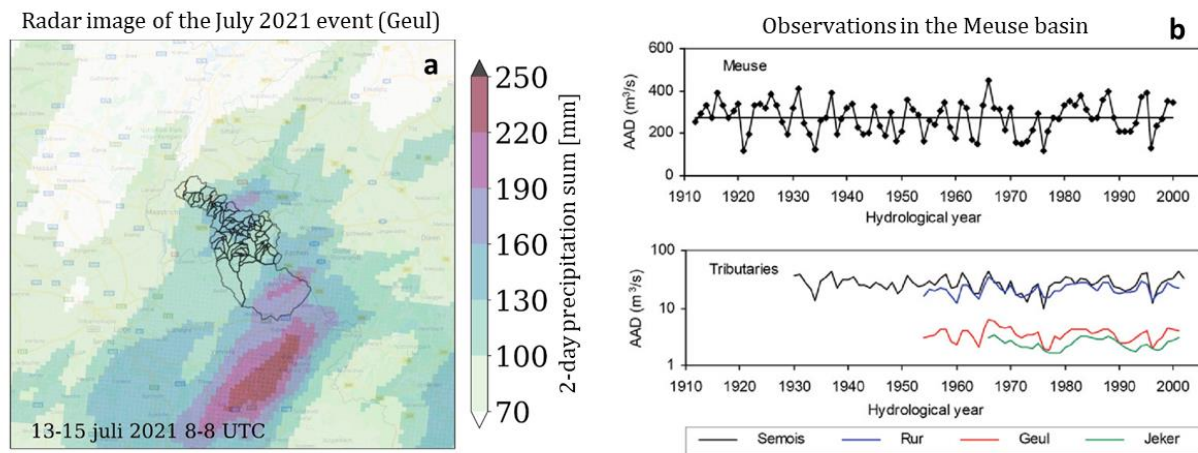


Figure 1.1 a) Radar image of the accumulation of precipitation over 2 days in the extreme July 2021 event in the Geul tributary of the Meuse b) Overview of the Annual Average Discharge in 1) the Meuse river and 2) several tributaries of the Meuse river. Measurements in the main river branch date back to approximately 1910, whereas measurements in the tributaries date back to 1930 at the latest (Kwadijk et al., 2016).

¹ The return period is defined as the inverse of the frequency of occurrence

1.1. State of the art for the Netherlands

As previously mentioned, the short length of both meteorological and hydrological observational timeseries prevents direct coupling of hydrological extremes to corresponding return periods. Derivation of hydrological return values that exceed the length of observations is therefore often carried out by statistical extrapolation of the observations. The complication of statistical extrapolation arises from the (partly) arbitrary selection of the extrapolation distribution, which impacts estimation of extremes. Figure 1.2a demonstrates extrapolation of the E-OBS precipitation observation dataset (72-years) in a catchment of the Meuse basin, using two different, commonly used, extreme value distributions. The different distributions display huge difference for large return periods, which indicates estimation of high return values based on statistical extrapolation is prone to statistical error (e.g. Van Den brink et al., 2003; Zeder et al., 2023).

Another disadvantage of statistical extrapolation is that it is only applicable on locations with observational data. This complicates the estimation of extreme values at arbitrary locations without data in the considered (sub)-basins. Moreover, gaining any insight on hydrograph progression of extreme events is impossible with statistical extrapolation, as the method only results in a single value, and does not provide information of the days surrounding the extreme.

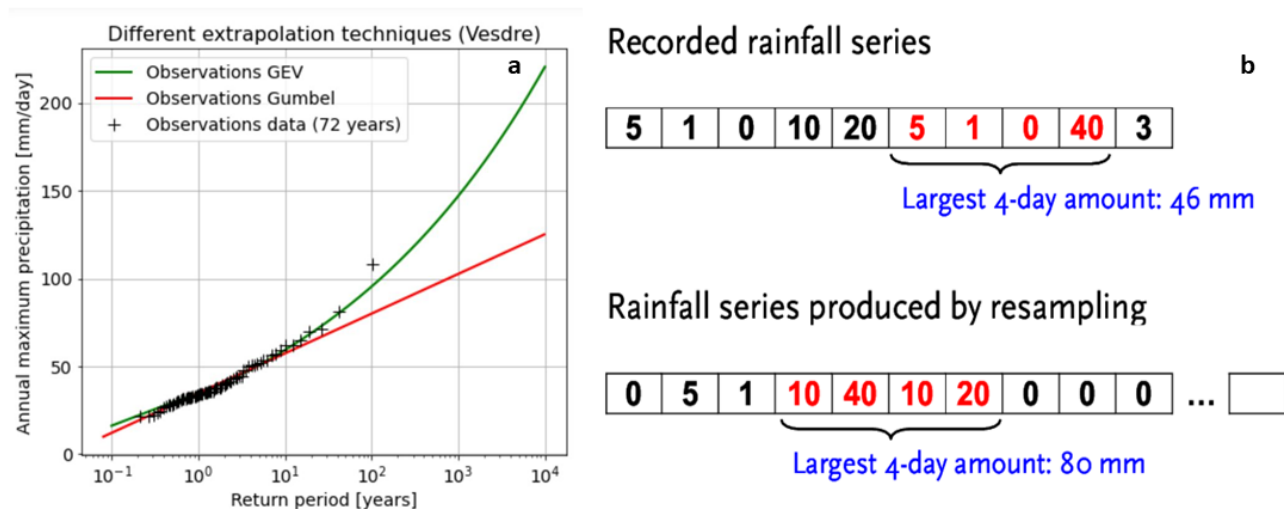


Figure 1.2 a) Visualisation of the influence of arbitrary choice of extrapolation technique on the provided return period with 72 years of E-OBS data from the Vesdre catchment (a subcatchment in the Meuse basin). Note that precipitation amounts differ approximately 25 mm/day for a 100 year return value and 50 mm/day for a 1000 year return value b) Schematic representation of the resampling process. Reordering of the historical days allows multi-day values to take higher values than observed in the historical sequence. This does not hold for single-day values of the generated timeseries (Hegnauer et al., 2014).

In order to address the limitations of statistical extrapolation in estimating discharge extremes, an alternative procedure called GRADE (Generator of Rainfall And Discharge Extremes) has been developed in the Netherlands by a consortium consisting of Rijkswaterstaat, Deltares and the KNMI (see section **Error! Reference source not found.**). In GRADE, a Weather Generator (WG) is used to generate extended meteorological timeseries (precipitation, temperature and radiation) of 50.000 years, by resampling observation data (Hegnauer et al., 2014). Note that there also exist other stochastic WG approaches (e.g. Nguyen et al., 2021), but due to familiarity the GRADE approach is further described in

this study. Although the daily extremes in the new synthetic dataset do not surpass those observed, the rearrangement of the dataset by resampling leads to larger multiday precipitation totals in the synthetic dataset compared to the original observations. This process has been visualized in Figure 1.2b (Hegnauer et al., 2014). Hydrological processes in large river basins typically exhibit a strong response to such large multi-day precipitation totals. After of the resampled timeseries in a hydrological model, feeding a hydrological model with the resampled timeseries will therefore contain several large discharge extremes that will exceed the observational dataset. In this way, GRADE enables the generation of largely extended timeseries (50.000 years) with increased discharge values, facilitating estimation of extreme return values directly from the timeseries and removing the need for statistical extrapolation. Another advantage is that the synthetic timeseries facilitates the creation of hydrographs for extreme events, supporting a more comprehensive analysis. Moreover, by employing an appropriate hydrological model, the GRADE procedure enables the identification of discharge extremes and their corresponding return values in unmonitored locations of the (sub)-basins.

For a considerable period now, GRADE has been instrumental in Dutch policy-making regarding flood protection. It has demonstrated that the use of synthetic precipitation data to estimate discharge and precipitation extremes holds promise as an alternative for statistical extrapolation. Nevertheless, the existing implementation of GRADE has known limitations, some of which were revealed after application of the extreme events of July 2021.

1.2. Problem statement

GRADE faces limitations when it comes to accurately estimating extreme discharge in small sub-catchments or tributaries of a basin. This is caused by the daily time step used in the WG, which is too coarse for adequate discharge estimation in these relatively small watersheds, with rainfall-runoff responses within a few hours, as observed during the flood events of July 2021. Simple calculations performed by Deltares also show fast rainfall runoff-responses in small catchments of the Meuse basin such as the Rur (0.31 days), the Geul (0.32 days) and the Vesdre (0.68 days). To accurately estimate discharge extremes in tributaries like these, a sub-daily time step is required, which is not (yet) facilitated in the GRADE procedure. Furthermore, it is worth repeating that the weather generator in GRADE only generates higher precipitation events when considering multi-day precipitation sums, but not for single-day values. Although the length of the observational dataset has been largely elongated by the resampling process, single-day values in the new sequence will never surpass the maximum value of the observational time series, which has been depicted in Figure 1.3a. The meteorological absence of daily extremes has consequences for the hydrological response to single-day precipitation. Catchments with hydrological responses to single-day or sub-daily precipitation will therefore likely have underestimated hydrological extremes when applying the GRADE procedure.

A similar effect can be detected for low multi-day precipitation totals. Resampling in GRADE is constrained by the values present in the original dataset, which means that the maximum values in the synthetic timeseries will never surpass a multiple (corresponding to the multi-day sum) of the maximum precipitation value in the original dataset. In simpler terms, the n-day sum generated by the weather generator can never exceed n times the maximum daily precipitation value found in the historical record. Furthermore, as the resampling approaches the multiple of the observational maximum (corresponding to the multi-day sum), the occurrence of maxima close to that value becomes increasingly rare. Consequently, for low multi-day precipitation totals, the synthetic timeseries may not

adequately capture extremes with high return periods, potentially leading to underestimation. As illustrated in Figure 1.3a, the underestimation becomes less significant (and shifts towards higher return levels) as the multi-day sum increases, which is likely related to the increased number of potential combinations. The relationship between precipitation and discharge implies that the inaccuracies present in the synthetic meteorological dataset will also impact the synthetic hydrological dataset. In large river basins such as the Rhine basin, where the hydrological response time to precipitation events is considerable and discharge extremes are predominantly influenced by large multi-day events, the prescribed shortcomings are not expected to have a significant effect for the return periods that are generally considered in policy-making. However, in smaller basins or tributaries that have a faster response to rainfall events (e.g., as observed in the events of July 2021), the underestimation of high precipitation extremes potentially leads to unrealistic representations of discharge. This may in turn hamper the accurate analysis of hydrological extremes.

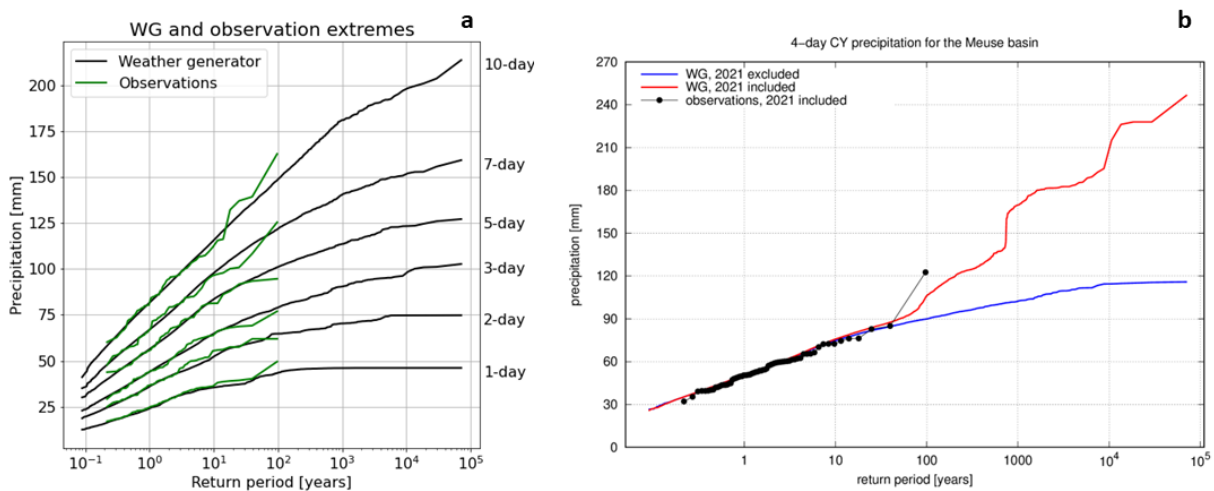



Figure 1.3 a) Visualization of the annual extremes for both the observations and the WG result for multiple multi-day sums in the Meuse basin. Low multi-day precipitation extremes show probable underestimation. This is less pronounced for high multi-day precipitation extremes b) Overshoot of precipitation extremes due to inaccuracies in the WG resampling technique. The figure shows the WG result before and after addition of the July 2021 extreme.

Moreover, the occasional occurrence of an extremely rare event in the observational dataset, with an expected return period much larger than the length of the dataset, results in unrealistic meteorological patterns in the synthetic timeseries. This issue becomes apparent when such an extreme event, like the one observed in July 2021, is added to the observational dataset. The current implementation of the weather generator faces difficulties in resampling events other than the one selected for the previous day when the extreme event is an outlier in the observational timeseries. This is due to the lack of other extremes with a similar magnitude to provide reference points for resampling. Consequently, the extreme event is overrepresented in the synthetic timeseries, leading to an artificial inflation of its occurrence and an overestimation of high multi-day extremes (see Figure 1.3b).

Furthermore, it is important to note that the weather generator used in GRADE does not simulate climate change, since it relies on resampling from past observations. However, numerous studies have indicated that precipitation events will undergo rapid changes due to climate change (e.g. O’Gorman, 2015). Consequently, the meteorological and discharge events generated by GRADE are valid for the



historical climate but may not accurately represent future climates. Given that flood protection requires careful planning, it is crucial to have insights into future hydrological and meteorological extremes for informed decision-making.

Although GRADE has demonstrated the potential of using generated timeseries for estimating discharge and precipitation extremes as a promising alternative to statistical extrapolation, its current operation is not without flaws, primarily due to the limited length of the observational timeseries. While application on larger hydrological entities like the entire Rhine basin may be less affected by the limitations of the weather generator, it can lead to inaccurate estimates of discharge return values in smaller tributaries. Therefore, to improve the estimation of meteorological and hydrological return values for these situations, a different approach is required.

1.3. Synthetic observations

Both statistical extrapolation and GRADE have demonstrated limitations due to the reliance on the short length of the observational datasets. Therefore, there is a strong demand for long observational datasets in these applications, which unfortunately do not exist.

As an alternative approach, use of synthetic timeseries generated by climate models can be considered to estimate meteorological and hydrological extremes. In the context of the KNMI'23 climate scenarios, the RACMO climate model forced by EC-Earth has generated over 1000 years of meteorological data (see section **Error! Reference source not found.**) representative for current climate after a bias correction. This synthetic dataset, either in its raw form or extended by the weather generator, can serve as observational input for hydrological and hydrodynamic models. This enables the generation of large timeseries of hydrological data that represent the current climate.


Use of the hydrological timeseries derived from the synthetic climate model data enables direct determination of extremes with return periods up to approximately 1000 years. This approach bypasses the methodological flaws associated with statistical extrapolation or the GRADE procedure. Furthermore, using the climate model data in the weather generator will likely shift the methodological flaws in extreme estimation towards larger return periods, which implies that higher extremes can be considered more reliable.

An additional advantage is that the climate model runs also contain meteorological data for future climate scenarios. As such, the approach of using a synthetic dataset to estimate hydrological extremes may also be extended for future climates, which can be essential information in policy making. Note that estimation of future extremes falls outside the scope of this research.

Another advantage of the RACMO model is that it generates meteorological data at an hourly time step, enabling generation of hydrological extremes at an hourly time step as well. This is crucial for the estimation of extremes in smaller basins or tributaries of the Meuse basin due to their fast rainfall-runoff response.

1.4. Research Goal

Using the synthetic meteorological dataset (like done in e.g. Van Den Brink et al., 2005) from the RACMO climate model provides a promising alternative for conventional techniques for estimation of meteorological and hydrological extremes due to the length of the dataset, its fine temporal resolution and its potential for analysis of future extremes. Nevertheless, it is crucial to acknowledge that the



pseudo-observations of the synthetic dataset have uncertain quality and must be investigated and compared with real observations. Hence, the objective of this study is to introduce the methodology of using synthetic data for estimating meteorological and hydrological extremes in basins of different shapes and sizes, to evaluate the quality of the meteorological RACMO dataset for this specific purpose and to provide insight in the additional potential of the synthetic RACMO dataset compared to observations. The focus in this report is on meteorological extremes. The hydrological follow-up is presented in a separate report by Couasnon et al. (2023).

2. Methodology

This research aims to present and evaluate a new approach for estimating discharge and rainfall extremes through the use of long synthetic time series produced by climate models, possibly after bias-correction (see e.g. Sunyer et al. (2012) for an overview of correction methods). The method is applied and tested in the Meuse basin and its tributaries, which will be introduced in Section 2.1. Following that, the different datasets used in this research are presented. In the final section, a more in-depth explanation of the methodology will be provided, including an explanation of the bias correction that is used to correct the synthetic data, the tests that are required to assess data quality and a brief overview of the hydrological follow up and its required meteorological variables.

2.1. Study area

The Meuse and its tributaries were subject to extreme floodings after the July 2021 precipitation events, proving the great significance of accurate extreme value estimates in this basin. Therefore, the Meuse river and its tributaries serve as an ideal setting to test the proposed approach. Furthermore, the social and economic impact caused by the floods has created good momentum for interregional collaboration in managing flood extremes. This research is conducted as part of the EMFloodresilience project, funded by the European Union, which aims to promote such interregional cooperation in and around the Meuse basin. In context of this collaboration, the focus of this research is specifically on the Meuse basin.

The Meuse originates in France and flows through Belgium and the Netherlands. Its basin, depicted in Figure 2.1a and b, also covers small parts of Germany and Luxembourg, with a few tributaries that feed the main river. The entire basin covers approximately 36,000 km². The Meuse basin exhibits significant variation in elevation, as it incorporates parts of rugged Ardennes and Eiffel and the gently sloping Lorraine region. Elevation differences throughout the basin can have an effect on meteorology and lead to varying annual precipitation totals around the basin, as shown in Figure 2.1a. Assessment of the synthetic timeseries is therefore required at the sub-basin level. Furthermore, the distinct topographical features result in varying response times of hydrology to rainfall in the different sub-basins, making investigation on the sub-basin scale essential from hydrological perspective as well. Hence, an analysis of the synthetic model data is executed on both the basin-scale and various sub-basins of the Meuse. Quality control on the sub-catchment scale also enables an assessment of the representativeness of the synthetic precipitation dataset across various spatial scales and it offers the opportunity to evaluate the competence of the hydrological response in catchments of different sizes, e.g. testing the significance of the temporal frequency of the synthetic data.

In this research, the sub-basins considered are the ones defined by the hydrological HBV model in GRADE. It is important to note that the hydrological computations in this study are not carried out by the HBV model but another hydrological model is used (see section 2.3.2). Table 1 provides an overview of the HBV tributaries. The index refers to the catchment number, as presented in Figure 2.1a.

Table 2.1 HBV-catchments and corresponding catchment area

Nr.	Name	Size (km ²)	Nr.	Name	Size (km ²)
135	Meuse at St Mihiel	2591	<i>143</i>	<i>Sambre</i>	<i>2741</i>
<i>136</i>	<i>Chiers</i>	<i>2196</i>	<i>144</i>	<i>Ourthe</i>	<i>1591</i>
<i>137</i>	<i>Meuse from St Mihiel-Stenay</i>	<i>1292</i>	<i>145</i>	<i>Ambleve</i>	<i>1043</i>
<i>138</i>	<i>Meuse from Stenay-Chooz</i>	<i>2247</i>	146	Vesdre	679

139	Semois	1212	147	Mehaigne	340
140	Viroin	530	148	Meuse from Namur-Liege	1437
141	Meuse from Chooz-Namur	1107	149	Jeker	455
142	Lesse	1304			

The results of this study will be predominantly demonstrated through visualization of four catchments with varying sizes and locations, as depicted in Figure 2.1b. In addition to the three highlighted catchments in Table 1, the entire Meuse basin upstream of Borgharen will also be considered. Additional or other catchments may be used to portray specific results more clearly. All the results will be visualized for all catchments in the Appendices.

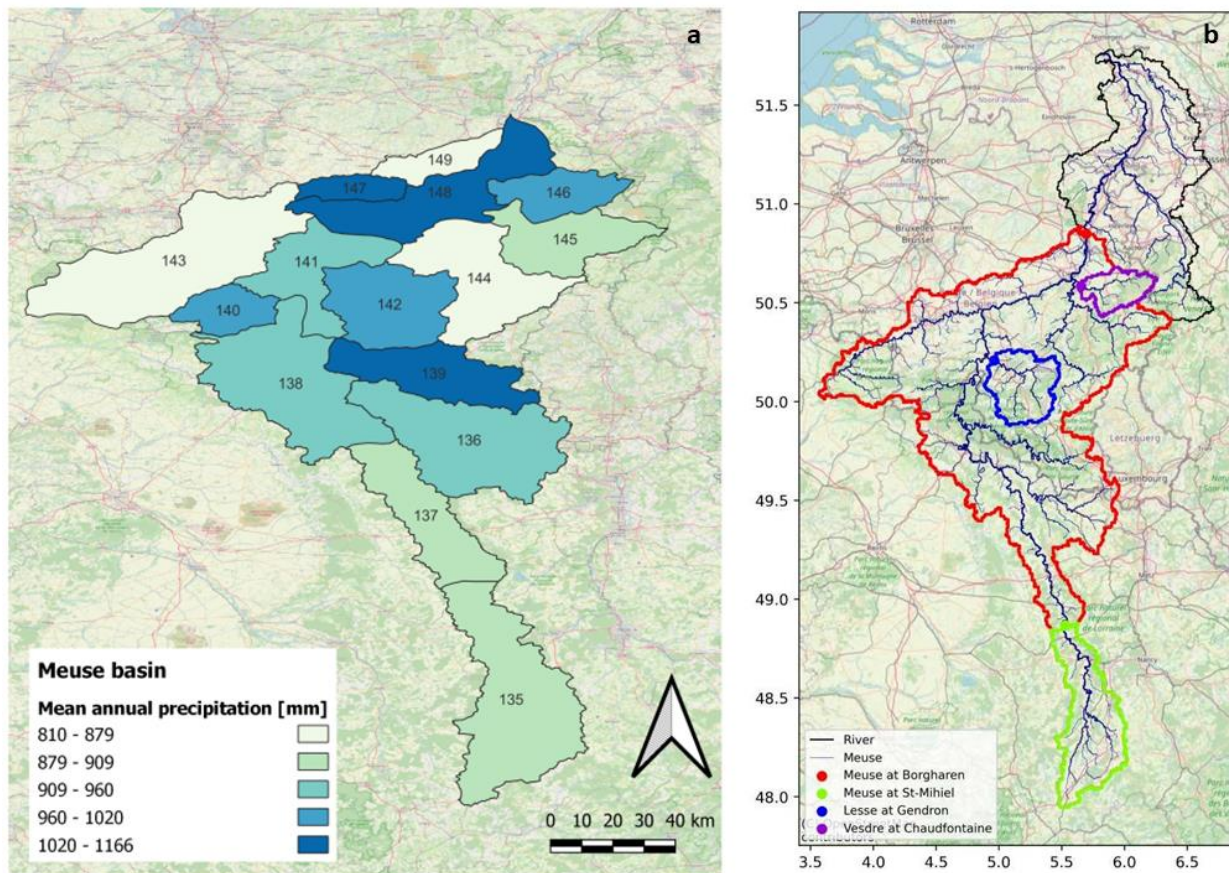


Figure 2.1 Overview of the Meuse basin in with a) different precipitation totals in different regions of the basin and their HBV catchment numbers and b) the outline of the catchments generally used for visualization of the results in this study. Note that these catchments have different locations and sizes. Numbers of the catchments are 135 – St. Mihiel (green), 142 – Lesse (blue), 146 – Vesdre (purple), all numbered catchments – Borgharen (red).

2.2. Data

There are two types of data that are considered in this study: The observational dataset on the one hand and the synthetic data generated by climate models on the other hand. The specific datasets that are used in this study are provided below.

2.2.1. Observations

The function of observations in this study is two-fold. On the one hand, they can be used to assess the quality of the synthetic datasets by comparing various indicators of the two datasets. On the other hand, observations are essential to correct model-induced biases present in the synthetic dataset (refer to Section 2.3.1 for more details about bias correction). In this study, the E-OBS dataset is used for both objectives. However, E-OBS data are only available with a daily time step, whereas the fast rainfall-runoff response in small sub-basins requires a dataset with a finer temporal resolution. Therefore, the genRE-based dataset for the Meuse basin is also used in this study, specifically for evaluation of the sub-daily synthetic data.

E-OBS dataset

E-OBS (Cornes et al., 2018) is a gridded observational dataset containing precipitation, temperature, sea level pressure, global radiation, wind speed and relative humidity data which covers much of Europe. The data is provided with a spatial resolution of 0.1 degrees, which is similar to approximately 11x11 km². For the relevant variables in this study, the E-OBS dataset is available from 1 January 1950 to present. The dataset is based on weather stations provided by the ECA&D and 84 other participating institutions. The stations used for the E-OBS dataset have been visualised in Figure 2.2 (Cornes et al., 2018). New versions of E-OBS are released twice a year, with updated timeseries and in some cases, new stations added. The version used in this study is E-OBSv26e, but for convenience the dataset will be addressed as E-OBS throughout the report. A comprehensive description of the E-OBS dataset, is found in Cornes et al. (2018).

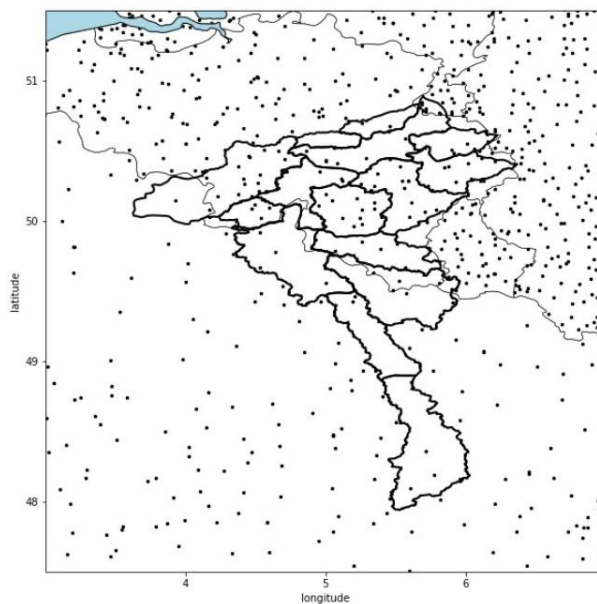



Figure 2.2 Overview of the stations in the Meuse basin used to create the E-OBS product (Cornes et al., 2018)

GenRE-based Meuse dataset

Van Osnabrugge et al. (2017) designed the GenRE approach to extend gridded climatological precipitation datasets in near-real time, which is required for e.g. operational flood forecasting and drought monitoring. Scaled by a climatological weighting factor based on monthly precipitation grids derived from climatological observation sets (such as E-OBS), sparse hourly precipitation data are



interpolated to a gridded dataset using inverse distance squared weighting. In other words, sparse hourly measurements from rain gauges are spatially distributed and scaled by the monthly climatology of a grid cell relative to the grid cell of the observation station. Bouaziz et al. (2020) then used the GenRE approach to interpolate hourly precipitation data in the Meuse basin. Hourly precipitation data from stations of Meteo France and Service public de Wallonie were spatially interpolated and scaled using the E-OBS gridded dataset. Note that the GenRE-based Meuse dataset is thus not completely independent of the E-OBS dataset. The GenRE based dataset for the Meuse basin spans from 2005 to 2017 and has a gridded resolution of approximately $1 \times 1 \text{ km}^2$.

2.2.2. Synthetic data

In this study the synthetic timeseries is considered as the meteorological output of the RACMO climate model. In this subsection, the general underlying principles of climate models are first explained, after which the specifics of the regional climate model RACMO and its meteorological output are described.

Climate models

General circulation models (GCM's) are a discrete representation of the earth's climate system. They simulate the transfer of energy and materials through the system of oceans, atmosphere and land, by using complex mathematical descriptions. The entire system is discretized in a three-dimensional grid around the earth and fluxes of energy and material can be exchanged between grid cells in all different directions, for every discrete model time step. The grid size and time step determine respectively the spatial and temporal resolution of the climate model. Note that increasing either of these resolutions will make the model computationally more expensive (e.g. increase the computation time). Given the present computational power of (super)computers, GCM's generally run at resolutions with an order of $100 \times 100 \text{ km}^2$.

Regional Climate models (RCM's) cover a much smaller spatial domain (e.g. a continent). Therefore, the spatial grid of climate models can be much finer (e.g. an order of $10 \times 10 \text{ km}^2$), implying they can show climatic behaviour on a much smaller scale and generally with higher accuracy. Note that climate systems depend on global processes, which is the reason that RCM's are driven by GCM's at their boundaries. In this research, the output of the RCM RACMO, forced by the GCM EC-EARTH, is used. A more in-depth description of these models and the resulting dataset is provided in the next section. The spatial domain of the RACMO dataset is provided in Figure 2.3.

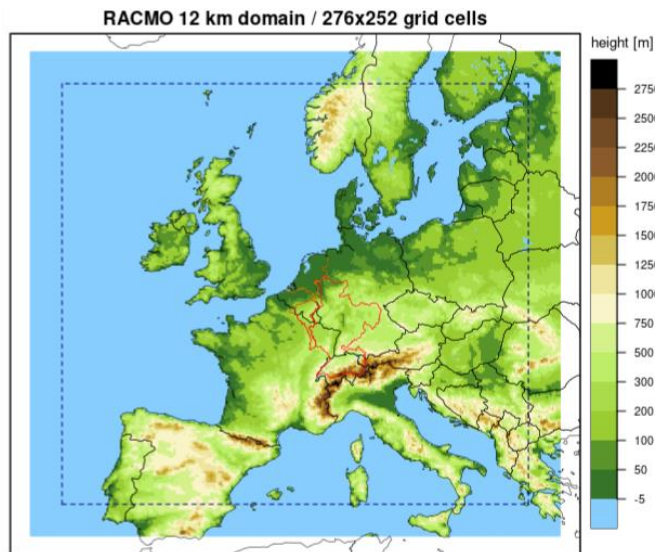


Figure 2.3 Overview of the RACMO domain (Van Dorland et al., 2023)

RACMO dataset


The GCM and RCM used in this study are respectively EC-EARTH3 (Döscher et al., 2022) and RACMO (Van Meijgaard et al., 2008). In the context of the KNMI-23 climate scenario's (Van Dorland et al., 2023) an ensemble of 16 climate simulations were generated with EC-EARTH3 with a resolution of 80x80 km² and then dynamically downscaled to a 12x12 km² grid covering Europe using RACMO. The variation between the ensemble members is achieved by initialising each member from a different part of an 1800 year long pre-industrial EC-EARTH3 run. Continuously, the 16 runs are forced with historical CMIP6 (intercomparison of climate models) forcing. This results in 16 different runs for comparable, historical climate, which can be used to distinguish the climate signal from natural climatic variability. At the end of model year 2014, the 16 historical runs are continued for SSP1.26, SSP2.45 and SSP5.85, up to the year 2165, providing climatic information for different greenhouse gas emission scenarios. Note that the ECEARTH3 runs have only been downscaled between model years 1950 and 2120. The primary objective of this research is to analyse extreme discharges with synthetic data in the present climate. Therefore, the meteorological model outputs from 1950 to 2014 for all 16 ensemble members have been used as the source data in this study, providing a dataset spanning a total of 1040 years for all relevant meteorological variables. Precipitation data is accessible at an hourly time scale, whereas the other meteorological variables are available at 3-hourly time scale.

2.3. Method

This section will provide a short elaboration of the approach to use synthetic data for extreme estimation. Apart from a description of the approach, synthetic data will be intercompared with observations, the bias correction used to account for systematic biases in the model is explained and an overview of the hydrological model for derivation of hydrological timeseries is provided. The section is finalized with a concise overview of the extreme value theory that is used in this report.

2.3.1. Approach

The approach of this research is an alternative of the prementioned GRADE approach. The approach of GRADE and the two alternative approaches that are considered in this study have been schematized in Figure 2.3a, b and c. As explained in Section 1.1, GRADE uses the WG to create a long synthetic



meteorological dataset. All relevant meteorological variables are subsequently used as input of a hydrological model and hydrodynamic model to eventually perform a frequency analysis based on the synthetic timeseries of 50,000 years. The advantage is that all return values of interest can be directly determined from the timeseries and no statistical extrapolation is required. This approach is therefore not prone to the arbitrary choice of extrapolation algorithm or statistical errors.

However, the major disadvantage of GRADE and in particular the WG, is that the resampling procedure exhibits methodical limitations. On the one hand, an overshoot of extremes (see section 1.2) can occur due to overpresence of a randomly occurring exceptionally extreme observation in the resampled precipitation dataset (see Van Voorst & Van Den Brink, 2022). On the other hand, resampling of the short dataset can lead to underestimation of high extremes for small multi-day precipitation totals due to the limits set by the resampling technique (see section 1.2) (Van Voorst & Van Den Brink, 2022). Furthermore, the WG is limited to the production of daily maxima, whereas sub-daily data (particularly precipitation extremes) are essential in small basins where the rainfall-runoff response is high. In addition, none of the conventional techniques incorporates climatic effects, which is essential information for flood protection measures against future flood events.

To account for several of the limitations, the GRADE procedure can be adapted by utilizing the synthetic timeseries of the RACMO climate model. Figure 2.3b depicts the first alternative, in which the WG is entirely bypassed. Instead, the synthetic RACMO timeseries are directly passed to the hydrological model. In this approach, the benefits of the large timeseries remain intact, while the limitations of the WG are eliminated. Return values can be directly determined from the timeseries up to approximately 100 years (the uncertainty of 1000 year return values from a timeseries of similar length is too high). To obtain larger extremes, statistical extrapolation can still be employed with less uncertainty compared to its application on short observational datasets.

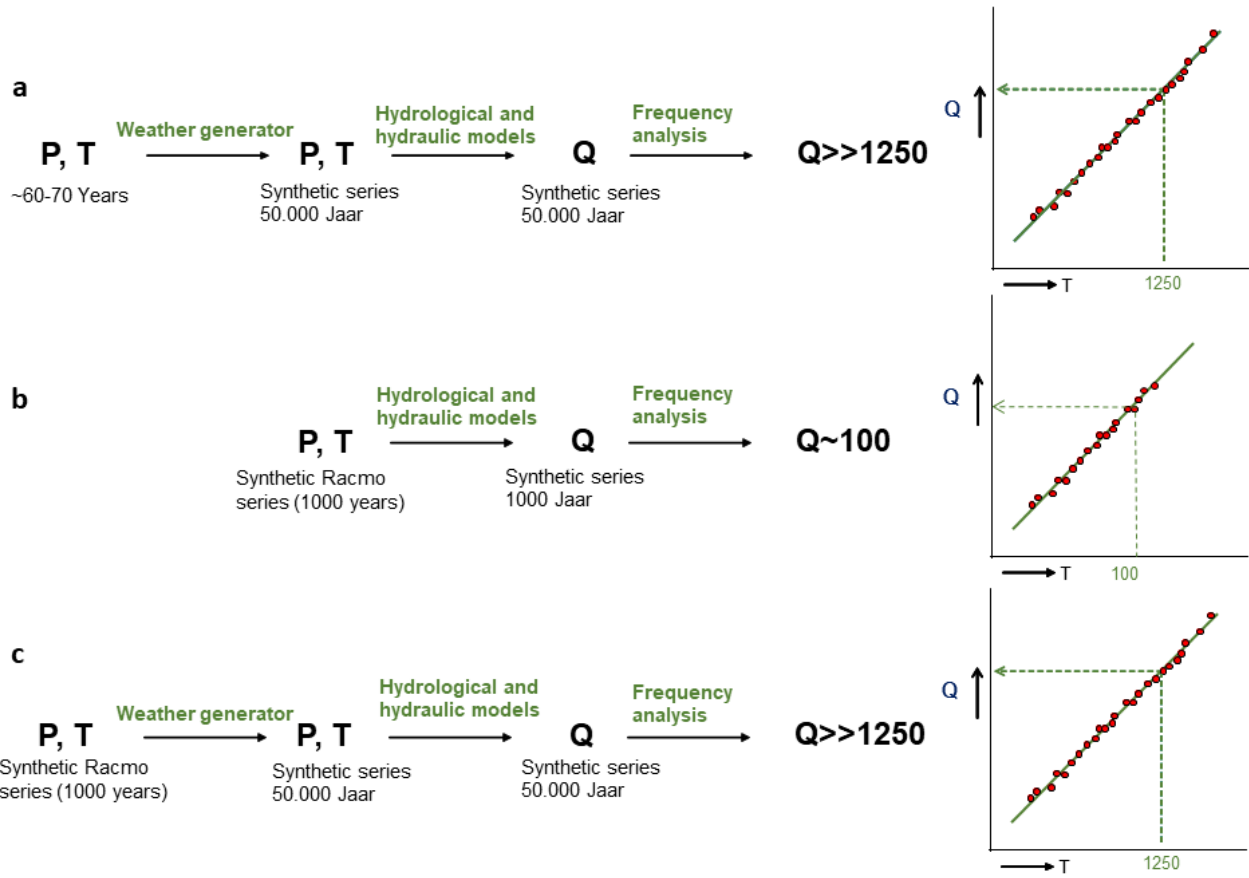


Figure 2.4 Three alternative approaches of using synthetic data being a) the original GRADE approach, b) the first alternative in which synthetic data are directly passed to the hydrological model, c) the second alternative in which synthetic RACMO data are used in

The second alternative (Figure 2.3c) is the utilization of the synthetic RACMO timeseries as an input of the WG. This leads to a longer hydrological timeseries than the first alternative. Besides, the to be resampled dataset is at least an order 10 times larger than the observational sequence, reducing the methodical error that causes over- or underestimation of the extremes. Application of the WG on the synthetic dataset will therefore provide high extremes with less uncertainty than the original WG and does not require statistical extrapolation to estimate extremes larger than 1000 years. However, the methodical flaws of the resampling procedure may still emerge for higher return periods.

The RACMO model provides meteorological data with a sub-daily frequency. Use of these data in the first described alternative allows for the analysis of hydrological responses to high, short-lasting precipitation extremes, particularly relevant in fast-responding basins. Note that the WG currently does not take hourly input. Return values on the sub-daily time scale can therefore only be estimated with the first alternative of the GRADE procedure. Furthermore, climate change can be incorporated in the GCM and RCM model runs. Both suggested GRADE alternatives can therefore potentially be applied for estimation of future extremes. However, this study first evaluates the use of climate model data to estimate extremes with historical data. Provided that results are satisfactory, evaluation of its application on future extremes is recommended for further research.

This study primarily focusses on the first GRADE alternative (b), including the impacts the longer timeseries has on the uncertainty of statistical extrapolation. The results of the second alternative will also be briefly discussed. It is important to note that the scope of this study ends with the analysis of the synthetic meteorological dataset. The discussion of hydrological results will be covered in Couasnon et al. (2023).. Section 2.3.2 does provide an overview of the hydrological model used for hydrological computation, including the required meteorological variables.

Comparing observations with synthetic data

The RACMO dataset differs from observations in several other ways than previously mentioned. To start with, the spatial density of the RACMO dataset is higher than that of official weather stations and the RACMO dataset provides a homogeneous distribution of data while the distribution of observational data is heterogeneous. Weather stations are generally more sparsely and not uniformly distributed over the spatial domain, whereas the climate model provides an equally representative value for every grid cell. Besides, the climate model is not susceptible to trends and inhomogeneities, such as changes in the environment, measurement equipment and methods. In general, RACMO offers a wide range of climate variables, with a large timeseries length, at relatively high spatial and temporal resolution. Observations will often fall short on at least one, or multiple of these variables. For instance, meteorological observations with an hourly time step are available for fewer variables, for a shorter time period and from fewer locations. Lastly, observational data generally originate from many different data sources, making acquisition challenging compared to the instantly available RACMO dataset.

On the other hand, observational data also have several benefits over synthetic data. Firstly, observations are generally considered as a factual representation of reality, providing an accurate description of climatology. The capability of climate model datasets to accurately describe climatology is unknown and topic of investigation in this research. It should be noted that observational datasets from different sources may yield varied results and that even for observations, there is no absolute truth. Secondly, the RACMO model may have difficulties in capturing meteorological processes that require a fine grid resolution (e.g. convection (Lucas-Picher et al., 2021)). Observation stations can provide direct measurements in which these processes are better represented.

The preceding comparison showed there are numerous advantages of the RACMO dataset relative to observations when regarding estimation of extremes. However, the quality of the RACMO dataset for this application is still unexplored and therefore one of the main focal points of this research. To improve the quality of the RACMO dataset, the first step is to account for systematic biases induced by the model. An overview of the bias correction applied to the synthetic RACMO data is provided in section 2.3.1.

Bias correction

Both GCMs and RCMs are prone to biases (e.g. Palmer et al., 2023). Sources of such model bias are e.g. discretisation of continuous environmental processes into model grids or simplifications of physical and thermodynamic processes (e.g. convection, surface roughness, orography). These biases have an effect on the model result, which needs a correction to compensate for these systematic biases. Over the years, different approaches have been developed to correct for model bias and reduce model errors. One of the techniques that has become increasingly popular is the quantile mapping (QM) technique (Themeßl, 2011; Cannon et al., 2015).

In QM, bias is corrected by comparing the quantiles of raw model output to observations. The method is based on the assumption that a climate model can more accurately project the rank of a variable of interest, than its actual values. Following this assumption, both the observations and model output are divided into different quantiles and using a quantile-depending correction function, model simulations are mapped onto the observation. This procedure has schematically visualised in Figure 2.4 (Kim et al., 2016), in which both the model output and observations are presented by a probability density function (pdf) and a cumulative distribution function (cdf).

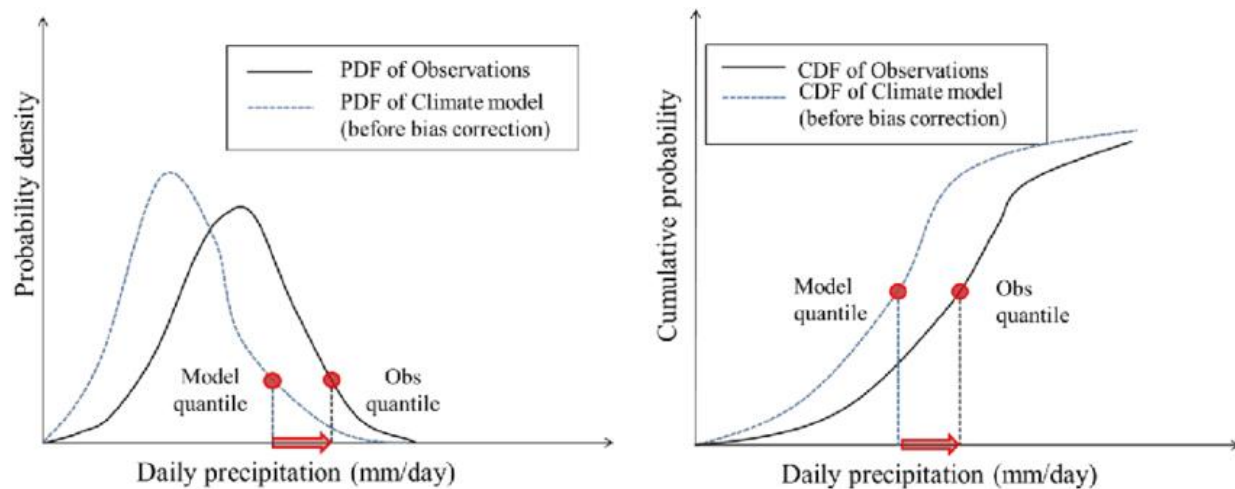


Figure 2.5 Schematic representation of the quantile mapping procedure for a bias correction

Provided that the observations and model results consist of an equal number of data points and the number of quantiles is to be chosen equal to the number of data points, the model output cdf will perfectly fit onto the observational cdf. However, such an approach would likely lead to overparameterisation. Besides, observations and model results are generally not equal in length. Therefore, both datasets are distributed into a limited number of quantiles. In this study, the quantiles are bound by the percentiles used for the KNMI climate scenario's (Van Dorland et al., 2023): quantile intervals of 0.05, with extra quantiles in the tails. The 0.99, 0.999 and 0.9999 quantiles are not directly calculated, but extrapolated from the 0.90 and 0.95 quantiles. For precipitation, we use the exponential distribution for this extrapolation,, and for the temperature, the Gaussian distribution is applied. In this way, stochastic uncertainty in the extreme quantiles is reduced.

The model result value corresponding to every percentile is mapped onto the observed value for the similar percentile. All model values between the percentiles are then interpolated between the new corrected values. This way, the cdf of the bias-corrected model is not entirely identical to the cdf of the observations, but only approaches it. The application of the QM bias correction in this research is similar to its application for the KNMI climate scenarios, which can be referred to for a more detailed description (report to be published on 9 October 2023). However, in this study precipitation quantiles higher than 0.99 have not been corrected, to avoid overcorrection of the large extremes.

It is essential for this study that the corrected model data are representative for current climate. This requires a stationary dataset without any climate signal, which requires detrending of the model dataset. The detrending process is explained in Figure 2.6. The QM correction is applied to subsets of 10 years of the raw model data (1950-1959, 1960—1969, etc.). Because there are 16 ensemble members in

the dataset that all cover the period 1950-2014, the subsets all contain 160 years of model data (except the 2010-2014 set, which contains 80 years). All subsets are corrected and detrended by mapping them onto the most recent part of the E-OBS dataset (1991-2020), making them most representative for current climate. Additionally, the QM correction is applied to every calendar month, because both magnitude and direction of the bias correction can vary seasonally. On average, there are approximately 160x30 (4800) raw model data points for every month for every grid point in every subset of 10 years. The observations contain approximately 30x30 (900) points per month. Note that the percentiles of the observational dataset are determined on the original observational grids and subsequently regridded towards the RACMO grid.

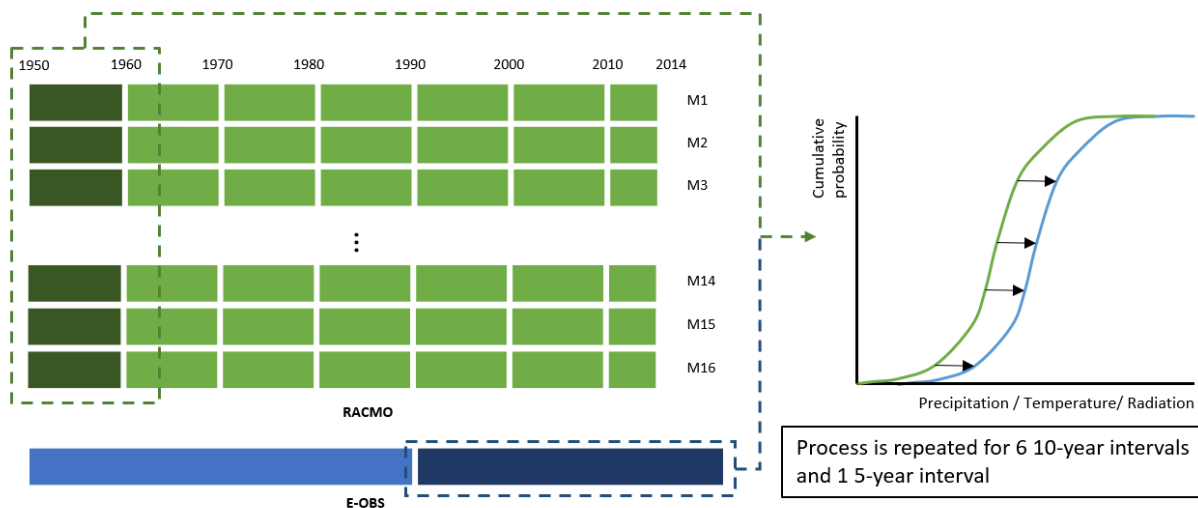


Figure 2.6 Schematic representation of the detrending procedure applied in this study.

The QM correction applied in this study is limited to the daily time scale, because E-OBS has no data available at higher frequency. Furthermore, the GenRE dataset for the Meuse basin is not long enough to use for a bias correction of the sub-daily model output. Since sub-daily data are a relevant part of this research, the sub-daily precipitation data are corrected by multiplication with the ratio of the corrected daily data and the raw daily data of the day of the specific event. For hourly data, this means that all 24 hours in a certain day have been multiplied with the same factor.

2.3.2. Hydrological model

To derive discharge extremes, the synthetic meteorological data must be transformed into a hydrological timeseries by application in a hydrological model. A gridded model is required for analysis of hydrological extremes on a small spatial scale, which is a scale that proved to be highly prone to flooding in the events of July 2021. This is why the gridded wflow model is used as hydrological follow up of this study. Although hydrological computations and analysis are not part of this study, in order to provide a complete overview of the method, a brief description of the wflow model is provided in this Section. The model description is directly obtained from Bouaziz and Buitink (2022). For a more comprehensive overview of the model refer to van Verseveld (2022).

The distributed hydrological modelling software wflow is a free and open source distributed hydrological modelling platform developed by Deltares and targeted to perform hydrological simulations using GIS

raster data, often based on global datasets (van Verseveld, 2022). The model calculates all hydrological fluxes at any given point in the model at a given time step, based on physical parameters and meteorological input data.

Different hydrological concepts exist within the wflow framework, including the wflow_sbm model concept and the wflow_flextopo concept. Within the wflow_sbm concept, alternative options exist to compute the river and land routing, either based on the kinematic wave or the local inertial approximation. The different concepts are described below.

Wflow processes

The wflow_sbm model is a physically-based distributed model. It includes a representation of dominant vertical hydrological processes for glaciers, snow, evaporation (interception, soil evaporation, open water evaporation, transpiration), infiltration depending on the fraction of paved and unpaved area, capillary rise, transfer of water through different layers in the unsaturated part of the soil and transfer of water from the unsaturated to the saturated store. When the soil is saturated or when precipitation exceeds the infiltration capacity, overland flow is generated. The main processes are schematized in Figure 2.7 and a detailed description of each process is available in van Verseveld et al. (2022) and in the online documentation (<https://deltares.github.io/Wflow.jl/dev/>). The code is open source and available on GitHub (<https://github.com/Deltares/Wflow.jl>).

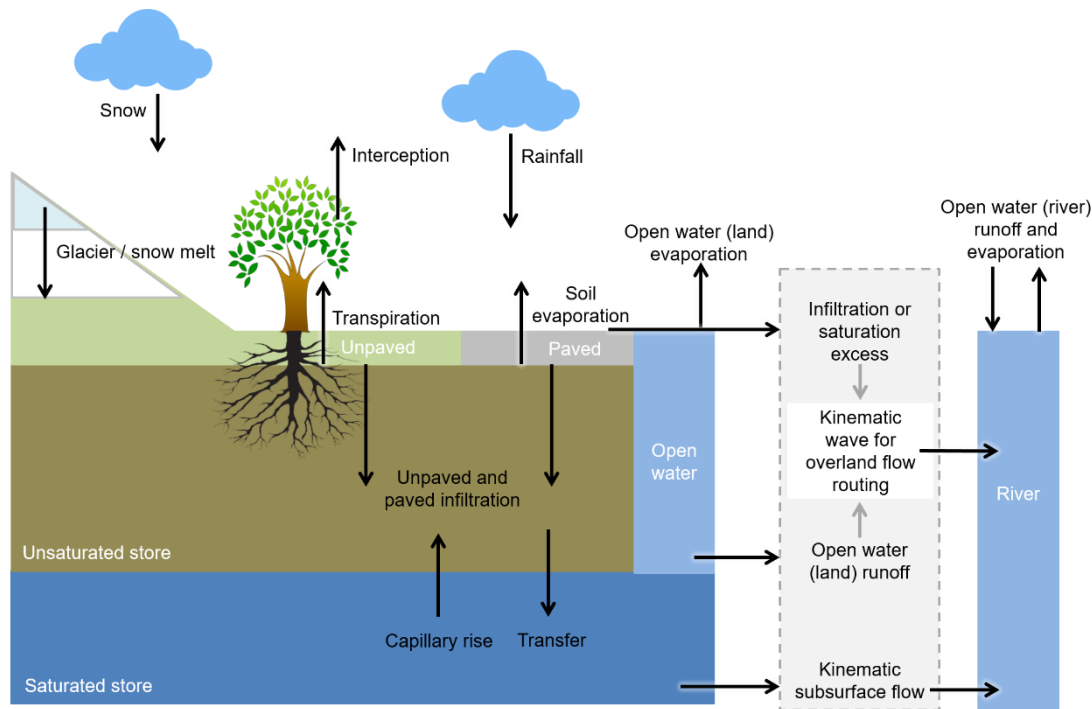


Figure 2.7 Schematic representation of the wflow_sbm concept

Water in the river, the subsurface and on land is transported downslope through the catchment along the river network. The kinematic wave is used for lateral subsurface flow. Several options are possible for the lateral processes of river and overland flow, including kinematic wave or local inertial approximation. For a more detailed description of the lateral processes, please refer to Bouaziz and Buitink (2022) and van Verseveld et al. (2022).

Meteorological input variables

The meteorological input required to run the wflow model consists of the following variables:

- Precipitation (P)
- Temperature (T)
- Potential evapotranspiration (PET)

The output of the RACMO model runs provides data for all variables but potential evapotranspiration. The latter is approximated with the Makkink evaporation formula (Makkink, 1957), which is proven in the Netherlands and often used for discharge modelling in the Meuse, using temperature and radiation data from the model as input variables. Precipitation is available up to an hourly time scale. The other meteorological variables are available up to a 3-hourly timescale and are downscaled to an hourly timestep with linear interpolation after the bias correction.

All meteorological variables have been bias-corrected using the QM approach, like described in section 2.3.1. As the E-OBS dataset has a daily timestep, the correction has been applied to the daily dataset. A 3-hourly representation of the bias-correction for R and MSLP is obtained by scaling the sub-daily value with the ratio of the corrected daily data and the raw daily data. For 3-hourly data, this means that 8 timesteps in a day are scaled with a similar factor.

To derive a correction for 3-hourly temperature, a slightly different approach is used. Instead of using mean T, sub-daily T is scaled using the difference between raw and corrected minimum and maximum temperatures following Equation 2.1.

$$T_{3h,n} = \frac{(T_{3h,o} - T_{d,min,o})(T_{d,max,n} - T_{d,min,n})}{T_{d,max,o} - T_{d,min,o}} + T_{d,min,n} \quad \text{Equation 2.1}$$

Note that this approach may lead to small discrepancies of mean daily temperature between the daily and hourly dataset. However, these differences are too small to influence the discharges.

Furthermore, Makkink PET is an empirical formula which is generally applicable to daily precipitation. To make sure annual average PET is similar for the daily and sub-daily datasets, the sub-daily PET dataset has been scaled with the total annual PET ratio between the daily and the sub-daily dataset.

For adequate functioning of the hydrological model, an adequate representation of the extremes of precipitation is the most important. Precipitation extremes will therefore be mainly considered in the results of this study. For the other variables, a decent representation of their distribution throughout the year is sufficient, which is presented in the annual cycles of Section 3.1.5

2.3.3. Extreme value analysis

The main focus of this research is to evaluate the quality and additional value of the synthetic RACMO timeseries for extreme estimation. Extreme value analysis, with its primary focus on the tail of the precipitation distribution, therefore plays an important role in this research. Two approaches for extreme value analysis are generally considered. Firstly, the peak over threshold method (POT), in which the peaks above a certain threshold are extracted from a continuous timeseries. For the second approach, the timeseries is distributed in blocks (years or seasons in this study) and the extreme value of every block is derived. The latter approach is used in this study. For a more comprehensive consideration of block maxima and peak over threshold, please refer to the (Van Den Brink et al., 2005).

In an extreme value analysis using annual extremes, a timeseries of annual maxima is obtained from the dataset. After sorting the annual extremes, the rank of each of the maxima then provides an indication of its return period. To estimate the probability of an extreme with rank n in dataset length m can be determined based on the probability plotting position formula as defined in Equation 2.2.

$$P = \frac{n + \alpha}{m + \beta} \quad \text{Equation 2.2}$$

The two undefined parameters α and β in this formula have been subject of decades of discussion. Often used is the formula proposed by Weibull (1939), also recommended by Gumbel (1942), in which $\alpha = 0$ and $\beta = 1$. But many alternatives have been discussed in literature. In this study, the alternative with which $\alpha = -0.3$ and $\beta = 0.4$ is used, which was proposed by Bernard and Bos-Levenbach (1955) and is commonly used within the GRADE consortium. The resulting probability plotting position is shown in Equation 2.3.

$$P = \frac{n - 0.3}{m + 0.4} \quad \text{Equation 2.3}$$

The return period is given by equation Equation 2.4, as defined by Buishand & Wijngaard (2007):

$$T = -\frac{1}{\log(P)} \quad \text{Equation 2.4}$$


Timeseries of extremes, especially short ones, are often described using extreme value distributions, which describe the behaviour of the extremes and allow for the extrapolation to return periods that are larger than the length of the dataset. The extreme value distribution that is most commonly used in this study is the Generalized Extreme Value (GEV) distribution (Jenkinson, 1955), which can capture various types of extreme behaviour. The GEV distribution combines the Gumbel (Type I), Fréchet (Type II) and Weibull (Type 3) families and its cumulative distribution function is provided with Equation 2.5 and Equation 2.6.

$$P = e^{-t(x)} \quad \text{Equation 2.5}$$

With:

$$t(x) = \begin{cases} \left(1 + \xi \left(\frac{x - \mu}{\sigma}\right)\right)^{-\frac{1}{\xi}} & \text{If } \xi \neq 0 \\ e^{-\frac{(x - \mu)}{\sigma}} & \text{If } \xi = 0 \end{cases} \quad \text{Equation 2.6}$$

The GEV distribution is defined by three parameters. The location parameter (μ) determines the centre of the distribution, the scale (σ) parameter controls the spread of the distribution and the shape parameter (ξ) determines its skewness. The latter parameter will often be addressed later in this study. A comprehensive description of the influence of the GEV-parameters on extrapolation is provided in Section 3.3. The parameters can be estimated by fitting the observed annual extremes to the GEV distribution. However, as mentioned before, extreme estimation based on a GEV fit with a small



observational dataset can be very uncertain. Note that the Gumbel distribution is a special case of the GEV distribution, i.e., when the shape parameter is equal to zero.

3. Results

This section provides a comprehensive analysis of the quality of the RACMO dataset and its potential, with specific focus on extremes. Firstly, long synthetic timeseries are compared with observations for different variables that are relevant for the estimation of hydrological extremes. Subsequently, the effect of climatic variability on the estimation of extremes in short datasets will be examined using the 16 ensemble members of the RACMO dataset separately. Thirdly, the main advantages of the length of the RACMO dataset will be further investigated through a statistical analysis, which is followed by addressing the seasonality of the meteorological extremes and how this may affect the hydrological perspective.

3.1. Long synthetic timeseries for hydrological application

To ensure an accurate representation of hydrological extremes, the climatology of the synthetic timeseries must be representative. For example, precipitation extremes have a large influence on the hydrological response of catchments, and must therefore be accurately portrayed in the synthetic RACMO dataset. To test this, precipitation extremes of the RACMO dataset are compared with observed extremes in this section.

The response of catchments to extreme precipitation is not linear and depends on various catchment characteristics. Representing these characteristics in a hydrological model is essential for adequate representation of discharge extremes. To ensure good representation of e.g. antecedent soil moisture, evaporation processes and snow melting processes in the hydrological model, the RACMO dataset must accurately reflect the distribution of meteorological variables throughout the year. This is why the annual cycle of all relevant meteorological variables is also compared with observations in this section.

3.1.1. Annual cycle

Figure 3.1 displays the precipitation annual cycle of E-OBS, GenRE, as well as the raw and corrected RACMO datasets. The plot represents the average daily precipitation for all calendar days throughout the year. Unless stated otherwise, the Figures depict the average over the catchment areas of the Meuse at Borgharen, the Meuse at St. Mihiel, the Lesse and the Vesdre. An overview of the annual cycle of all catchments is provided Appendix 6.1.

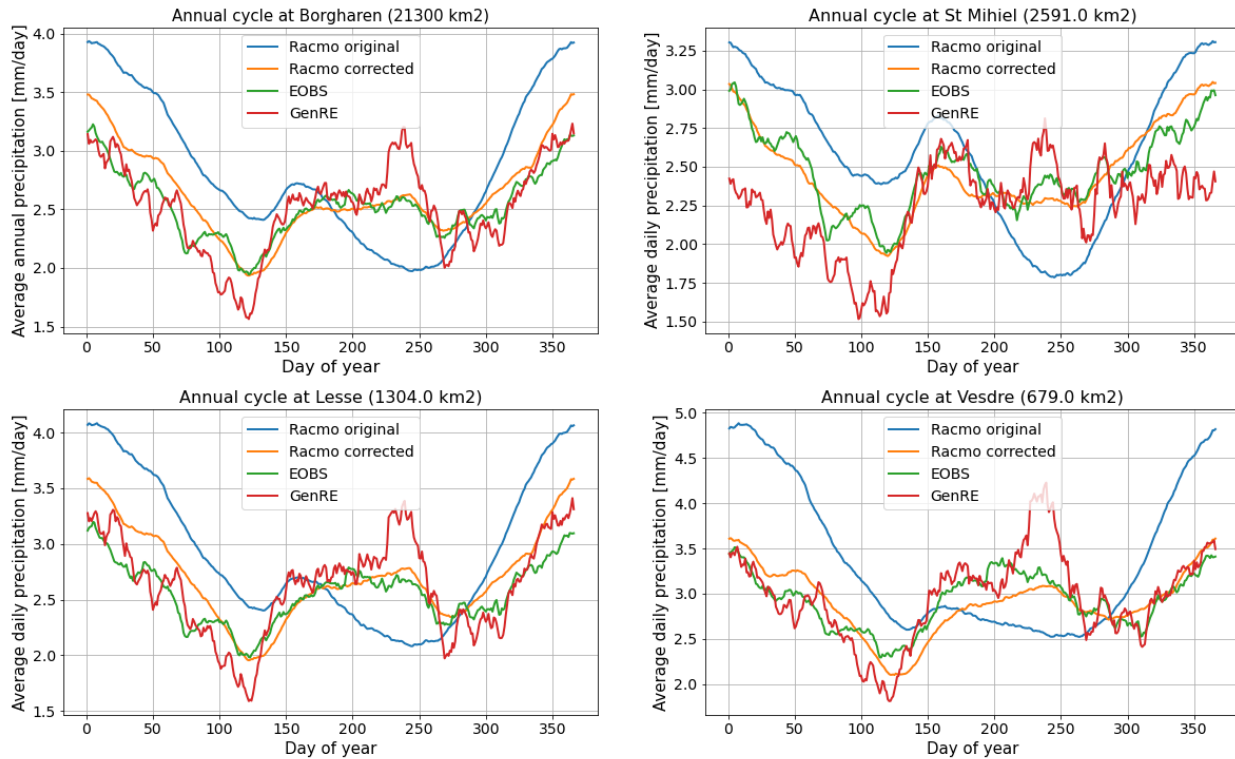


Figure 3.1 Overview of the annual cycles of RACMO (original and corrected), E-OBS and GenRE, averaged over the catchment areas of the Vesdre, Lesse and the Meuse upstream of St. Mihiel and Borgharen. The annual cycle presents the average daily precipitation falling on a certain day of the year based on all years in the dataset and in each ensemble member.

To have an adequate climatological representation, the distribution of precipitation throughout the year in RACMO must match with that of observations. The results show a great improvement in resemblance between RACMO and observations after bias-correction, indicating that the bias-correction performs well. Where the raw RACMO data exhibit considerably higher precipitation averages during winter and spring compared to observations, and slightly lower values during summer, the corrected dataset has drier springs and wetter summers, better matching both observational datasets. Note that the E-OBS dataset is used for quantile mapping of the RACMO dataset, but the alternative GENRE dataset (with fewer years) also shows good resemblance to the distribution of precipitation throughout the year in the corrected RACMO dataset. Consequently, after bias correction, the annual distribution of precipitation in the RACMO dataset is considered suitable for application in the hydrological model.

Figure 3.2 shows the annual cycle of the other meteorological variables that are required in the hydrological model (T, and PET), averaged over the Meuse basin at Borgharen. Here, the raw RACMO dataset, the corrected RACMO dataset and E-OBS are compared.

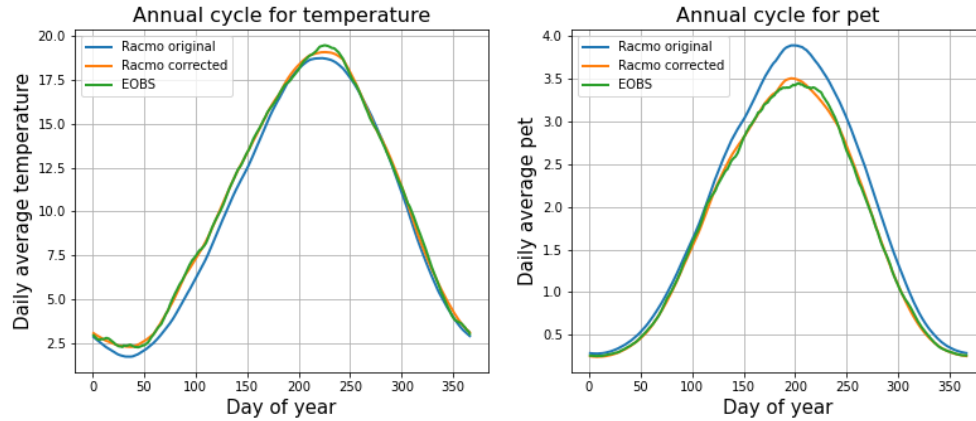


Figure 3.2 Annual cycles of daily average temperature and pet for the Meuse catchment upstream of Borgharen.

For both temperature and PET, the bias-corrected RACMO results compare very well with E-OBS. This indicates that the bias correction is performing well and both temperature and PET data are well represented in the hydrological model by the RACMO dataset. Note that bias-correction is rather inessential for the temperature data, as the raw model result already compares very well with observations.

3.1.2. Annual multi-day extremes

A comparison between the annual extremes of the RACMO dataset and observations is provided for a daily and 5-day precipitation sum in Figure 3.3 and Figure 3.4. Note that the raw RACMO data is not included in the Figures. This is because a large part of the data points in the extreme value plots originate from the upper 0.95 quantile of the annual timeseries, which was not subjected to a bias correction in this study. As a result, the differences between raw and corrected RACMO extremes are minimal and therefore, only the corrected RACMO dataset is shown in the Figures. To give an indication of the magnitudes of the precipitation maxima, the 1-day and 5-day sum of July 2021 have been added to the Figures. An overview of the annual extremes in other catchments is given in Appendix 6.3.

With the exception of the GenRE dataset in St. Mihiel, all datasets exhibit a strong similarity to each other for both considered multi-day sums. This indicates that extremes are well represented in the corrected RACMO dataset, at least within the temporal domain covered by the observational datasets. As such, the climate model effectively captures the dynamics around singular daily precipitation extremes and inter-daily extreme precipitation patterns are also well represented and closely resemble reality. The resemblance of RACMO and observation data increases confidence that the model accurately represents the larger extremes that exceed the temporal range covered by observations. In general, the RACMO dataset shows to have great quality regarding precipitation extremes on daily and greater than daily scales and is therefore suitable for application in hydrological models to estimate discharge extremes.

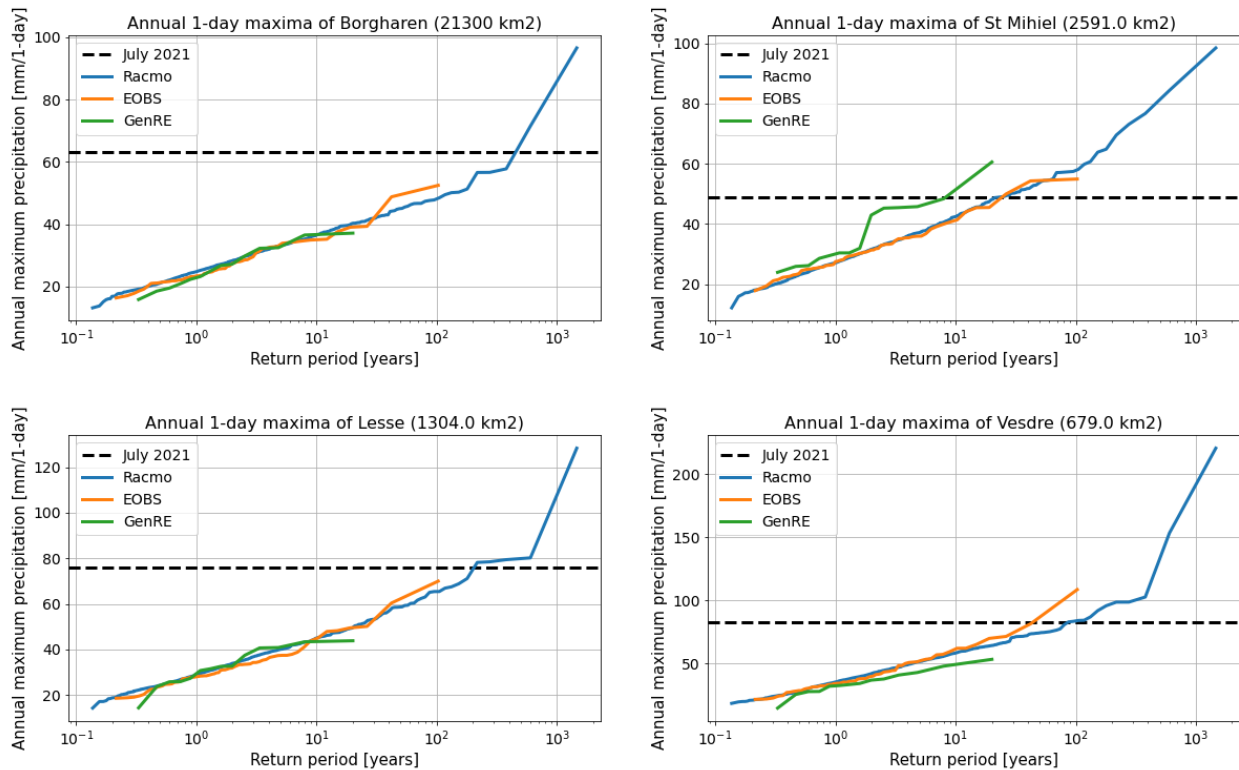


Figure 3.3 Overview of daily annual maximum precipitation of RACMO, E-OBS and GenRE, averaged over the catchment areas of the Vesdre, Lesse and the Meuse upstream of St. Mihiel and Borgharen.

Figure 3.3 and Figure 3.4 highlight one of the advantages of the large synthetic dataset. While extreme determination directly from the observational dataset is limited to return values of only a few decades, the RACMO dataset directly plots extreme estimation with return periods exceeding 1000 years. Besides, the longer dataset reveals potential behaviour and trends that can only be investigated with larger datasets and that were previously undiscovered. For example, the curvature of the extreme value plots can now be analysed and estimated in much greater detail and with much smaller uncertainty compared to previous studies with observations alone. The E-OBS dataset for both 1 and 5-day precipitation totals in the St. Mihiel catchment may for instance suggest downwards curving behaviour for return periods larger than 100 years. The RACMO dataset however suggests entirely opposite behaviour. A few of these new insights, including the shape of the curvature, but also the difference between summer and winter events in large datasets, are further explored in sections **Error! Reference source not found.** and 3.4.

The July 2021 daily and 5-daily precipitation sums are shown for comparison purposes. Note that in several catchments, the daily and 5-daily sums of precipitation can become substantially larger than the July 2021 event according to the RACMO simulations. Particularly in the Vesdre, daily precipitation totals were simulated to be more than twice as large as the July 2021 event. Also note that July 2021 has a relatively low RE return period in the Vesdre according to the RACMO simulations, even though severe floods occurred in this basin. This discrepancy may be related to the rapid rainfall-runoff response of the Vesdre, potentially indicating that a daily time window is too large for the high runoff response.

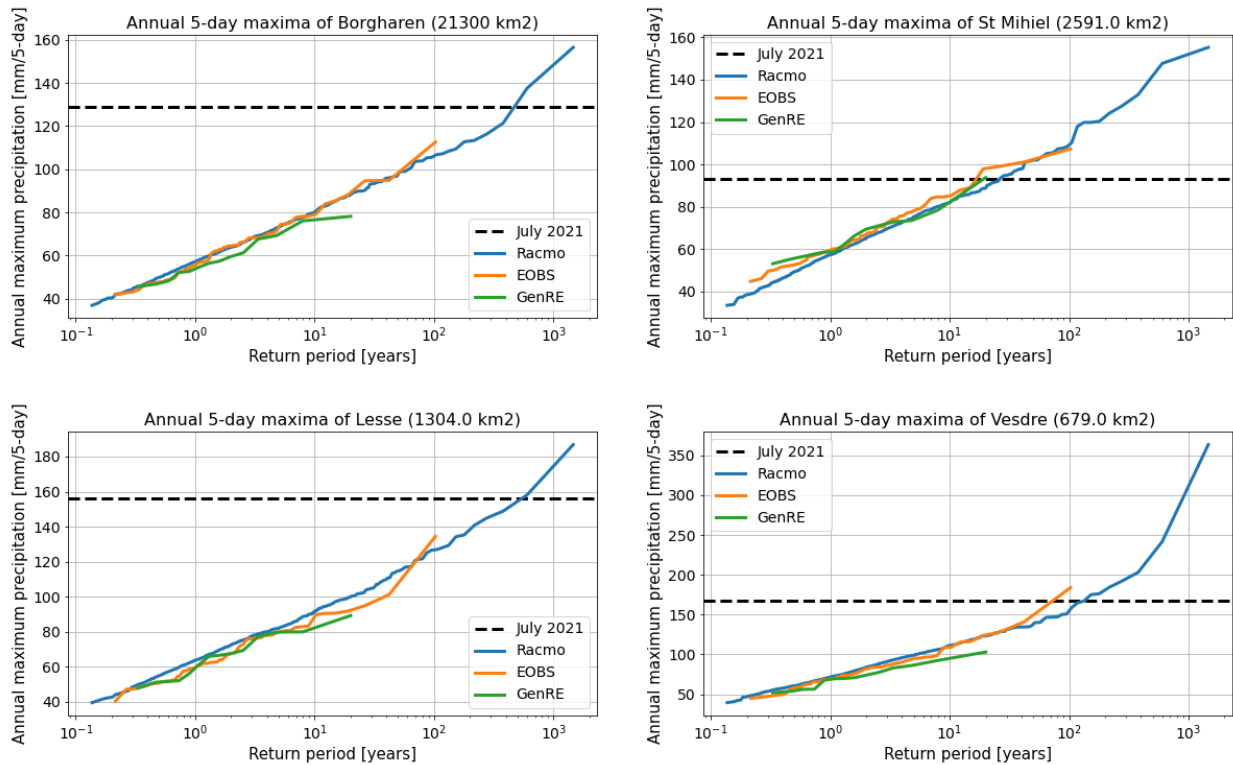


Figure 3.4 Overview of 5-daily annual maximum precipitation of RACMO, and E-OBS and GenRE, averaged over the catchment areas of the Vesdre, Lesse and the Meuse upstream of St. Mihiel and Borgharen.

3.1.3. Annual sub-daily extremes

Although RACMO successfully captures extreme precipitation events at the daily scale, an adequate sub-daily description of precipitation is also important to allow accurate description of the fast hydrological response of several smaller catchments. Figure 3.5 and Figure 3.6 compare hourly and 6-hourly annual precipitation extremes between the RACMO dataset and the GenRE dataset. Only the GenRE dataset is used as comparing dataset because E-OBS does not provide hourly data. Hourly and 6-hourly maxima of the July 2021 storm were not available and are therefore not presented in these figures. An overview of the annual extremes in other catchments is also given in Appendix X.

The results show a reasonable agreement between GenRE and RACMO for the length of observations, specifically for the Borgharen and Vesdre catchments. However, there are slight discrepancies between the two datasets when the St. Mihiel and Lesse catchments are considered. It should be noted that Figure 3.1, Figure 3.3 and Figure 3.4 reveal a considerable difference between the E-OBS and GenRE datasets, particularly in the St. Mihiel catchment. This may indicate that the observed offset in Figure 3.5 does not only stem from the RACMO dataset, but could also be influenced by potential shortcomings in the observational dataset. Besides, the observational timeseries only spans 12 years, which challenges a comparison with the 1000-year timeseries. Regarding 6-hourly data, the plots show a stronger agreement with the GenRE observation dataset. Resemblance is particularly improved for the Lesse catchment and slightly better for the Meuse upstream of St. Mihiel. These results give a first indication that RACMO can also be used at a sub-daily scale (6-hourly and potentially hourly) in hydrological analysis of extremes, but a more detailed description on the reliability of the sub-daily RACMO data is provided in section 3.2.

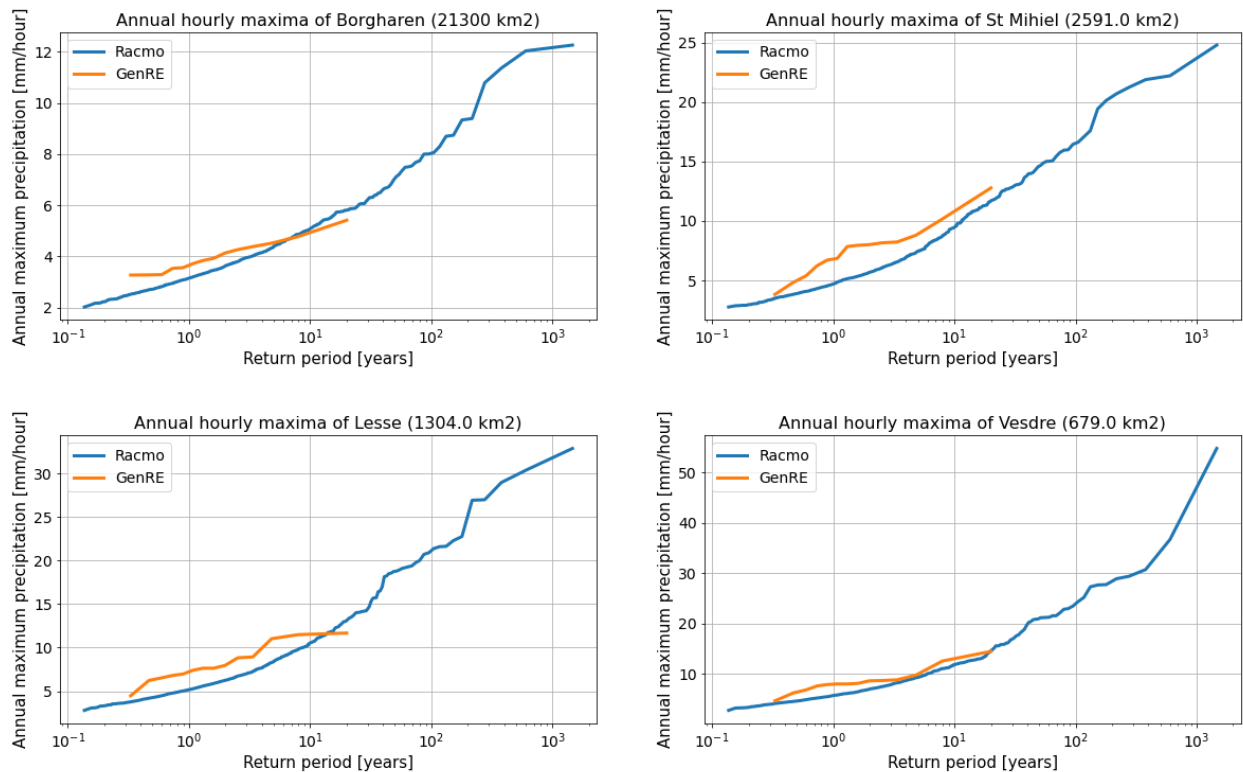


Figure 3.5 Overview of hourly annual maximum precipitation of RACMO and GenRE, averaged over the catchment areas of the Vesdre, Lesse and the Meuse upstream of St. Mihiel and Borgharen.

Apart from their comparison with observations, the hourly RACMO extremes can also be tested based on literature. Hourly extremes generally show an upward curvature in extreme value analysis (e.g. Beersma et al., 2019). This upward curvature is found for RACMO in all catchments, indicating that the tail behaviour of hourly extremes is well represented by the RACMO model. It is striking that the short hourly observational dataset does not exhibit the upwards curvature accurately for most catchments, which is presumably related to the short length of the dataset. This once again highlights the value of the long synthetic datasets.

Although the July 2021 event has not been plotted, it is important to note that the 6-hourly precipitation extremes in the Vesdre simulated by RACMO have reached values that are substantially higher than the observed precipitation sums of July 2021. During this event, discharge extremes were reported within 6 hours after the precipitation peaks. With similar catchment response to the RACMO precipitation extremes, discharge extremes based on the RACMO extremes will likely even reach higher discharges than reported in 2021, which is confirmed by Couasnon et al. (2023). A closer examination of the most extreme Vesdre event is conducted in section 544.2. Furthermore, the hourly and primarily the 6-hourly Vesdre show a clear inflection point in the graph. The origin of this inflection point is further discussed in section 3.4 and section 4.2.

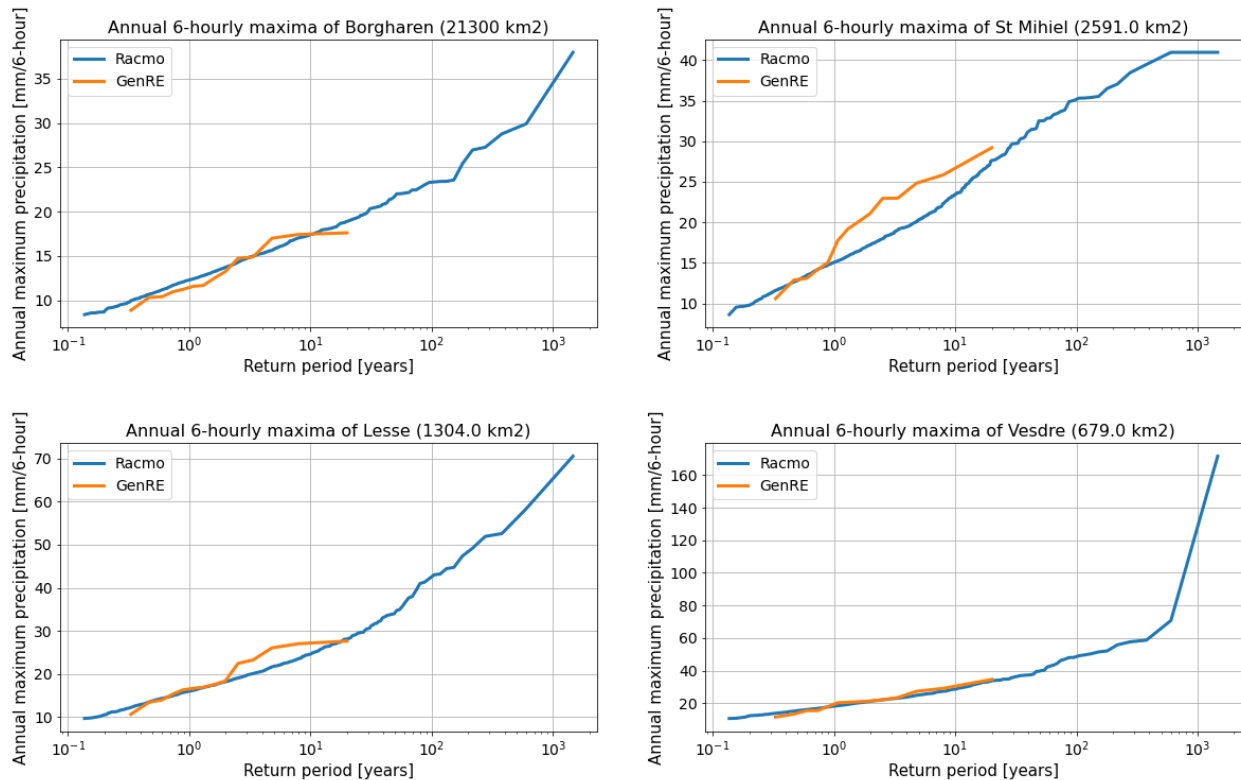


Figure 3.6 Overview of 6-hourly annual maximum precipitation of RACMO and GenRE, averaged over the catchment areas of the Vesdre, Lesse and the Meuse upstream of St. Mihiel and Borgharen.

3.1.4. Daily cycle

Similar to the annual cycle, the distribution of daily precipitation can be analysed using a daily cycle, like depicted in Figure 3.7, in which the hourly precipitation is averaged over all days in the year. Because the daily distribution of precipitation is more pronounced in summer, the daily cycle of summer precipitation is also shown in Figure 3.8. Note that the signal of the raw RACMO model results is similar to that after applying a bias correction. The only effect of the correction is a vertical shift of the signal. This results from the fact that the bias correction does not distinguish between different hours and as such, the daily spread shown in these figures are entirely subject to the performance of the RACMO model.

In both Figures, the shape of daily cycles of RACMO and observations is quite similar, especially after bias correction. The minima, maxima and the distribution of hourly precipitation therefore all seem well described by the RACMO model. The behaviour of short precipitation events is thus simulated reasonably well by the model, which is particularly important in summer. Note that the Figures show a slight phase lag, with the corrected RACMO dataset being ahead of observations, which is not uncommon in RCMs with parameterized convection (e.g. Rio et al., 2009). However, for the extreme statistics considered in this study, the timing of precipitation extremes on a daily scale is not of great relevance and will not impact the study results. Do note that the discrepancy in timing between hourly RACMO and observations should be considered for application in studies with other focal points.

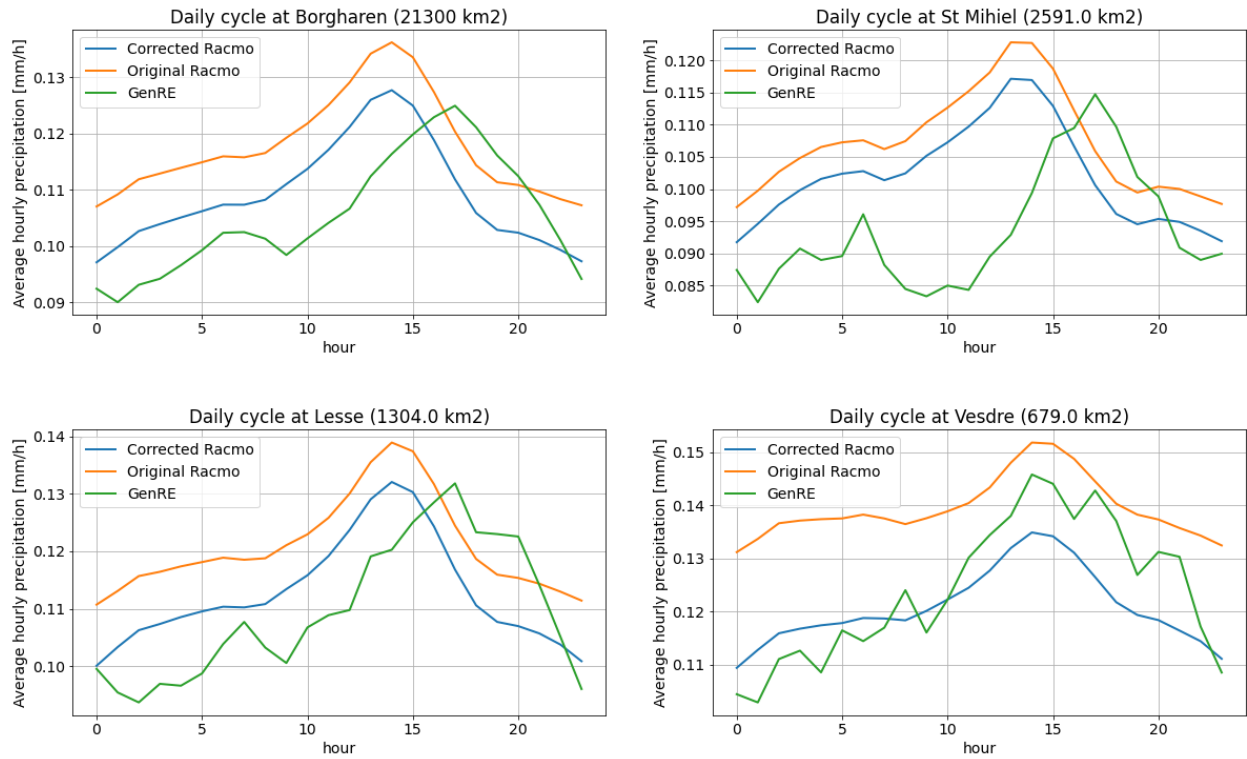


Figure 3.7 Overview of the daily precipitation cycle of RACMO (original and corrected) and GenRE, averaged over the catchment areas of the Vesdre, Lesse and the Meuse upstream of St. Mihiel and Borgharen.

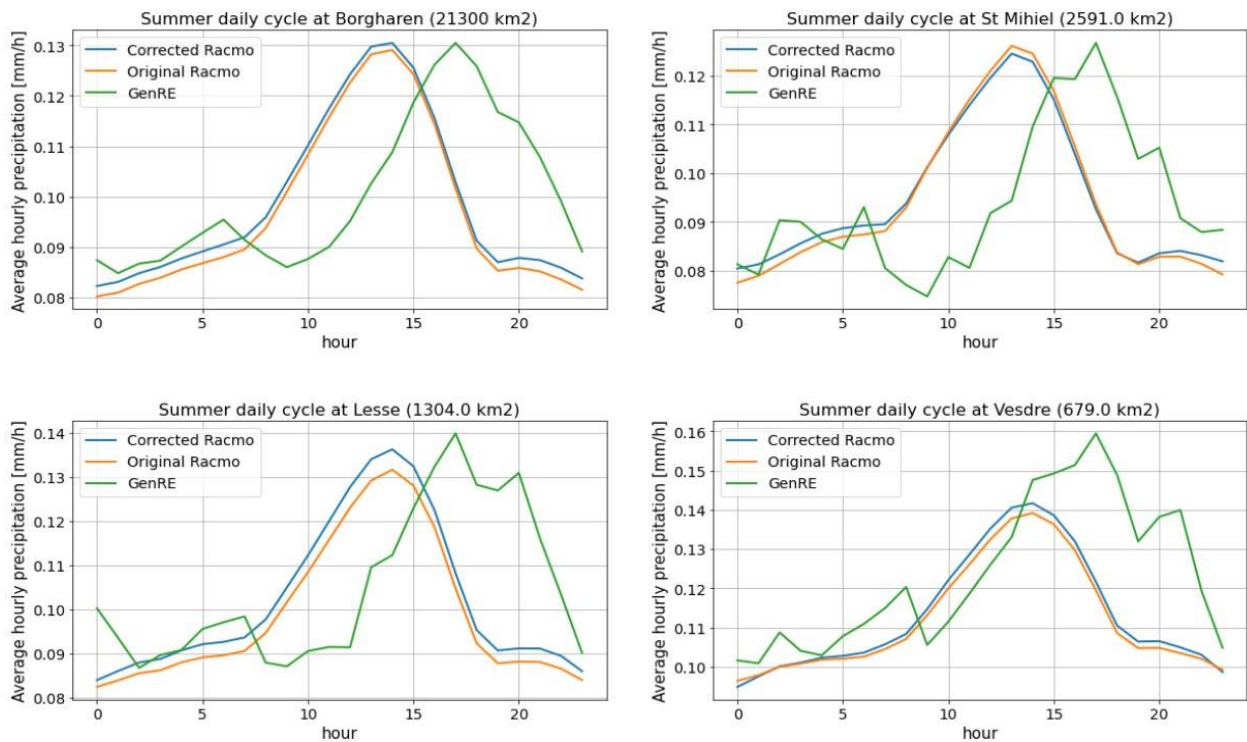


Figure 3.8 Overview of the daily precipitation cycle in summer of RACMO (original and corrected) and GenRE, averaged over the catchment areas of the Vesdre, Lesse and the Meuse upstream of St. Mihiel and Borgharen.

3.1.5. Weather generator

As explained in the methodology, there are two alternatives of the existing GRADE approach. In the first alternative, the 1000 year spanning synthetic timeseries is directly used as input of the wflow model. For return periods larger than 1000 years, statistical extrapolation can be applied, which is extensively discussed in section 3.3. The second alternative is to use the synthetic RACMO dataset as input of the WG. A brief extreme value analysis of this approach is provided in this section. Note that the analysis is limited to time windows of a day or larger, as the WG only runs with a daily input. The annual extremes of the corrected RACMO dataset and E-OBS dataset, both before and after WG resampling, are depicted in Figure 3.9 and Figure 3.10 for respectively a 1 and 5-day sum. The WG plots for the other catchments can be found in Appendix 6.4.

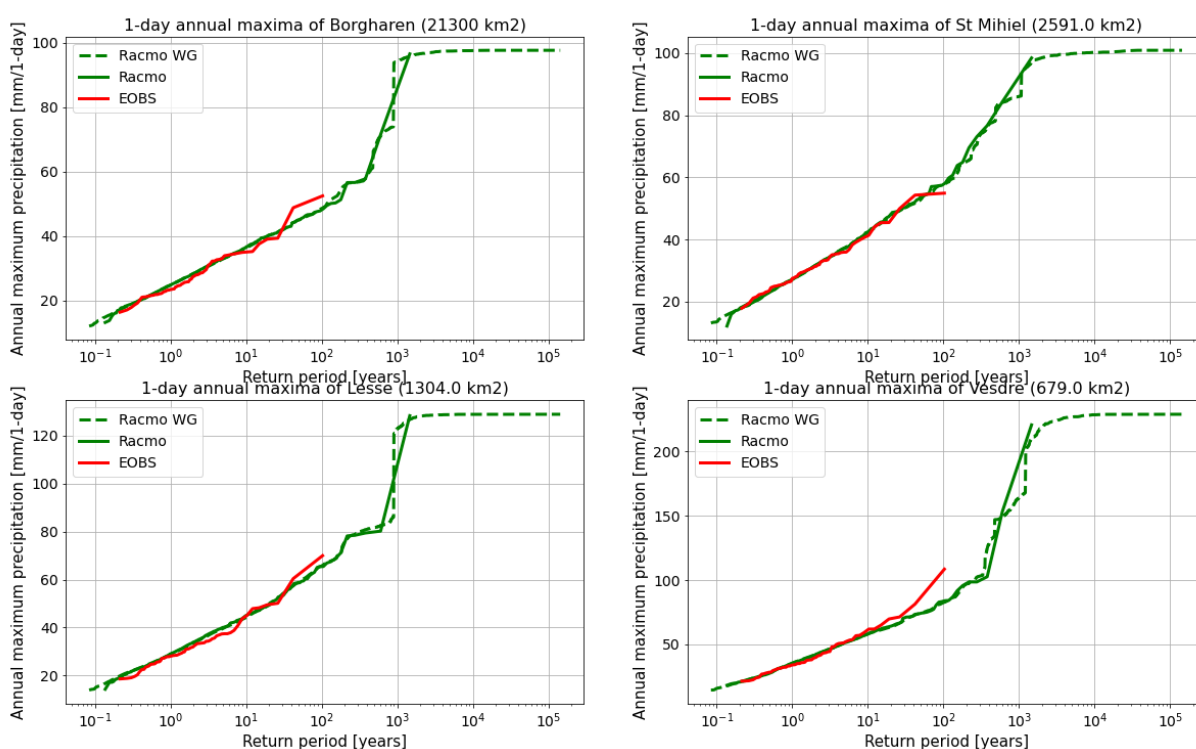


Figure 3.9 Annual maximum precipitation for a 1-day precipitation sum for RACMO (with and without WG resampling) and E-OBS

The main disadvantages of the WG are also visible in Figure 3.9 and Figure 3.10. Resampling of daily precipitation sums will never exceed the maxima that are in the original RACMO dataset. Use of the WG for a 1-day precipitation sum is therefore not useful. As mentioned in section 1.2, use of the WG becomes more plausible for 5-day precipitation extremes. Return periods can be estimated for durations exceeding 100.000 years. Note that the WG result of the RACMO dataset displays several jumps, which are likely caused by methodical flaws of the WG. However, over- or underestimation of the WG occurs much later when the RACMO dataset is used as resampling dataset compared to the observational dataset.

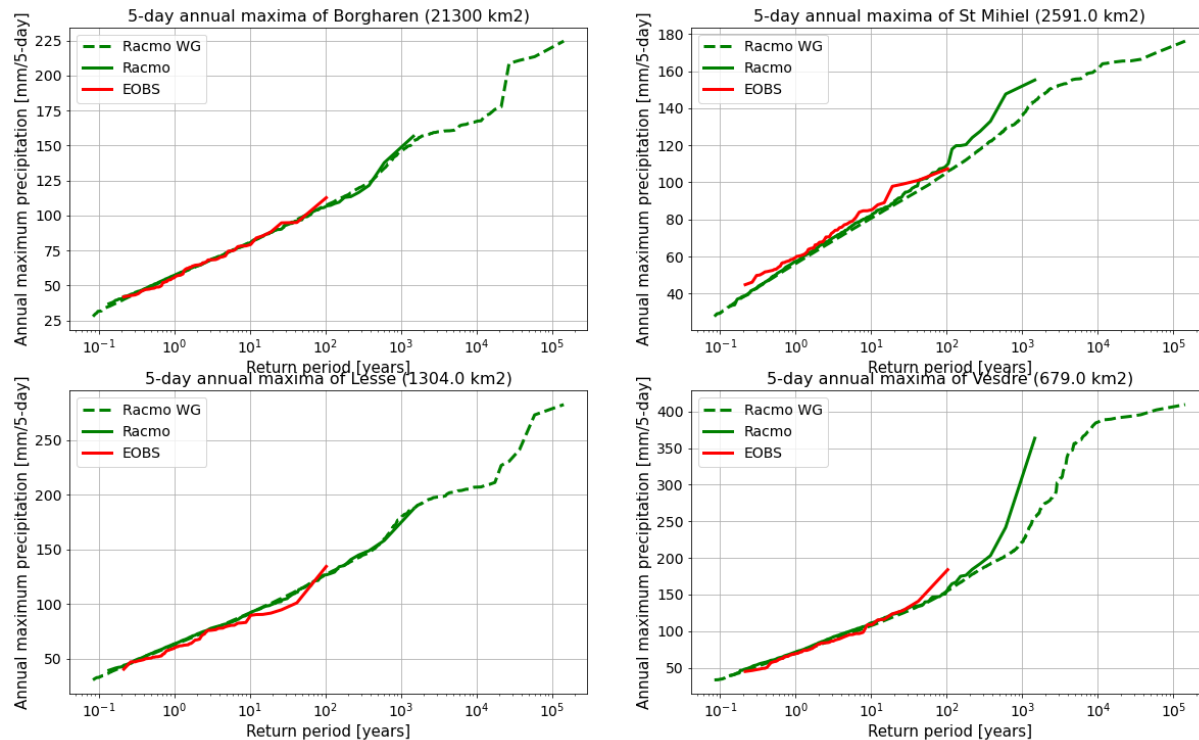


Figure 3.10 Annual maximum precipitation for a 5-day precipitation sum for RACMO (with and without WG resampling) and E-OBS

Note that the WG can not be used for estimation of precipitation extremes with a daily time window or lower, whereas catchments in the Meuse basin are likely to respond to such short sub-daily precipitation. Depending on the results of this study, it may therefore be valuable to conduct additional research to create an hourly version of the WG.

3.1.6. Overview of RACMO return values

Table 3.1 provides an overview of the return values for all considered catchments within the Meuse basin and the basin as a whole for both an hourly and a daily duration. The return values have been obtained by fitting a GEV distribution to the annual extremes and extracting the maximum value corresponding to each relevant return period. For return periods exceeding the RACMO dataset length (greater than 1000 years), the GEV fit on the WG result has been used. As a measure to determine the offset of the GEV from the data points, the most extreme empirical value is added to the table (which has a plotting position around a return period of 1400 years). In Appendix 6.5, tables with return values for a 2,3 and 5-day sum are presented.

In general, comparison of the RACMO results with different observational datasets in the previous section of this chapter has shown that the bias-corrected RACMO data appears to be adequate for hydrological simulations to estimate discharge extremes. The return values corresponding to 1, 10 and 100 year return periods as presented in Table 3.1 can therefore be considered as accurate estimates (with increasing uncertainty for larger return periods), for both daily and sub-daily timesteps. Besides, assuming that the statistical uncertainty reduces with the square root of the size of the dataset, the statistical uncertainty of the daily return values in Table 3.1 is approximately 4 times smaller than that of observations, while the reduction is almost 10-fold for sub-daily data. However, even with the reduced

statistical uncertainty, the derivation of return values higher than 100 years is still subject to substantial uncertainty (either due to the statistical uncertainty of the GEV distribution or due to the imperfections of the WG) and should therefore be treated carefully. Comparisons of the differences between the maximum empirical return value and the GEV 1000 year return value suggest similar caution. Do note that the plotting position of the maximum empirical return value is also uncertain and can therefore be an over or underestimation of the true value as well.

Table 3.1 Overview of different precipitation return values of the Meuse basin and its catchments for a daily and hourly sums. Results are presented in millimeters per timestep.

RP (years)	<i>Hourly sum</i>					<i>Emp</i> ~1400	<i>Daily sum</i>						<i>Emp</i> ~1400
	1	10	100	1000	10000		100000	1	10	100	1000	10000	
Meuse	3.1	5.0	8.0	12.8	12.3	24.7	36.8	49.6	63.2	79.8	96.9	96.5	
St. Mihiel	4.7	9.1	17.9	35.2	24.8	27.2	42.5	59.2	77.7	103.4	130.5	98.4	
Chiers	4.9	9.4	19.0	40.0	23.9	29.7	44.7	61.3	79.6	95.7	115.0	91.1	
Stenay	4.9	9.8	21.4	48.9	27.9	28.7	45.1	64.7	88.2	111.2	141.1	137.6	
Chooz	5.0	9.4	18.7	38.5	40.9	30.6	45.2	60.5	76.3	96.8	117.0	128.0	
Semois	5.5	10.3	21.3	46.1	39.0	34.7	51.6	67.8	83.3	99.4	114.6	104.9	
Viroin	5.5	11.2	24.2	54.5	39.0	28.9	45.1	65.4	91.0	120.2	157.5	117.5	
Namur	5.1	10.3	21.7	46.8	54.8	26.3	42.0	63.5	93.0	132.3	187.3	139.7	
Lesse	5.2	10.3	21.2	44.3	32.9	28.9	45.4	64.5	86.7	120.0	157.5	128.4	
Sambre	4.6	9.1	18.0	35.4	31.3	26.6	41.9	60.2	82.2	105.5	134.7	97.0	
Ourthe	5.0	10.0	21.3	46.9	43.5	29.3	46.5	65.0	84.9	114.2	144.1	82.7	
Ambleve	5.5	11.2	24.0	52.5	45.2	32.7	53.9	78.4	106.8	138.5	175.9	136.5	
Vesdre	5.7	11.5	23.3	47.1	54.8	34.8	58.8	86.8	119.5	154.2	196.1	220.6	
Mehaigne	5.3	11.5	25.0	54.9	42.3	26.2	43.5	66.3	96.3	132.3	181.9	115.5	
Liege	4.8	9.3	17.4	31.9	48.9	26.9	43.8	66.5	97.1	125.4	168.7	119.8	
Jeker	5.3	11.4	23.6	48.4	62.0	26.6	43.8	65.9	94.3	128.7	174.7	132.5	

The availability of long synthetic data has enabled the analysis of an entirely new domain of return values that was previously unexplored. Although absolute values of the high return periods may still be prone to statistical uncertainty, the length of the dataset suggests a more reliable description of the curvature of extreme value plots, which is elaborated upon in sections 3.2 and 3.3. Such an accurate description is potentially even more important than achieving an exact resemblance with observations for lower extreme values, because it will often be a dominant factor in the statistical approximation of precipitation extremes corresponding to very high return values. A more detailed analysis of the advantages of long synthetic data regarding the curvature of extreme value plots is provided in section **Error! Reference source not found.**

3.2. Ensemble members of the synthetic dataset

The main advantage of the synthetic RACMO dataset, as has been addressed multiple times, is its length compared to observations. However, the dataset is not generated through a continuous simulation. Instead, 16 simulations of 65 years were executed, all of which are different but representative for the current climate. This approach allows for the examination of the climatic variability within the RACMO

dataset. For example, the spread of annual extremes over a similar climate can be examined, to provide an understanding of the degree to which extreme values of the different datasets may vary within similar climatic conditions. Furthermore, the climatic spread along the ensemble members can be used to assess whether the observed values fall within the expected climatic variability of RACMO. Analysis of climatic variability of the RACMO model based on the different ensemble members is provided in this section.

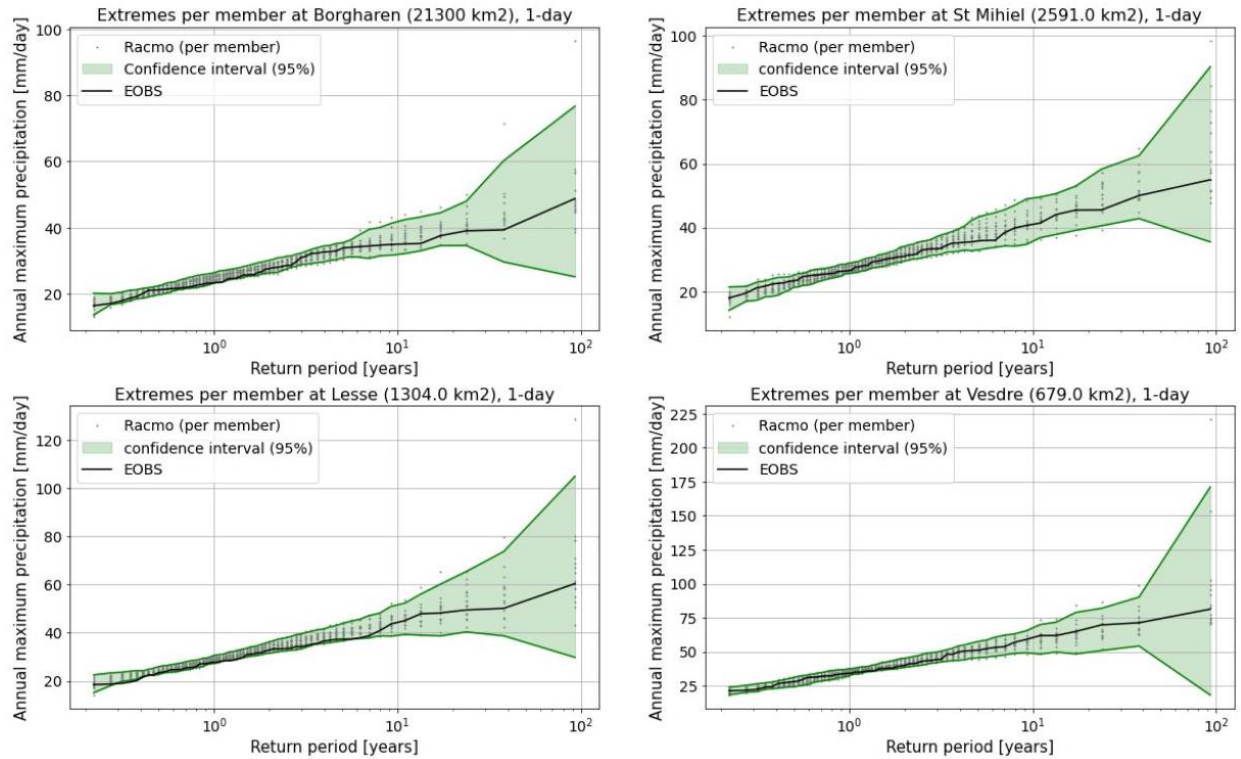


Figure 3.11 Daily Annual maximum precipitation for all 16 RACMO members separately and the E-OBS dataset, including a confidence interval based the spread of the 16 RACMO members.

The climatological spread of the precipitation extremes in the RACMO dataset is shown in Figure 3.11, Figure 3.12 and Figure 3.13 for respectively a daily, hourly and 6-hourly time step. The annual extremes for all 65-year long datasets (16 members) have been matched with their corresponding return period. The 2.5th to 97.5th percentile range, which we refer to as the ensemble spread of the extremes has been determined using all 16 members, being an indicator for the spread of the member extremes in similar climatic conditions. The daily RACMO dataset has been compared to the E-OBS observations, which have a similar length as the individual ensemble members of the RACMO dataset. To compare the hourly and 6-hourly data, the GenRE dataset is used. To ensure a good comparison for these time steps, the 16 ensemble members have been divided into 5 segments of 12 years each, resulting in a timeseries length similar to that of the observations.

Both the percentile range and the individual RACMO points show an increasing spread for larger return periods across all catchments. Depending on the region, the spread starts becoming more pronounced for return values of 5-10 years when regarding the daily datasets. The large variety of the high daily extremes shows that estimating such extremes with the given dataset length becomes progressively less

reliable². This loosely suggests that a dataset of approximately 65 years is suitable for estimating extreme values up to approximately 10 years. Larger return periods show a significant spread and estimation of corresponding return values is therefore not very reliable. As observational datasets are generally not much longer than the individual members of the RACMO dataset, estimation of large extremes based on these datasets is highly prone to the accidental occurrence of an extreme event, given the substantial possible variation in a given climate. Consequently, the reliability of high extreme estimates from observational datasets is limited.

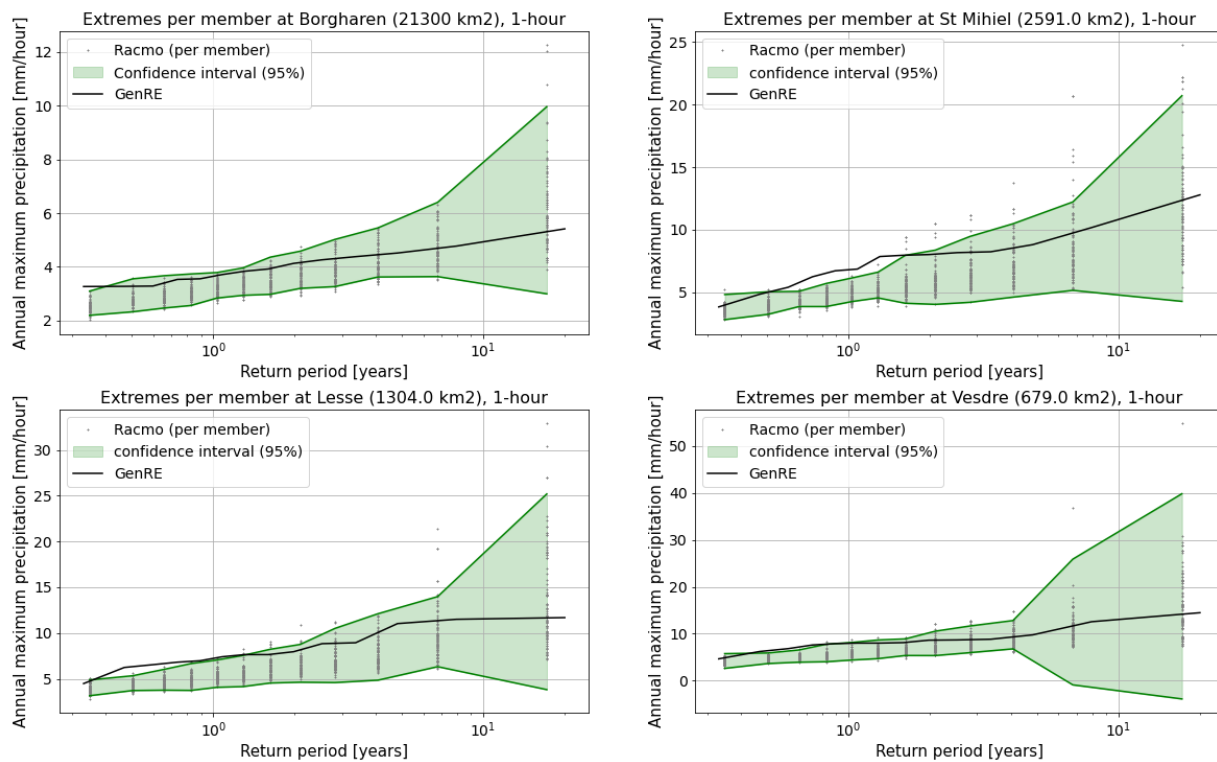


Figure 3.12 Hourly Annual maximum precipitation for all 16 RACMO members separately and the GenRE dataset, including a confidence interval based the spread of the 16 RACMO members

In the even shorter hourly and 6-hourly datasets (with 12 years of data), the climatic variability in precipitation extremes is already more pronounced and exponentially increasing for return periods between 1 and 5 years. This implies that datasets with a sub-daily timestep, which are typically available for a limited time span like the GenRE dataset, cannot be used to estimate extremes with return periods larger than 5 years. Consequently, determining large sub-daily precipitation and discharge extremes using currently available datasets proves to be extremely insecure. In general, whether using a daily or sub-daily time step, there is a significant need for larger datasets, emphasizing the crucial necessity of using large synthetic datasets.

² The low bound of the confidence interval starts decreasing for larger return periods and should technically be constrained.

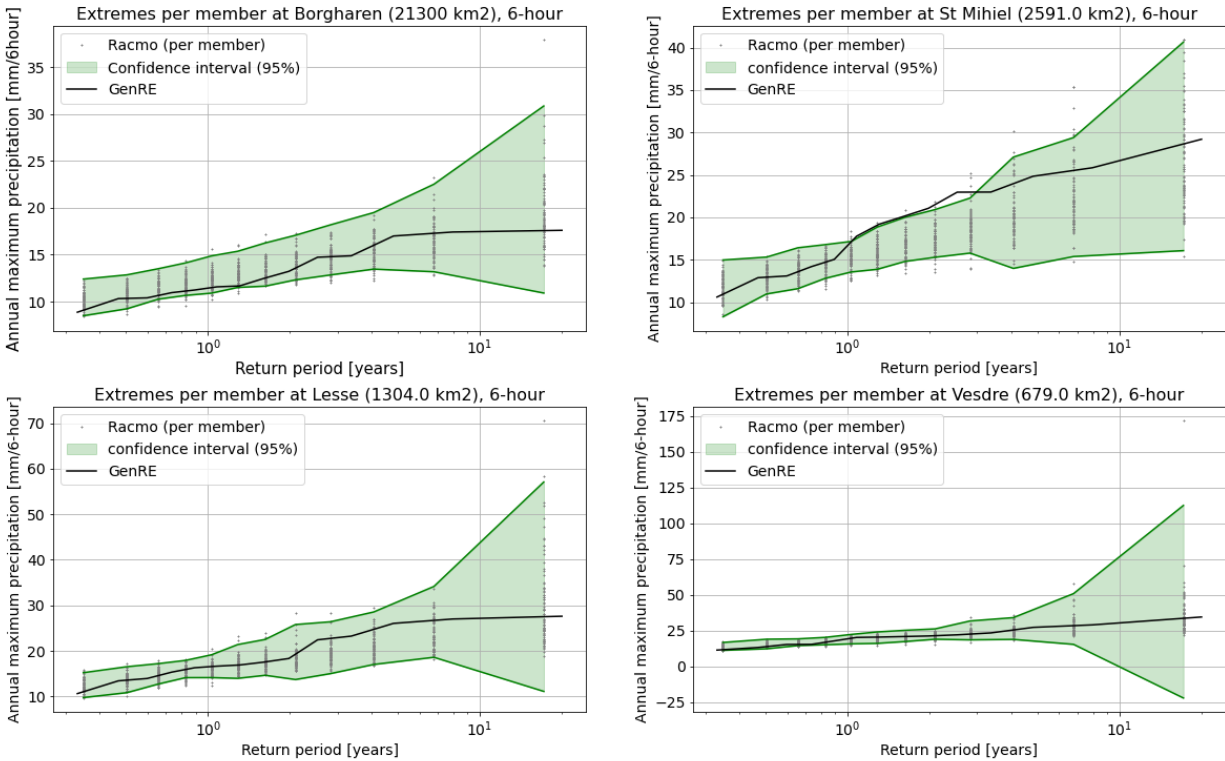



Figure 3.13 6-Hourly Annual maximum precipitation for all 16 RACMO members separately and the GenRE dataset, including a confidence interval based the spread of the 16 RACMO members

Figure 3.11 shows that the observational datasets generally fall within the confidence interval set by the daily RACMO dataset. This indicates that the observations are consistent with the expected variability of the RACMO dataset. In other words, the observations could be considered as a 17th ensemble member of the RACMO dataset in most catchments. This statistical consistency implies that the observations are comparable to the RACMO dataset in terms of extreme precipitation on a daily timescale, again confirming the reliability of the synthetic dataset for estimating precipitation extremes on this time scale.

The only catchment in which observations are not entirely enclosed by the RACMO confidence interval is the Semois catchment (see Appendix 6.6.1), where the middle extremes are slightly lower than the lowest bound of the RACMO confidence interval. Note that this discrepancy may be attributed to the fact that there is a considerable likelihood of one outlying sequence among the 15 catchments. Alternatively, it is possible that the differences between the modelled RACMO extremes and observation extremes in the Semois catchment are of more systematic nature. Particularly the orography of the catchment, being an elongated valley, can be difficult to capture in the RACMO 12x12 grid size of the RACMO model.

The sub-daily data can also be tested by examining if the observations fall within the confidence intervals of the RACMO ensembles as presented in Figure 3.12 and Figure 3.13. The figures show slightly more outlying data points compared to the daily RACMO dataset. However, the majority of the data points in the observational dataset still fall within the confidence intervals. This reaffirms that the sub-daily RACMO datasets (in particular the 6-hourly dataset, but even the hourly dataset) provide a



reasonably accurate description of annual extremes. This is particularly important for smaller catchments where the fast response of extreme runoff can not be adequately estimated by using a daily time step.

There are several catchments in [Figure 3.12](#), for which some of the observed extremes fall outside the RACMO confidence intervals. As the observational dataset only spans 12 years, these deviations could potentially be related to the high statistical uncertainty of the observational extremes. Besides, [Figure 3.1](#) shows there can be a considerable difference between the two observational datasets in some catchments (e.g. St Mihiel), indicating that the quality of the observational datasets is not consistent either. Overall, the observations follow a similar pattern as the RACMO dataset, with a few points that exhibit distinct behaviour. Note that most of the offsets are mitigated when considering a 6-hourly time step.

In general, observational precipitation extremes fall almost entirely within the confidence intervals set by the climatic variability of RACMO for daily and even sub-daily time steps. In other words, the climatic description of extremes is considered to be comparable between observations and the RACMO dataset. This demonstrates that the RACMO dataset provides a reliable estimation of precipitation extremes, which is crucial for the hydrological follow-up of this study. Furthermore, the large climatic spread of the RACMO dataset for high extreme return values has shown that estimation of extremes around or above the length of the dataset is rather unreliable. This once again stresses the importance of a longer dataset.

3.3. The GEV shape parameter

Previous results have shown that the length of the dataset is important for the estimation of high extremes. Besides the improved statistical uncertainty, long timeseries also enable improved evaluation of the shape of the extreme value plots, due to the increased availability of data points within the 100 to 1000 year range. The shape of extreme value plots is generally described by a GEV distribution, which is defined by a location, scale and shape parameter, as previously described in [section 2.3.3](#). The location and to a lesser extent the scale parameter can be estimated adequately based on a relatively short timeseries. The shape parameter, which mainly controls the shape of the distribution's tail, requires a longer dataset for an adequate estimate, because longer datasets have more datapoints and therefore provide more information on the tail of the distribution. Gordon et al. (2015) has illustrated the influence of all GEV parameters on an extreme value plot as depicted in [Figure 3.14](#).

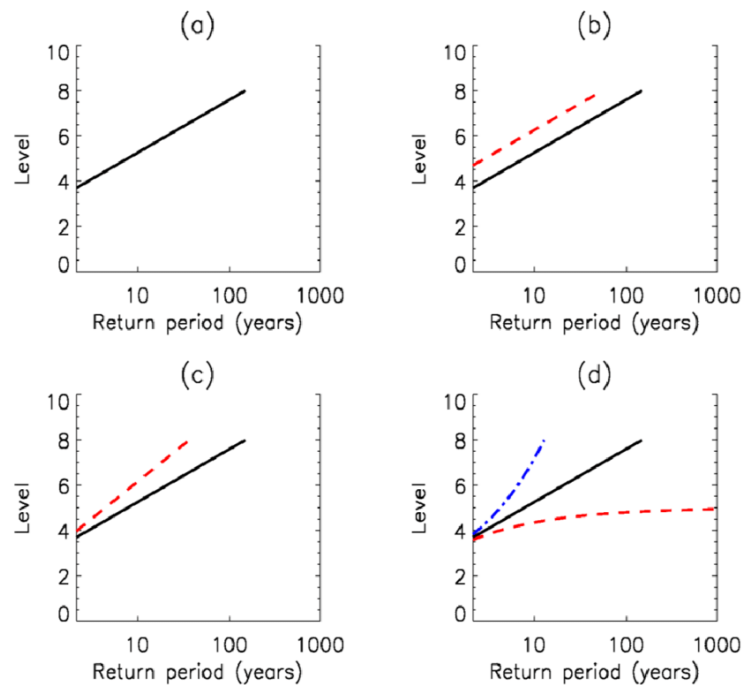


Figure 3.14 Overview of the influence of the GEV-parameters on the extreme value plots (Gordon et al., 2015), with b) the influence of the location parameter, c) the influence of the scale parameter and d) the influence of the shape parameter

This Figure suggests that the value of lower extremes is predominantly influenced by perturbations of the location parameter. However, middle and high extremes are especially reliant on changes in the scale and to larger extent the shape parameter. Generally speaking, an adequate estimate of high extremes is primarily dependent on the shape parameter of a GEV distribution, which is best estimated by larger datasets. In other words, an accurate description of the curvature in the extreme value plots, which is more accurately described by the long RACMO data compared to the shorter observations, is of higher importance for the representation of large extremes than a decent comparison between observations and the RACMO dataset in the lower return period domain. A more detailed analysis of the curvature of the RACMO extremes and the shape parameter of the corresponding GEV distributions is provided in this section.

3.3.1. Daily GEV distributions

Figure 3.15 shows the GEV distributions fitted to the annual extremes (daily timestep) of each separate RACMO member using maximum likelihood estimation in red, the combined RACMO timeseries in green and E-OBS in black. The individual datapoints, that were the foundation of the GEV fits, are also plotted in corresponding colour. The GEV distributions of the other catchments is provided in Appendix 6.7. There is an enormous spread between the GEV fits of the different ensemble members in all catchments and even the sign of the shape parameter (indicating upwards or downwards curvature) deviates between the different ensemble members. This indicates that the climatological spread of the ensemble members also leads to a significant deviation in the statistical representation of extremes. Any GEV based on a limited amount of data, such as the observational dataset, is therefore unreliable for estimation of high return values and has the risk of under- or overestimating extreme events.

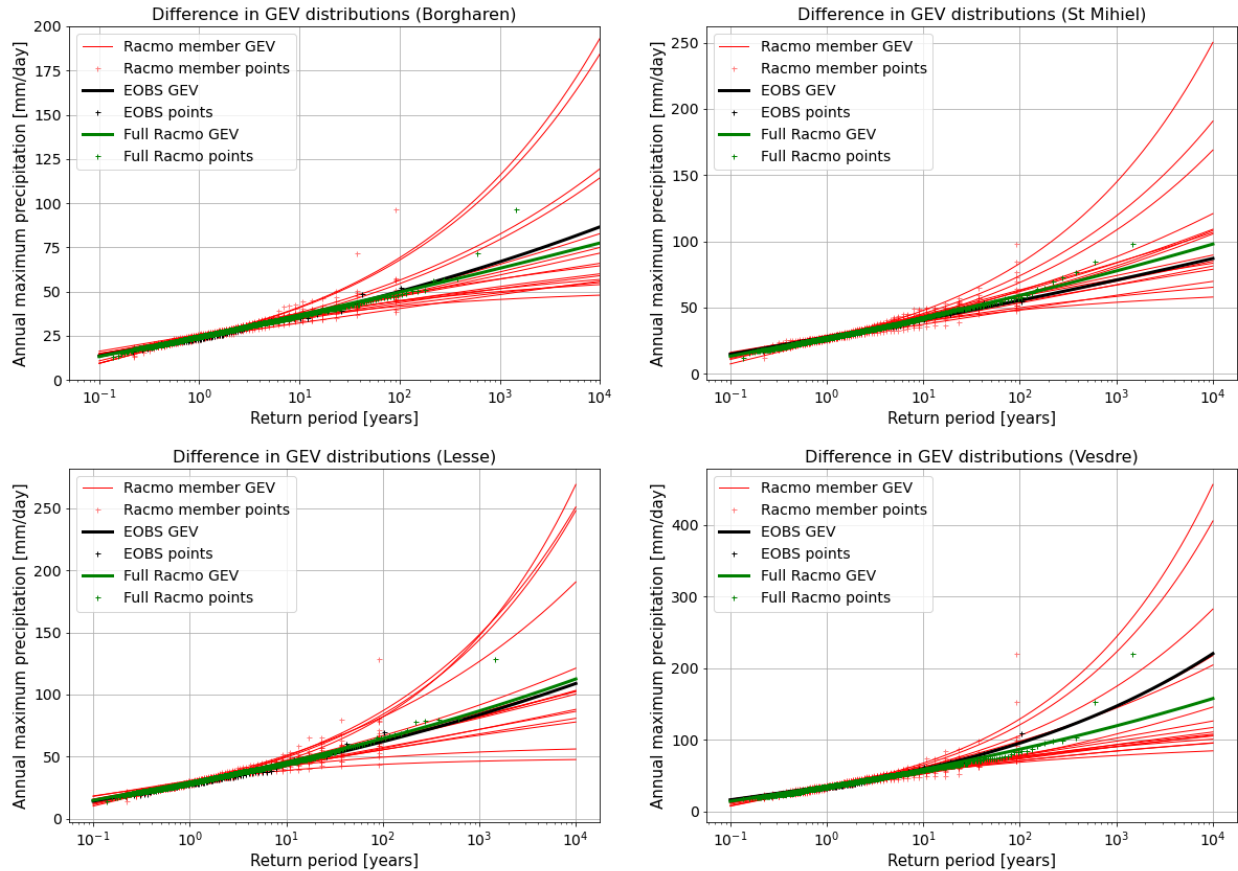


Figure 3.15 GEV distributions fitted to the daily annual extremes all separate RACMO member, the combined RACMO dataset and the E-OBS dataset.

The curvature of the separate RACMO members is strongly influenced by outliers due to the limited number of datapoints. Short observational datasets may experience similar effects. The larger RACMO dataset is only lightly impacted by the outlying datapoints and therefore generally gives a better representation of the trend of the extremes. In several catchments (e.g. catchments Sambre or Jeker in Appendix 6.7.1), there is a substantial difference between the GEV of E-OBS and the GEV of RACMO, even in the direction of the curve. As the RACMO timeseries likely provides a better estimate of the shape parameter, it is likely to assume that the statistical description of extremes based on observations in these catchments is not adequate. Particularly in catchments where the GEV gives substantially lower extremes for observations than for RACMO, the risk of underestimating extremes using a statistical approach is high.

The curvature of the long RACMO GEV distributions differs between the various catchments of the Meuse basin. The shape parameter ranges from positive (downwards curvature) to negative (upwards curvature). In most cases, the curvature of the daily extremes is not extremely pronounced. The Borgharen and Chooz catchments for example seem to be well captured by a Gumbel distribution, which has a straight line and a shape parameter of 0. In general, the curvature of the GEV distributions seems to be catchment specific. The influence of catchment characteristics on the shape parameter, such as the size and location of the catchments, is analysed together with the temporal influence on the shape parameter in section 3.3.3.

Appendix 6.7.2 shows the GEV distributions fitted to the annual extremes of separate RACMO members, the combined RACMO timeseries and observations for a 5-day precipitation sum. The differences between observations and the synthetic RACMO are also evident for these multi-day sums. In many catchments, even the sign of the shape parameter differs between the two GEV representations. Note that the long RACMO timeseries almost all have a shape parameter of zero or larger (downwards curvature).

3.3.2. Hourly GEV distributions

The variation in GEV representation between short and long timeseries can also be analysed for an hourly time step. Figure 3.16 presents the GEV distribution fitted to the hourly annual for the separate RACMO ensemble members, the long RACMO timeseries and the GenRe observational dataset. Note that the hourly GenRe dataset is considerably shorter in length than the daily E-OBS dataset. The effects of the dataset length are apparent when addressing the differences between the GEV's of observations and the long RACMO timeseries. In many catchments, the observational shape parameter is positive, whereas all RACMO members, including the long timeseries, curve upwards. Beersma et al. (2019) showed that a GEV distribution of hourly maxima generally curves upwards, corresponds well with the RACMO simulations. The observational GEV's on the other hand, often do not reproduce an upwards curvature, implying that any high return value estimates based on statistical extrapolation of the short observational timeseries is likely an underestimation of reality. As such, estimation of large hourly extremes is a lot more reliable when the RACMO dataset is considered.

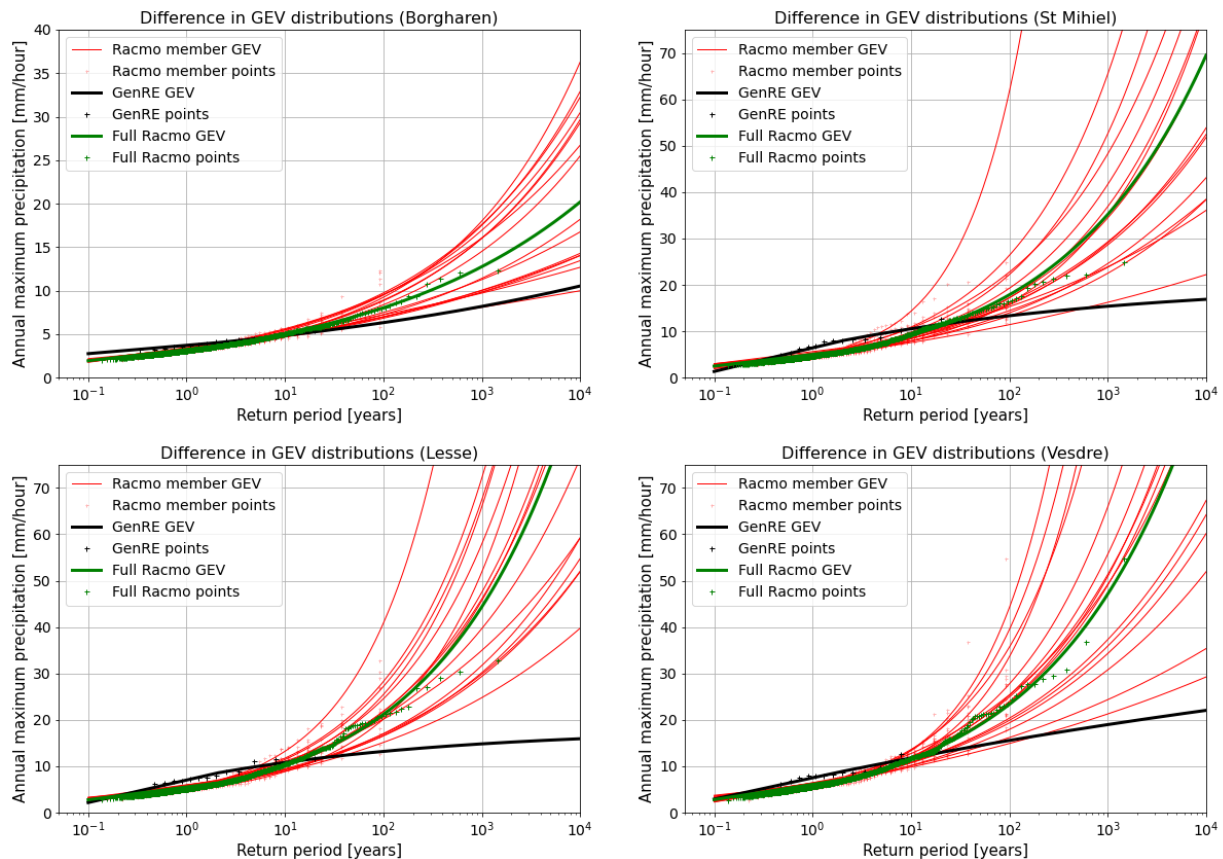


Figure 3.16 GEV distributions fitted to the hourly annual extremes of all separate RACMO member, the combined RACMO dataset and the E-OBS dataset.

Although all RACMO member GEV's show upwards curvature, there is still a large variety between them. This indicates that any hourly datasets of approximately 65 years can also exhibit a significant difference in their statistical representation.

3.3.3. Temporal and spatial spread of the shape parameter

As discussed before, the curvature of return value plots is an essential determinant for the estimation of high extremes. This section will discuss the potential influence of temporal and spatial effects on the curvature (defined by the shape parameter), based on the long synthetic timeseries with a more stable curvature.

Figure 3.17 presents the shape parameter of the GEV fit for different time windows per catchment, considering both RACMO and observations (E-OBS for a daily time step, GenRE for an hourly time step). The shape parameter of the observations exhibits a large spatial variation over the catchments for all time windows, whereas the RACMO dataset shows a relatively constant distribution of the shape parameter per time step. In other words, the shape parameter of observations appears to have a random spatial distribution for all time steps, contrary to the RACMO timeseries which shows a relatively comparable spatial distribution of the shape parameter, which increases for larger time windows. In general, it is clear that the increase of dataset length leads to a decrease in randomness of the shape parameter, enabling further investigation of potential patterns of this curvature. Note that the value of the shape parameter of the daily RACMO dataset ranges around a value of -0.1 . This is a value that is often found in literature (e.g. Papalexiou and Koutsoyiannis, 2013). Besides, a value of -0.1 has been linked with the physical process of the extreme precipitation in Wilson & Toumi (2005), suggesting a physical meaning of the shape parameter. Refer to section 4.2 for a more detailed discussion about the shape parameter.

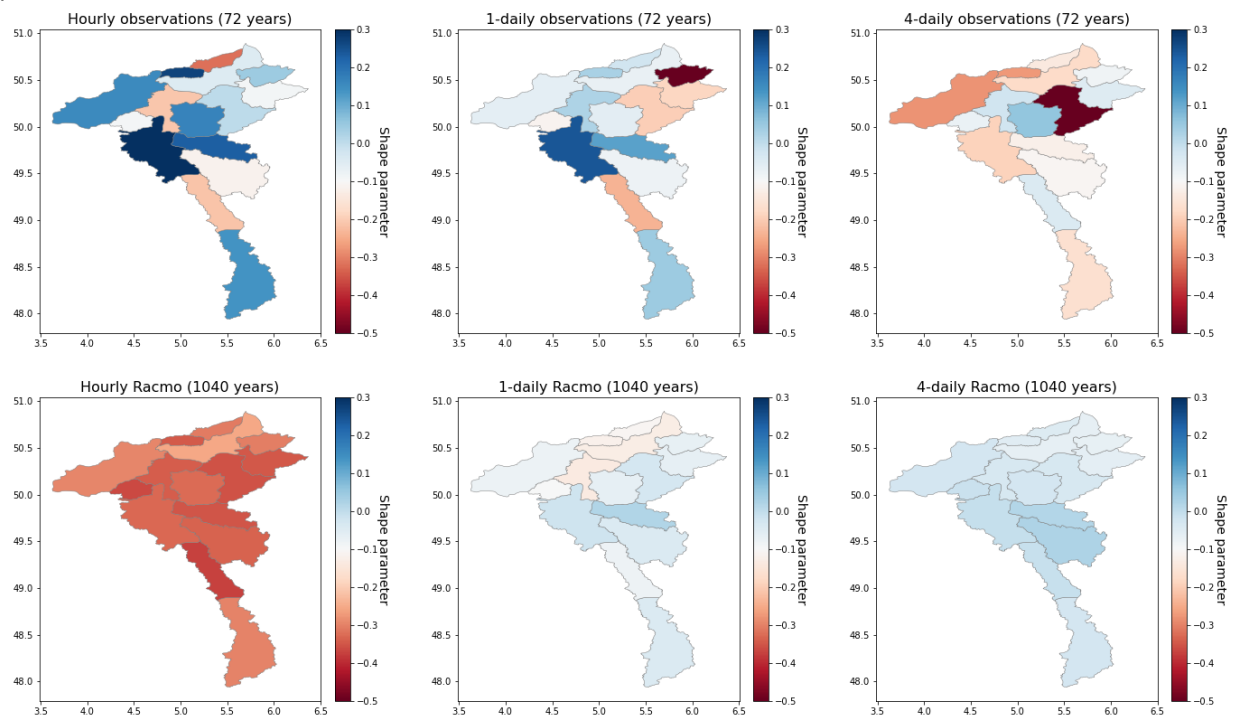


Figure 3.17 Spatial distribution of the shape parameter of the GEV distribution for the catchments in the Meuse basin based on E-OBS and RACMO.

Figure 3.17 provides evidence that the influence of catchment size (averaging precipitation over different sizes) on the shape parameter and the curvature of extremes is considerably smaller compared to the influence of the considered time window for catchments in the Meuse basin. This finding is supported by Figure 3.18, in which the influence of catchment size on the shape parameter of the RACMO GEV distributions is presented for four different time windows. Each point represents the shape parameter of a single catchment. The trendlines are plotted, including their corresponding R^2 value. The plots show a marginal increase in the shape parameter with catchment size. However, the low R^2 value of all trendlines suggests that the variation of the shape parameter between the catchments is only slightly represented by the catchment size. In general, for the relative size differences of catchments in the Meuse basin, averaging precipitation over different catchment sizes has a limited effect on the curvature of the GEV distribution. The earlier mentioned effect of the considered time window on the curvature of the GEV distribution is well captured by Figure 3.18.

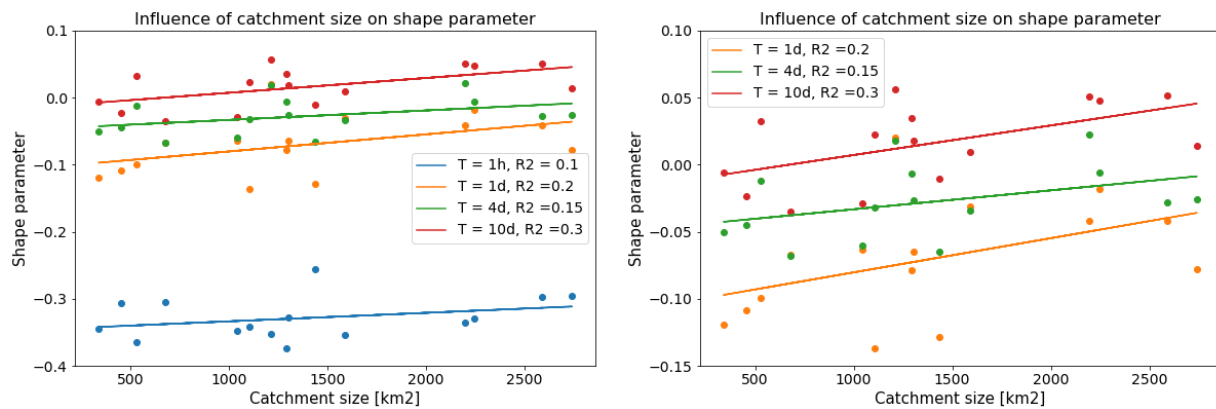


Figure 3.18 The influence of catchment size on the shape parameter for 4 different parameters, based on the RACMO dataset

In conclusion, the GEV shape parameter appears stable in RACMO, with values that are confirmed by literature. The shape parameter from observational records is less stable, which is caused by the short record length. Note that the scale and location parameter is expected to be better estimated using observations, as this is less dependent on record length and the RACMO parameters may be affected by model bias. However, in this study, the stability of the shape parameter is more relevant than potential model bias in the RACMO dataset, because the shape parameter is the determining parameter for high return value estimates. Therefore, for large return periods, the RACMO data will provide a considerably better estimate of return values than the observations, as the decrease in statistical uncertainty of the shape parameter outweighs an increase of model uncertainty regarding the scale and location parameter. Refer to section 4.2 for a more detailed discussion about model uncertainty and statistical uncertainty.

3.4. Seasonal effects

The meteorological and hydrological events of July 2021 were exceptional for the summer period. Precipitation accumulated to amounts that were never observed before in that season. It is important to consider whether this summer event was an incidental extreme or not. To provide more insight into summer extremes, their likelihood of occurrence and their extremity compared to winter events, the

influence of seasonality on extremes is analysed in this section. Note that the summer is defined as the half year with months April, May, June, July, August and September. The winter is defined as the half year covering the remaining months.

Figure 3.19 - Figure 3.21 give annual extremes for the summer and winter half year, for respectively a daily, 10-daily and hourly time window. Both the RACMO dataset and observations are depicted in the plots. The 10-day precipitation sum is not representative for the hydrological response in the Meuse basin, but has been chosen to distinguish several entirely different time windows. An overview of all catchments is provided in Appendix 6.8.

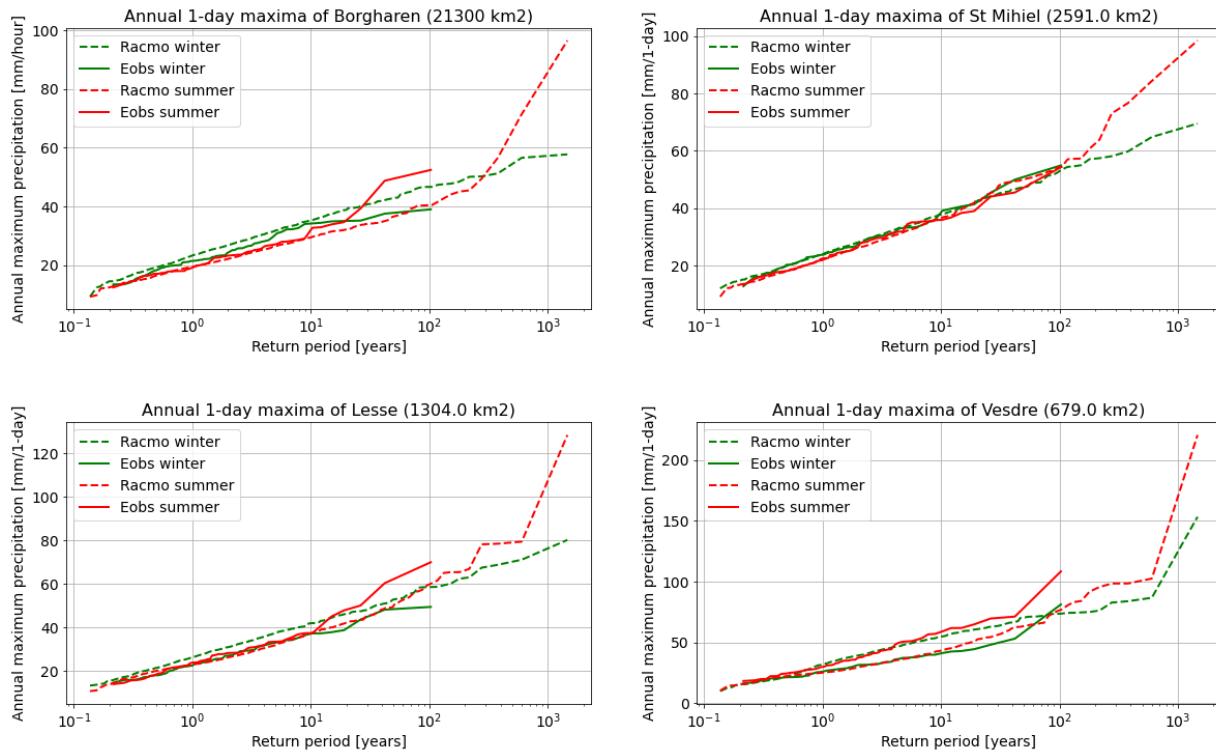


Figure 3.19 1-day summer and winter annual extremes in different catchments of the Meuse basin

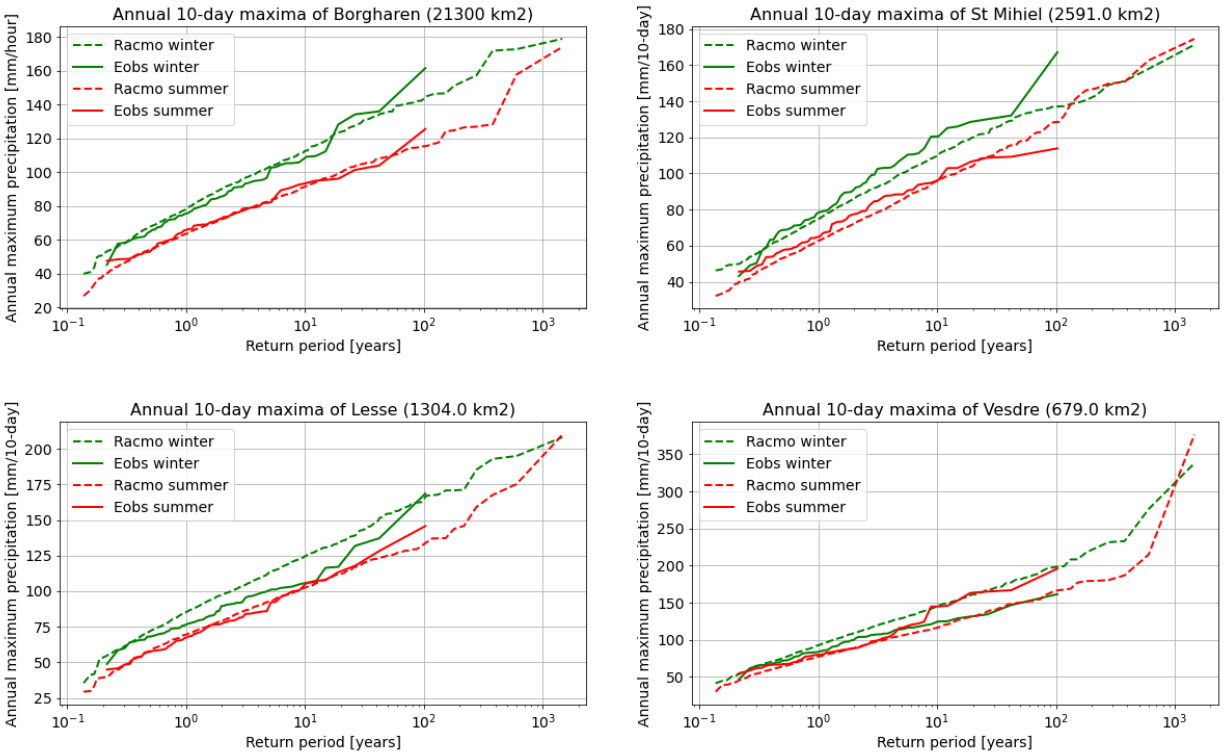


Figure 3.20 10-day summer and winter annual extremes in different catchments of the Meuse basin

In most catchments, winter maxima with a daily time step are higher for the low and middle extremes compared to summer maxima. However, the summer maxima have a clear inflection point and generally have a rapid increase in extremity for high return values. As depicted, summer extremes will often surpass winter extremes for higher return values. While low daily extremes are often slightly smaller in summer than in winter, high extremes seem to be particularly dominated by summer events. Like experienced in July 2021, summer events can be as extreme, or even extremer than winter events according to the RACMO simulations. As such, increased awareness of the potential magnitude of precipitation extremes in summer and the corresponding flood risk is essential. Evidently, extremes exhibit different behaviour in summer and winter due to the different nature of precipitation in both seasons. Therefore, daily precipitation data must be described with a double population (instead of a

combined GEV for calendar year maxima). More implications on the existence of a double population are given in section 4.2.

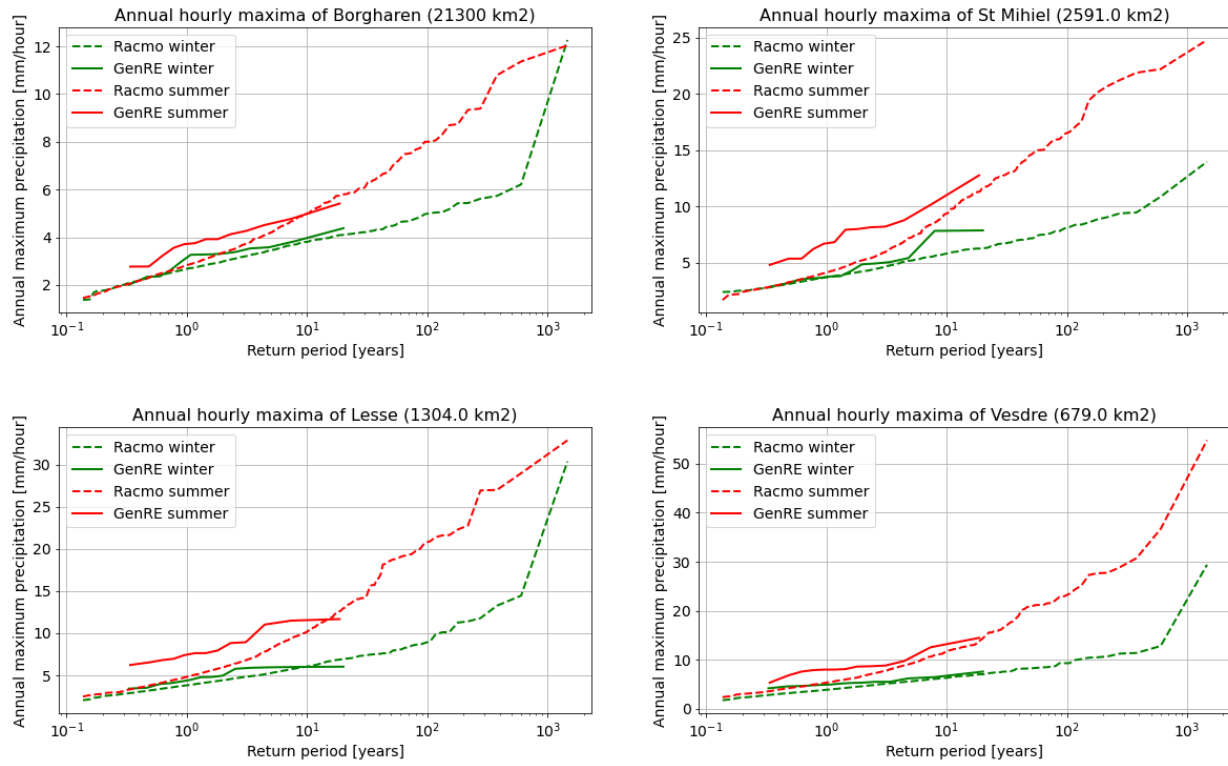


Figure 3.21 1-hour summer and winter annual extremes in different catchments of the Meuse basin

Figure 3.20 shows that 10-day precipitation extremes are consistently larger in winter than in summer, which corresponds well with the long-lasting frontal precipitation that typically occurs. Vice versa, the hourly precipitation (Figure 3.21) is consistently higher in summer compared to winter across almost all catchments. This is caused by the short intense precipitation events that typically occur in summer. In both cases, the annual extremes can therefore be captured statistically by using 1 population. However, summer events may require a double population, related to the dewpoint temperature (see section 4.2). The results show that summer or winter dominance depends on the time window and there are time windows for which summer extremes become gradually more extreme than winter extremes for larger return periods. The occurrence of high discharge extremes in summer (potentially even larger than the winter extremes) is therefore dependent on the rainfall-runoff response time of catchments, where fast-responding catchments are more likely to experience high summer extremes. Note that the discharge yield in catchments is not linear to precipitation and is dependent on catchment characteristics.

Although this study mainly focusses on precipitation extremes, the final aim of this research is to provide reliable estimates of discharge extremes as well. It is important to note that the hydrological response to precipitation is not linear and that hydrological results and conclusions may therefore differ from the meteorological results. It is therefore strongly recommended to also regard the hydrological report of Couason et al. (2023). One example of the non-linearity of the hydrological response is the spatial distribution of the precipitation event. The two largest (summer) precipitation events for

Borgharen are presented in Figure X. Note that the nature of these events differs, which could also lead to an entirely different hydrological response. Furthermore, although these summer precipitation extremes have a larger basin-average result than in July 2021, the discharge yield is not larger than that of July 2021 (Couasnon et al., 2023). As such, the hydrological analysis of the meteorological results presented in this study is essential.

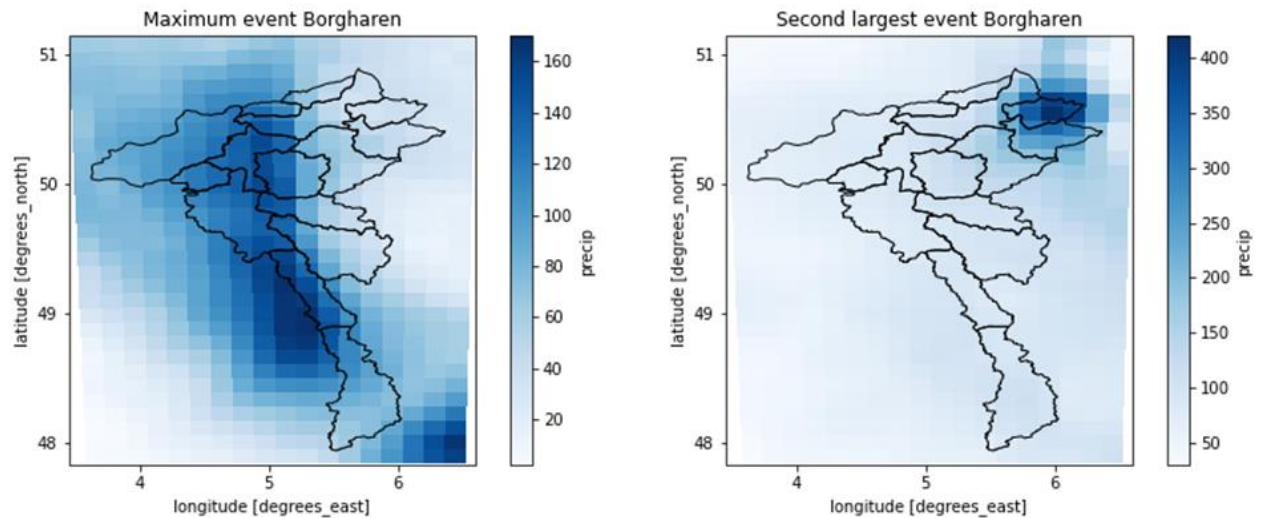


Figure 3.22 Overview of the two maximum events in Borgharen (both summer events). There is a clear spatial spread between the two figures, which may lead to an entirely different hydrological response.

4. Conclusions, Discussion & Recommendations

4.1. Conclusions

This study describes and explores the approach of using synthetic data from the RACMO climate model in order to improve extreme return value estimates of precipitation and discharge. The results of this study show:

- The climatology of RACMO precipitation extremes in the Meuse area **compare very well** with observations³.
- The extensive length of RACMO reveals a range of extreme values that was previously unanalysed, providing a more plausible way to estimate the tails of annual precipitation extremes. These results are therefore a promising step in the direction of improved large return value estimates.
- The **statistical uncertainty** in the estimation of extreme precipitation is strongly reduced by the use of RACMO data: the use of 16 members results in a statistical uncertainty that is (roughly) 4 times smaller than the use of observations only⁴ for daily data. For hourly data, for which only 12 years of (gridded) data are available, the effect is a reduction with a factor of almost 10.
- The estimations of the GEV shape parameter from observed precipitation maxima are spatially inconsistent. Long timeseries provide a more reliable estimate of the shape parameter.
- Averaging in time substantially increases the GEV shape parameter⁵. Spatial averaging may slightly increase the GEV shape parameter, but this effect is less pronounced.
- The clear distinction between the GEV distributions of summer and winter events in RACMO may indicate the existence of a double population (see section 4.2) and a transition between the dominance in magnitudes from winter to summer maxima. How and whether this effect is also translated into discharge extremes is described in the hydrological report of Couasnon et al. (2023).

4.2. Discussion

Additional explanations and insights can be provided for several results and conclusions presented in this report:

- RACMO is – as all climate models are - prone to systematic **model biases**. This leads to too high precipitation amounts in winter, and too low amounts in summer. As described earlier, the distribution of precipitation throughout the year can have a large effect on the amount of water in the soil, which is an essential parameter in discharge modelling. To ensure that these biases do not affect the discharge results, the applied Quantile Mapping bias correction leads to removal of the bias in the annual cycle. This holds both for precipitation, temperature and (potential) evaporation. No bias correction is applied for the most extreme quantiles ($P > 0.99$).
- It is well known that RCM's like RACMO underestimate the extreme hourly precipitation amounts when compared with station data. The reasonable agreement of RACMO and observations found in this study may be caused by the fact that, in this analysis, the comparison

³ The quantiles up to 0.99 are bias corrected in order to get a correct annual cycle.

⁴ Assuming that the statistical uncertainty reduces with the square root of the increase of the size of the dataset.

⁵ The shape parameter becomes less negative, i.e. tends to a lighter tail.

is done over spatial averages. This may lead to largely reduced precipitation amounts of the observations compared to the point data of rain gauges (see Lombardo et al., 2006).

- The RACMO data adds value to the observational data only if the **reduction in statistical uncertainty is large relative to the introduced RACMO model uncertainty**. As already indicated, the model uncertainty is removed in the annual cycle, and absent in extreme (daily) events. The question that remains is: **“Can we trust the GEV shape parameter of the (hourly and daily) extreme precipitation as derived from the RACMO data?”**[§] We think that this is indeed the case, and we have the following arguments:
 - The value of the GEV shape parameter as derived from the daily precipitation RACMO data is close to the value of -0.1 , as given by Papalexiou and Koutsoyiannis (2013) and others.
 - Even if the location and/or scale parameter of the RACMO-based GEV distribution is biased, it is well possible that the shape parameter is unbiased. We have several reasons for this:
 - The shape parameter is a dimensionless parameter, which already indicates that it has a more generic meaning than e.g. the location parameter (which is very sensitive to orographic effects, to the way that precipitation is parameterized in models, etc.). The fact that the shape parameter is often assumed to be constant over a region - and can then be estimated by combining all station records in that region (as done by e.g. Beersma et al. (2018)) - sustains this assumption.
 - Wilson and Toumi (2005) give a fundamental distribution of heavy rainfall, which they connect with the physical process of the extreme precipitation. This again leads to the value of -0.1 of the shape parameter (see Van den Brink & Konnen 2011).
The physical process that Wilson and Toumi (2005) describe are well described by RCM's like RACMO, which makes the estimated shape parameter trustworthy. This is confirmed by the agreement in the value of -0.1 between observations and model(s).
 - A more comprehensive consideration of the added values of climate models is given in the Appendix A of De Valk & Van den Brink (2023).
- Results of this study show that extreme precipitation events from summer and winter may originate from **different populations**, with distinct parameters of the corresponding (GEV) distributions. Whether this finding has consequences for the estimation of very extreme return values depends on different aspects:
 - For hourly precipitation extremes in the Meuse area, the summer maxima are always higher than the winter maxima (see Figure 3.21 both for the RACMO data and observations). This implies that all the annual maxima are summer events. This is caused by convection, which is much more pronounced in summer than in winter.
 - For 10-day extremes, it is vice-versa: all annual maxima originate from winter, and the corresponding extreme value distribution is single populated.

[§] The question is not primarily whether the GEV distribution is the correct distribution, but whether the curvature of the distribution is realistic and not a model artefact.

- However, for 1-day (and also for 6-hourly) maxima, some of the event occur in summer, and some in winter, with an increased probability for summer events for larger return periods. Stated otherwise, this implies that, on an extreme value plot, there is a smooth transition from the less extreme events originating from winter to the most extreme events originating from summer. The return period for which both extremes are of the same order is hard to determine, as it depends on many factors, like the exact duration, the size of the area over which is averaged, etc.

It is precisely this range from 1-hourly to 24-hourly extremes that are crucial in the formation of extreme discharges for the (sub)catchments of the Meuse. The consequence is that fitting an extreme value distribution on a single population may fail for extrapolation purposes. Depending on the return period where the summer events exceed the winter events, it may result in either under- or overestimation.

Special attention should be paid to situations when this so-called 'transition point' occurs at a return period that exceeds the length of the (observational) dataset, but is lower than the return period that is used for design criteria: due to its rarity it is unlikely that events from the second (but severe) population are found in the observational record, but they dominate the return values of the design criteria. The RACMO data shows clear indication that this situation may occur (even more pronounced in the discharge results than in the meteorological results, see Couasnon et al. (2023)). It is very well possible that the July 2021 event is an illustration of this hazardous situation, which emphasises the need for further research on the possible existence of double populations in the annual maxima.

- The concept of double populations in precipitation extremes is well known. E.g., Lenderink et al. (2017), and Beersma et al. (2018) showed the existence of a second population of extremes within the summer season, strongly related to the dewpoint temperature: Dewpoint temperatures above 17.5°C can be part of a second population. It is likely that the distinction between summer and winter extremes as found in this study is related to the distribution of summer events into 2 dewpoint temperature related populations. Therefore, it is recommended to explore how this dewpoint temperature influences precipitation extremes in RACMO. Although the **intensity** of the second population may be affected by model bias, its **existence** is clearly indicated by the results of this study and by Lenderink et al. (2017) and Beersma et al. (2018).
- As an illustration, an analysis of the event that caused the largest precipitation amounts for the Vesdre catchments (see QR-code below) shows that, from a synoptical perspective, the event is realistic, and even shows features that reminds to the July 2021 event, e.g. the slow-movement of the system, leading to huge amounts of precipitation in a relatively small area. This indicates that – although being very extreme – the largest simulated RACMO events have a realistic character and have to be taken seriously.



4.3. Recommendations

The aforementioned conclusions and discussion points have led to the following suggestions for future research and implementation.

- We recommend to **repeat the analysis** of this report with 2 datasets:
 - The RACMO dataset as generated for the KNMI 2014 climate scenario's. This dataset also consists of 16 members for the 1950-2014 period; however the driving GCM differs from the one used in the KNMI 2023 case (EC-Earth2.3, that differs in resolution, land-use and parameterizations). If – despite these differences – the estimation of the GEV shape parameter agrees with the values as presented now, it is a strong indication of the robustness of the derived shape parameter
 - The SEAS5 dataset (see Van Voorst & Van den Brink, 2021), which consists of 8,500 years of data. This dataset is fully independent of the RACMO data, and also considerably larger. Again, reproduction of the shape parameter will strongly confirm the reliability of the model data. Also, the length of the dataset allows for a more thorough investigation of the behaviour of summer and winter events (although the resolution of SEAS5 is lower than that of RACMO).
- If the analysis of the suggested datasets confirms the findings of the current study, it is recommended to use the RACMO data (combined with wflow discharge calculations) for design criteria. A hybrid solution is to use the RACMO shape parameter and derive the location- and scale (GEV) parameter from the observational data in order to find an optimal balance between statistical- and model uncertainty.
- An in-depth analysis of the meteorological situations that lead to the most extreme precipitation events (or, even better: the most extreme discharge events) may shed new light on the dynamical aspects that leads to these extreme situations; this may also help to understand the July 2021 situation, or the existence of a potential double population.
- A logical and interesting follow-up of the current research is to examine the effect of climate change on the (extreme) precipitation amounts and corresponding discharges. The RACMO dataset also contains 16 ensemble members for resp. the ssp126, ssp245 and ssp585 Shared Socioeconomic Pathways (SSPs), up till 2120 (ssp126 and ssp245) or 2165 (ssp585). This gives the opportunity to determine the effects of those SSP's on the climate in the Meuse area. Also here, the role of the dew point temperature can be investigated.
- As the domain of RACMO is much larger than the Meuse area, other basins like the Rhine and the Vecht can also be used as study area to repeat this study. Besides, the extensive RACMO domain allows for the analysis of the coincidences of high discharges on the Meuse and the Rhine, or coincidences of high discharges and large storm surges.

5. References

- Beersma, J., Versteeg, R., Hakvoort, H. (2018). *Neerslagstatistieken voor korte duren* (No. 2018-12). STOWA. Retrieved from <https://www.stowa.nl/sites/default/files/assets/PUBLICATIES/Publicaties%202018/STOWA%202018-12%20HR.pdf>
- Beersma, J., Hakvoort, H., Jildera, R., Overeem, A., Versteeg, R. (2019). *Neerslagstatistiek en -reeksen voor het waterbeheer 2019* (No. 2019-19). STOWA. Retrieved from <https://www.stowa.nl/sites/default/files/assets/PUBLICATIES/Publicaties%202019/STOWA%202019-19%20neerslagstatistieken.pdf>
- Bernard, A., & Bos-Levenbach, E.J. (1955). The plotting of observations on probability-paper.
- Bouaziz L.J.E. & Buitink J. (2022). Developments of the wflow Meuse and Rhine hydrological models in 2022. Deltareport (11208037-002-ZWS-0005).
- Bouaziz, L. J., Steele-Dunne, S. C., Schellekens, J., Weerts, A. H., Stam, J., Sprokkereef, E., ... & Hrachowitz, M. (2020). Improved understanding of the link between catchment-scale vegetation accessible storage and satellite-derived Soil Water Index. *Water Resources Research*, 56(3), e2019WR026365.
- Buishand, A., & Wijngaard, J. (2007). *Statistiek van extreme neerslag voor korte neerslagduren* (No. 295). KNMI. Retrieved from <https://cdn.knmi.nl/knmi/pdf/bibliotheek/knmipubTR/TR295.pdf>
- Cannon, A. J., Sobie, S. R., & Murdock, T. Q. (2015). Bias correction of GCM precipitation by quantile mapping: how well do methods preserve changes in quantiles and extremes?. *Journal of Climate*, 28(17), 6938-6959.
- Couason, A., Riveros, A., Bouaziz, L. (2023). *Evaluation of discharge extremes in the Meuse river and her tributaries*. To be published.
- Cornes, R. C., van der Schrier, G., van den Besselaar, E. J., & Jones, P. D. (2018). An ensemble version of the E-OBS temperature and precipitation data sets. *Journal of Geophysical Research: Atmospheres*, 123(17), 9391-9409.
- De Niel, J., Demarée, G., & Willems, P. (2017). Weather typing-based flood frequency analysis verified for exceptional historical events of past 500 years along the Meuse river. *Water Resources Research*, 53(10), 8459-8474.
- De Valk C., van den Brink, H. (2023). *Update van de statistiek van extreme zeewaterstand en wind op basis van meetgegevens en modelsimulaties* (No. 406). KNMI. Retrieved from <https://cdn.knmi.nl/knmi/pdf/bibliotheek/knmipubTR/TR406.pdf>
- Döscher, R., Acosta, M., Alessandri, A., Anthoni, P., Arsouze, T., Bergman, T., Bernardello, R., Boussetta, S., Caron, L.-P., Carver, G., Castrillo, M., Catalano, F., Cvijanovic, I., Davini, P., Dekker, E., Doblas-Reyes, F. J., Docquier, D., Echevarria, P., Fladrich, U., Fuentes-Franco, R., Gröger, M., v. Hardenberg, J., Hieronymus, J., Karami, M. P., Keskinen, J.-P., Koenigk, T., Makkonen, R., Massonnet, F., Ménégoz, M., Miller, P. A., Moreno-Chamarro, E., Nieradzik, L., van Noije, T., Nolan, P., O'Donnell, D., Ollinaho, P., van

den Oord, G., Ortega, P., Prims, O. T., Ramos, A., Reerink, T., Rousset, C., Ruprich-Robert, Y., Le Sager, P., Schmith, T., Schrödner, R., Serva, F., Sicardi, V., Sloth Madsen, M., Smith, B., Tian, T., Tourigny, E., Uotila, P., Vancoppenolle, M., Wang, S., Wårlind, D., Willén, U., Wyser, K., Yang, S., Yepes-Arbós, X., and Zhang, Q. (2022). The EC-Earth3 Earth system model for the Coupled Model Intercomparison Project 6. *Geosci. Model Dev.*, 15, 2973–3020. <https://doi.org/10.5194/gmd-15-2973-2022>

Gordon, C., Cheong, W. K., Marzin, C., & Rahmat, R. (2015). Singapore's Second National Climate Change Study-Climate Projections to 2100-Report to Stakeholders. *Centre for Climate Research Singapore, Singapore*.

Gumbel, E. J. (1942). Simple tests for given hypotheses. *Biometrika*, 32(3/4), 317-333.

Hegnauer, M., Beersma, J. J., Van den Boogaard, H. F. P., Buishand, T. A., & Passchier, R. H. (2014). Generator of Rainfall and Discharge Extremes (GRADE) for the Rhine and Meuse basins. Final report of GRADE 2.0. *Deltares and KNMI*.

Jenkinson, A. F. (1955). The frequency distribution of the annual maximum (or minimum) values of meteorological elements. *Quarterly Journal of the Royal Meteorological Society*, 81(348), 158-171.

Kim, K. B., Kwon, H. H., & Han, D. (2016). Precipitation ensembles conforming to natural variations derived from a regional climate model using a new bias correction scheme. *Hydrology and Earth System Sciences*, 20(5), 2019-2034.

Kreienkamp, F., Philip, S. Y., Tradowsky, J. S., Kew, S. F., Lorenz, P., Arrighi, J., ... Wanders, N. (2021). Rapid attribution of heavy rainfall events leading to the severe flooding in Western Europe during July 2021.

Kwadijk, J., Arnell, N.W., Mudersbach, C., de Weerd, M., Kroon, A., Quante, M. (2016). Recent Change—River Flow. In: Quante, M., Colijn, F. (eds) *North Sea Region Climate Change Assessment*. Regional Climate Studies. Springer, Cham. https://doi.org/10.1007/978-3-319-39745-0_4

Lenderink, G., Barbero, R., Loriaux, J. M., & Fowler, H. J. (2017). Super-Clausius–Clapeyron scaling of extreme hourly convective precipitation and its relation to large-scale atmospheric conditions. *Journal of Climate*, 30(15), 6037-6052.

Lombardo, F., Napolitano, F., & Russo, F. (2006). On the use of radar reflectivity for estimation of the areal reduction factor. *Natural Hazards and Earth System Sciences*, 6(3), 377-386.

Lucas-Picher, P., Argüeso, D., Brisson, E., Trambly, Y., Berg, P., Lemonsu, A., Kotlarski, S., & Caillaud, C. (2021). Convection-permitting modeling with regional climate models: Latest developments and next steps. *Wiley Interdisciplinary Reviews: Climate Change*, 12(6), e731. <https://doi.org/10.1002/wcc.731>

Makkink, G. F. (1957). Testing the Penman formula by means of lysimeters. *Journal of the Institution of Water Engineers*, 11, 277-288.

Nguyen, V. D., Merz, B., Hundecha, Y., Haberlandt, U., & Vorogushyn, S. (2021). Comprehensive evaluation of an improved large-scale multi-site weather generator for Germany. *International Journal of Climatology*, 41(10), 4933-4956.

O’Gorman, P. A. (2015). Precipitation extremes under climate change. *Current climate change reports*, 1, 49-59. <https://doi.org/10.1007/s40641-015-0009-3>

Palmer, T. E., McSweeney, C. F., Booth, B. B., Priestley, M. D., Davini, P., Brunner, L., ... & Menary, M. B. (2022). Performance based sub-selection of CMIP6 models for impact assessments in Europe. *Earth System Dynamics Discussions*, 2022, 1-45.

Papalexiou, S. M., & Koutsoyiannis, D. (2013). Battle of extreme value distributions: A global survey on extreme daily rainfall. *Water Resources Research*, 49(1), 187-201.

Rio, C., Hourdin, F., Grandpeix, J.-Y., and Lafore, J.-P. (2009), Shifting the diurnal cycle of parameterized deep convection over land, *Geophys. Res. Lett.*, 36, L07809, doi:[10.1029/2008GL036779](https://doi.org/10.1029/2008GL036779).

Sunyer, M. A., Madsen, H., & Ang, P. H. (2012). A comparison of different regional climate models and statistical downscaling methods for extreme rainfall estimation under climate change. *Atmospheric Research*, 103, 119-128.

Themeßl, M.J., Gobiet, A., & Leuprecht, A. (2011). Empirical-statistical downscaling and error correction of daily precipitation from regional climate models. *International Journal of Climatology*, 31(10), 1530-1544.

Van den Brink, H. W., Konnen, G. P., & Opsteegh, J. D. (2003). The reliability of extreme surge levels, estimated from observational records of order hundred years. *Journal of Coastal Research*, 376-388.

Van den Brink, H. W., Können, G. P., & Opsteegh, J. D. (2005). Uncertainties in extreme surge level estimates from observational records. *Philosophical Transactions of the Royal Society A: Mathematical, Physical and Engineering Sciences*, 363(1831), 1377-1386.


Van den Brink, H. W., Können, G. P., Opsteegh, J. D., Van Oldenborgh, G. J., & Burgers, G. (2005). Estimating return periods of extreme events from ECMWF seasonal forecast ensembles. *International Journal of Climatology: A Journal of the Royal Meteorological Society*, 25(10), 1345-1354.

Van den Brink, H. W., & Können, G. P. (2011). Estimating 10000-year return values from short time series. *International Journal of Climatology*, 31(1), 115-126.

Van Dorland, R., Beersma, J., Bessembinder, J., Bloemendaal, N., van den Brink, H., Brotons Blanes, M., Drijfhout, S., Haarsma, R., Krikken, F., Le Bars, D., Lenderink, G., van Meijgaard, E., Reerink, T., Selten, F., Severijns, C., Siegmund, P., Sterl, A., Overbeek, B., de Vries, H., Wichers Schreur, B., van der Wiel, K. (2023). *KNMI National Climate Scenarios 2023 for the Netherlands* (No. 2023-02). KNMI. Retrieved from https://cdn.knmi.nl/system/data_center_publications/files/000/071/902/original/KNMI23_climate_scenarios_scientific_report_WR23-02.pdf

Van Meijgaard, E., Van Ulft, L. H., Van de Berg, W. J., Bosveld, F. C., Van den Hurk, B. J. J. M., Lenderink, G., & Siebesma, A. P. (2008). *The KNMI regional atmospheric climate model RACMO, version 2.1* (p. 43). De Bilt, The Netherlands: KNMI.

Van Osnabrugge, B., Weerts, A. H., & Uijlenhoet, R. (2017). genRE: A method to extend gridded precipitation climatology data sets in near real-time for hydrological forecasting purposes. *Water Resources Research*, 53(11), 9284-9303.



Van Verseveld, W. J., Weerts, A. H., Visser, M., Buitink, J., Imhoff, R. O., Boisgontier, H., ... & Russell, B. (2022). Wflow_sbm v0. 6.1, a spatially distributed hydrologic model: from global data to local applications. *Geoscientific Model Development Discussions*, 1-52.

Van Voorst, L., van den Brink, H. (2021). *Improving the GRADE weather generator by using synthetic datasets from RACMO and SEAS5* (No. 398). KNMI. Retrieved from <https://cdn.knmi.nl/knmi/pdf/bibliotheek/knmipubTR/TR398.pdf>

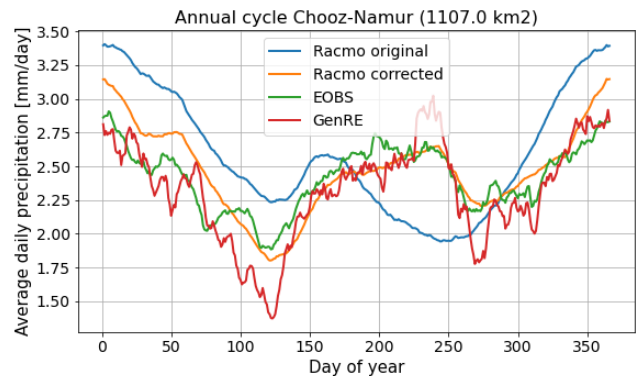
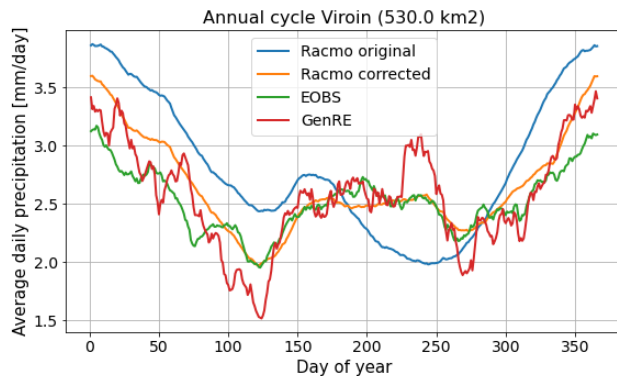
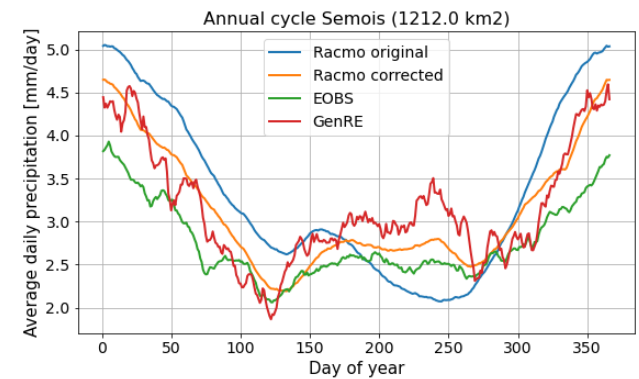
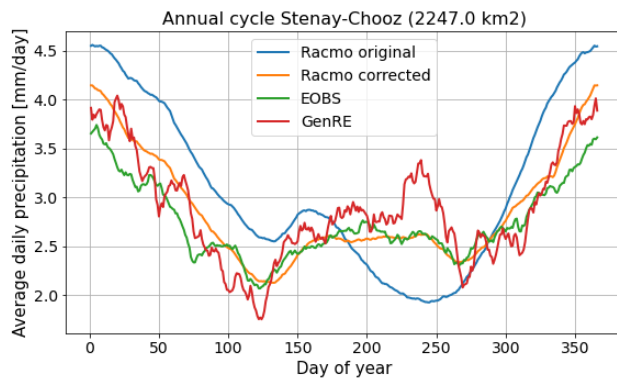
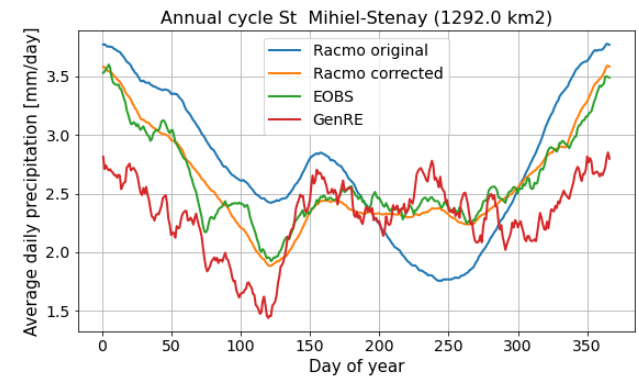
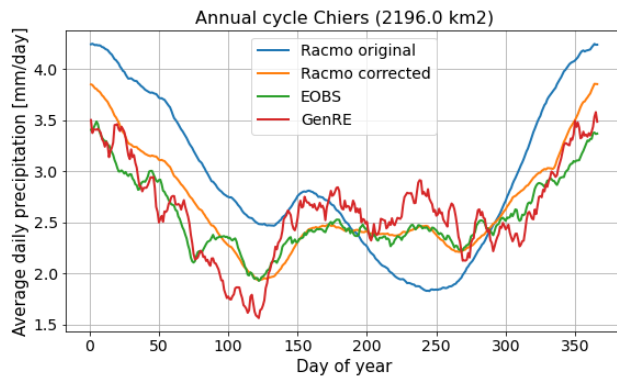
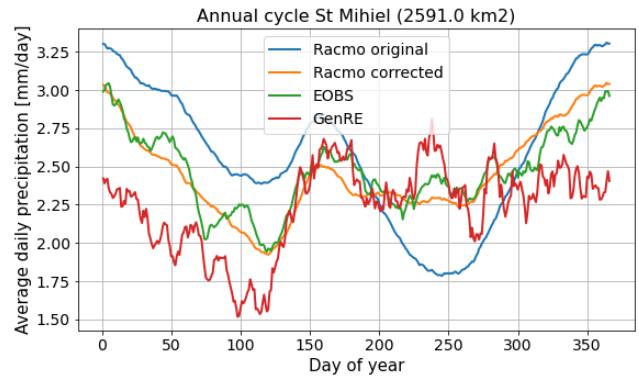
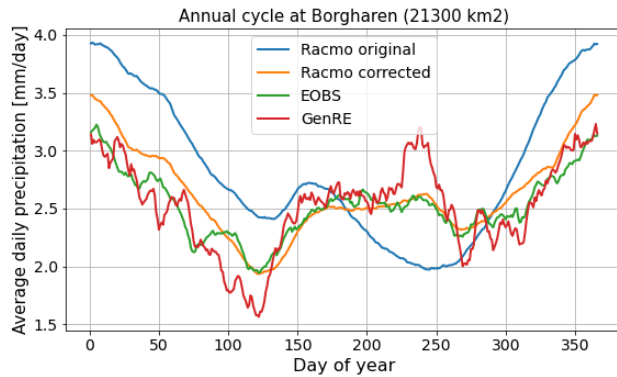
Weibull, W. (1939). A statistical theory of strength of materials. *IVB-Handl.*

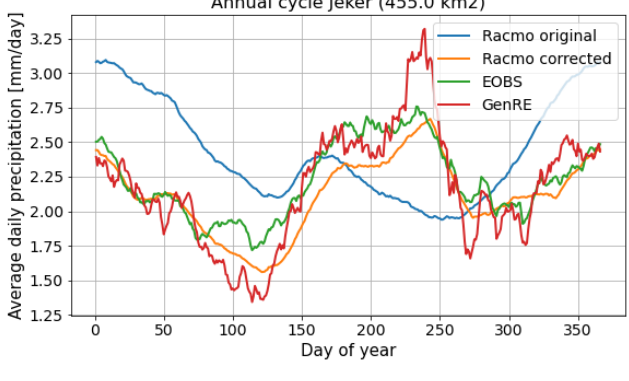
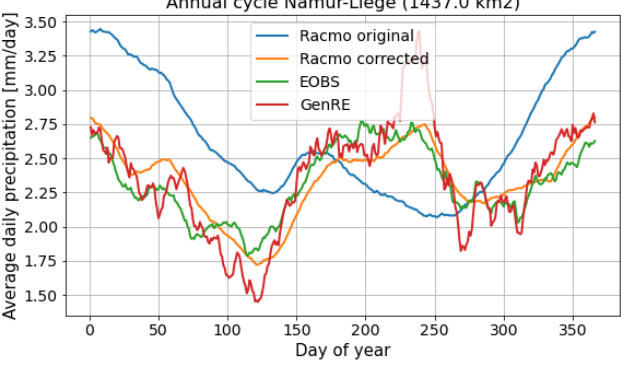
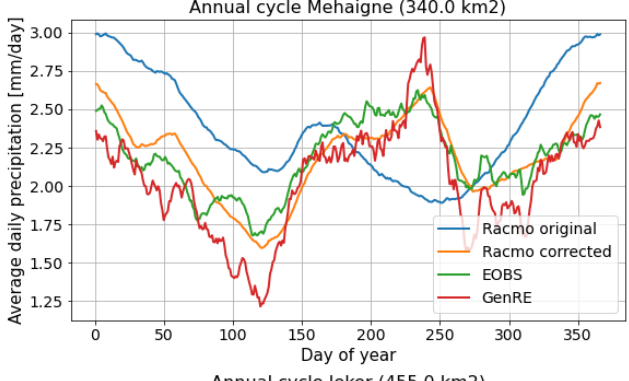
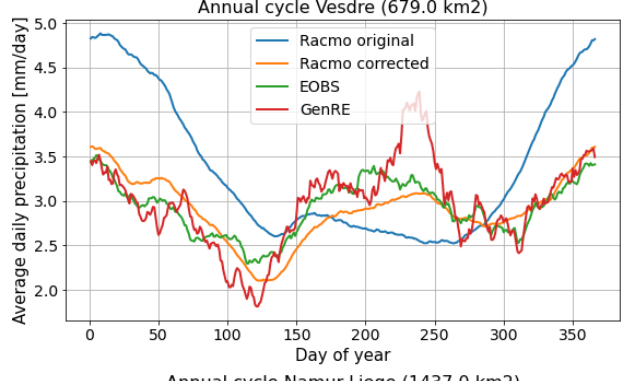
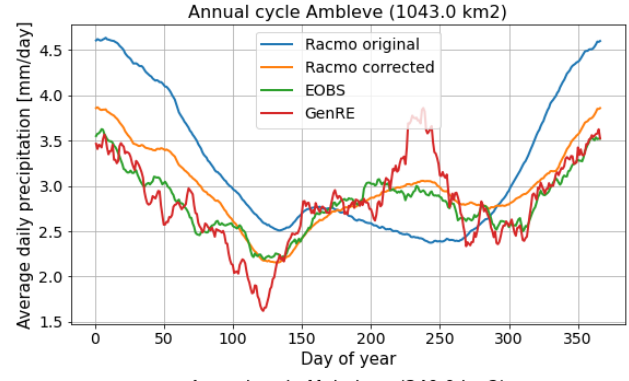
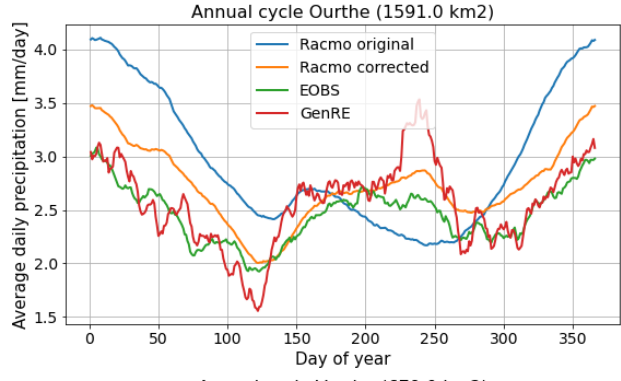
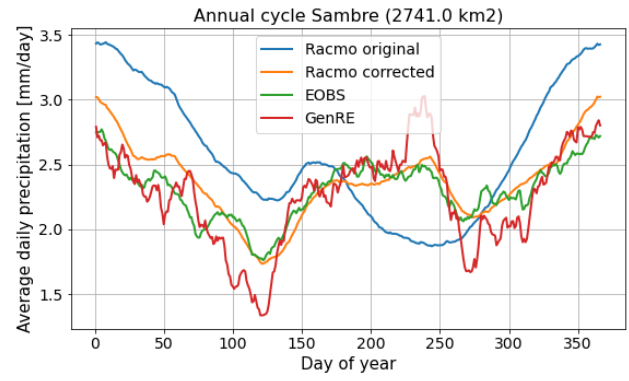
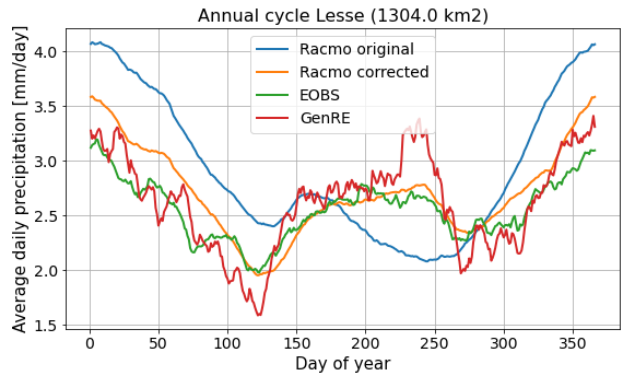
Wilson, P. S., & Toumi, R. (2005). A fundamental probability distribution for heavy rainfall. *Geophysical Research Letters*, 32(14).

Zeder, J., Sippel, S., Pasche, O. C., Engelke, S., & Fischer, E. M. (2023). The effect of a short observational record on the statistics of temperature extremes. *Geophysical Research Letters*, 50, e2023GL104090. <https://doi.org/10.1029/2023GL104090>

6. Appendices

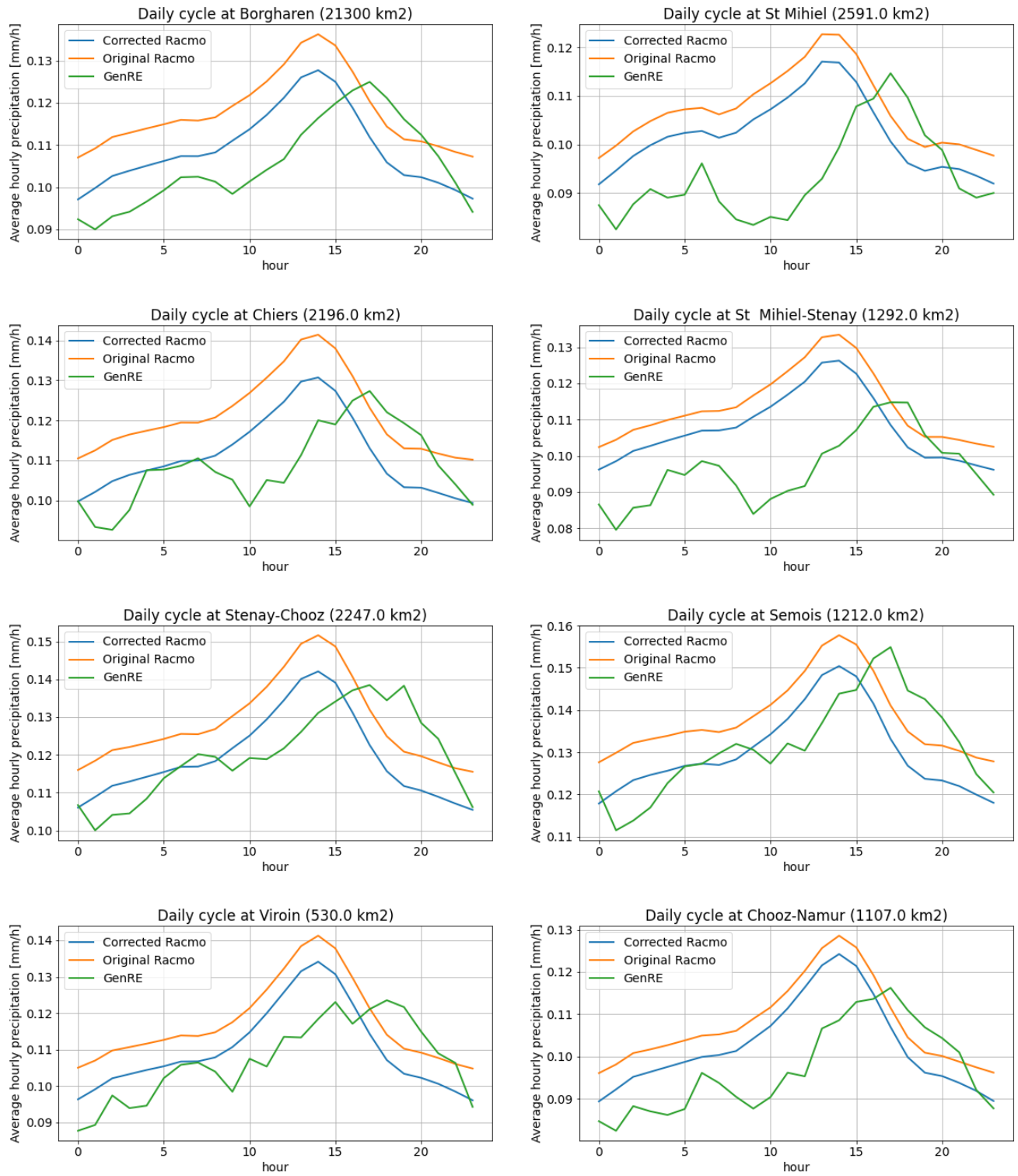
6.1. Annual cycles

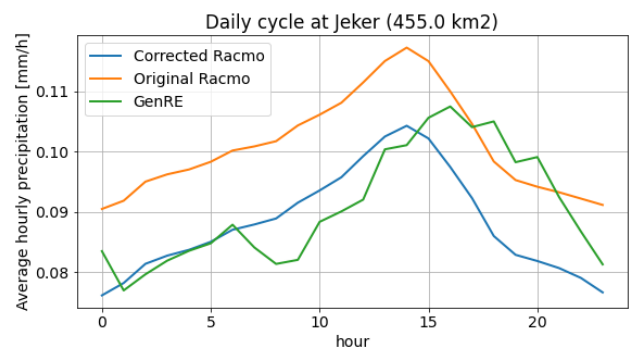
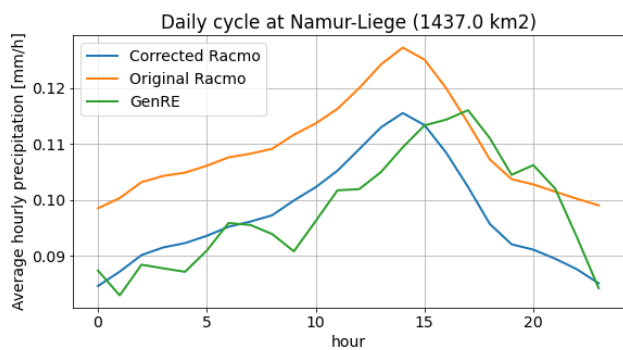
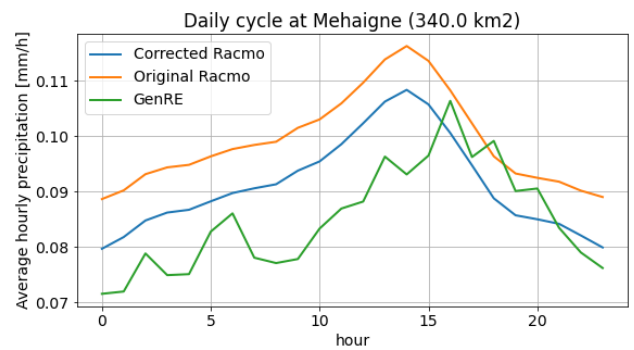
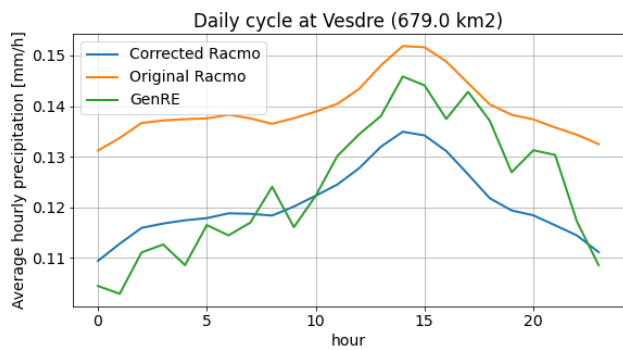
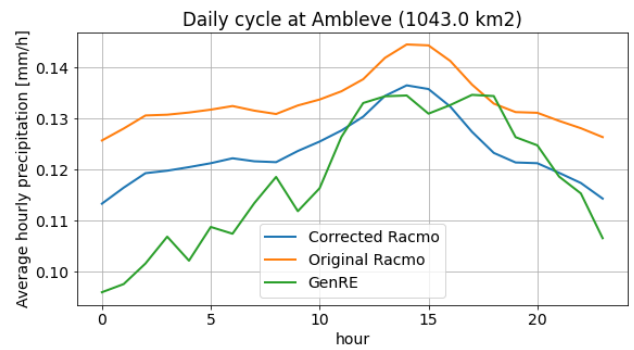
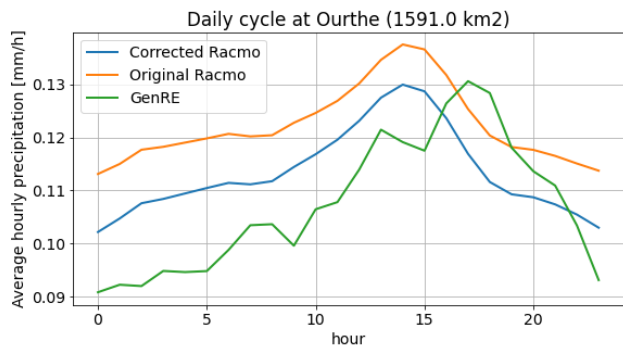
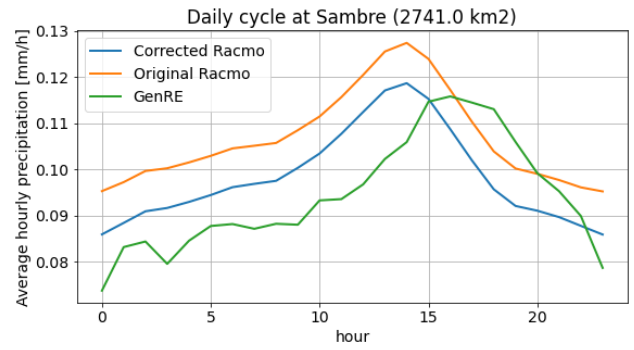
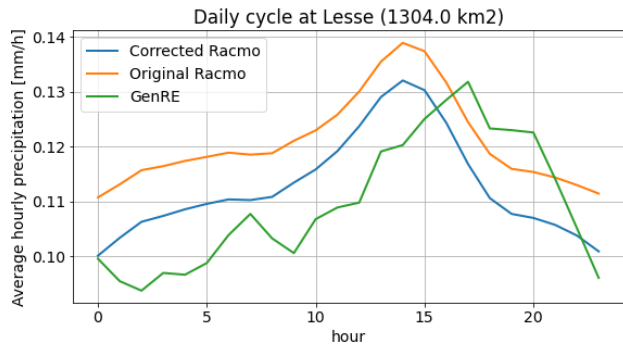




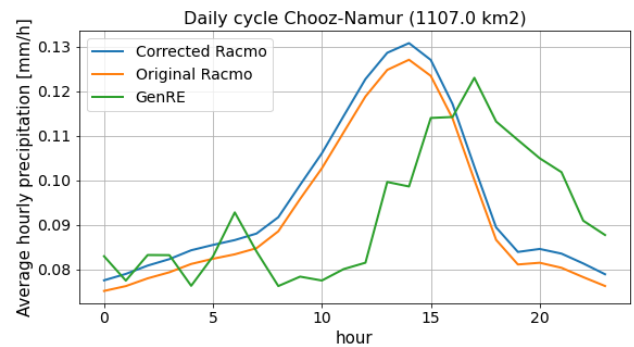
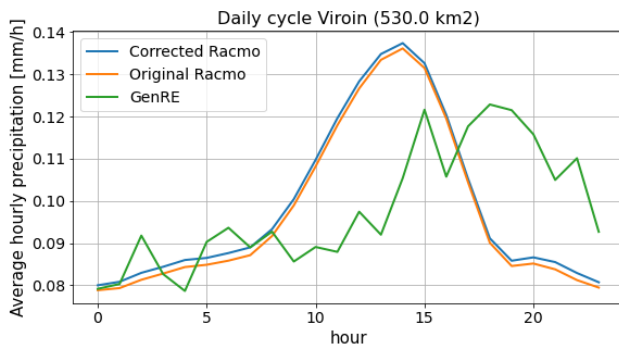
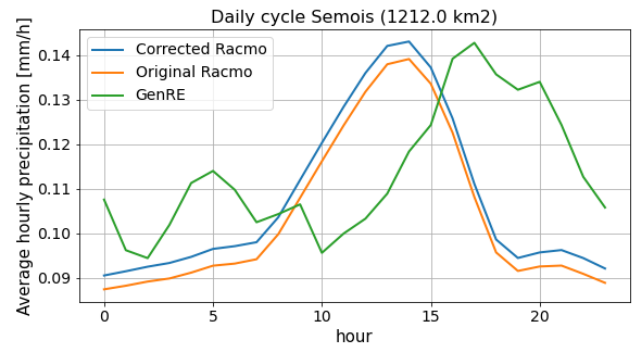
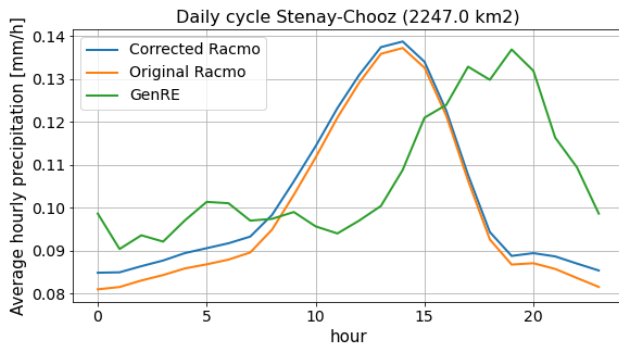
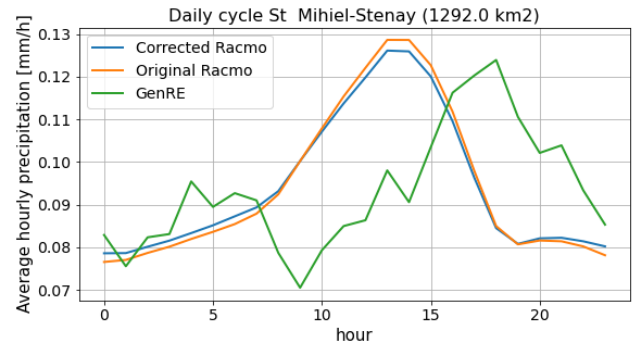
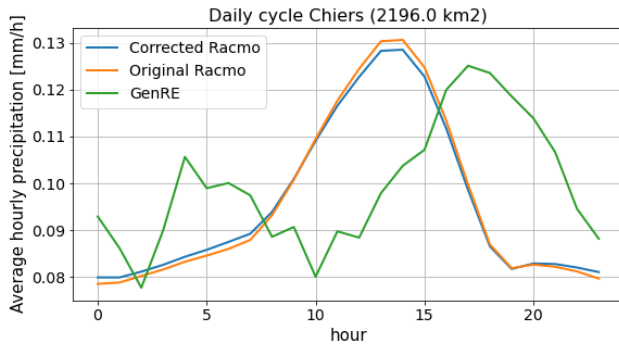
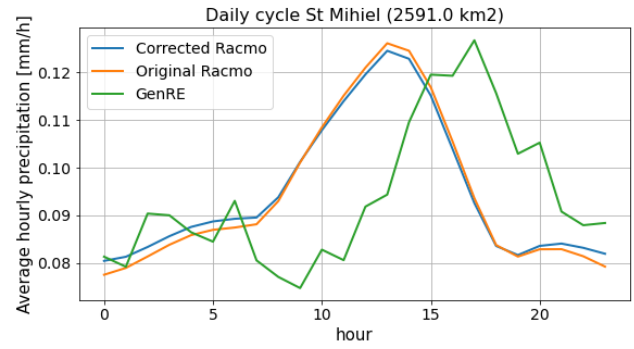
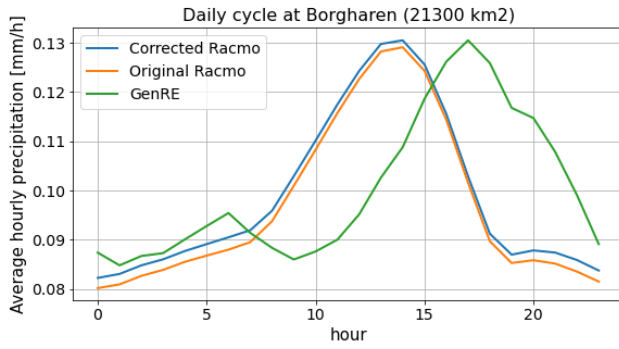
6.2. Daily cycles

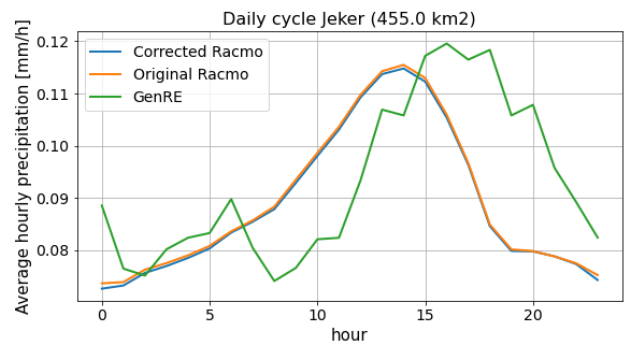
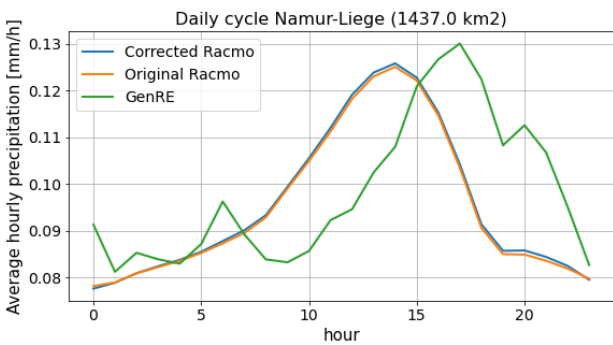
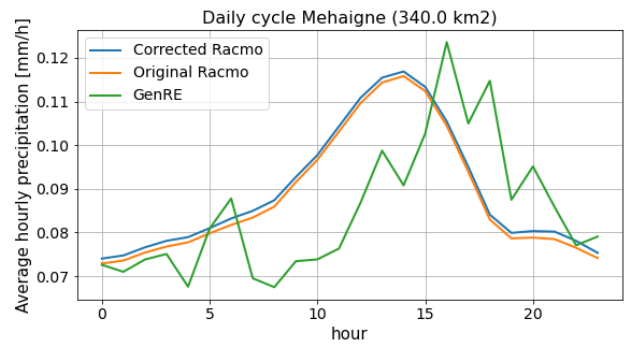
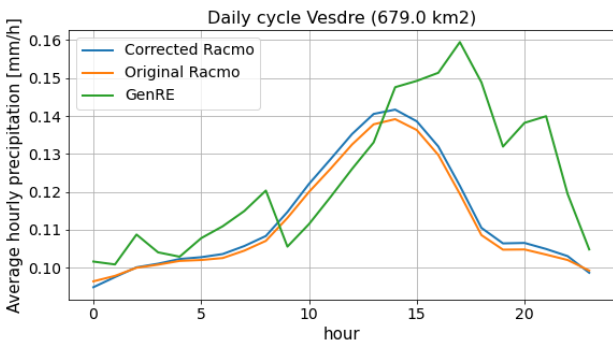
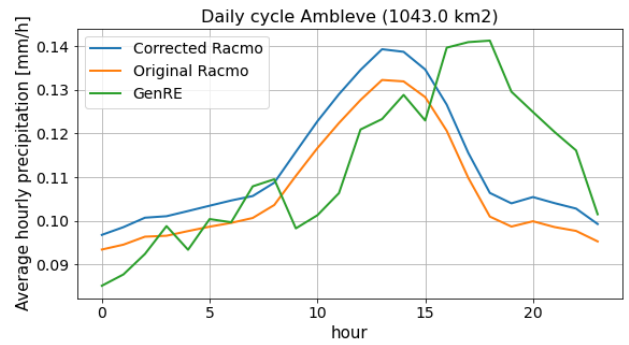
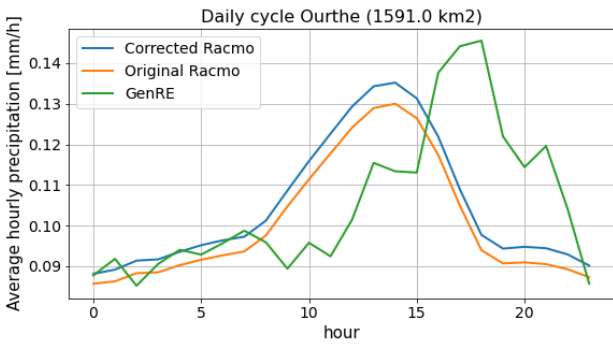
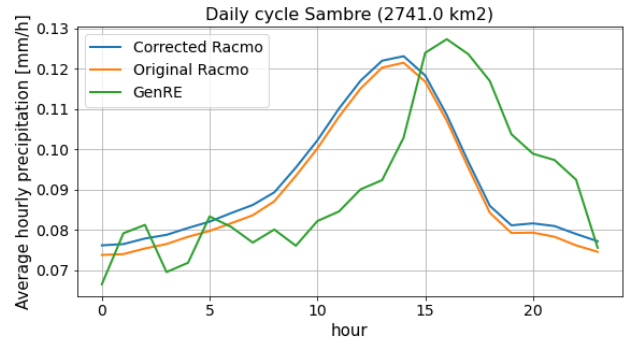
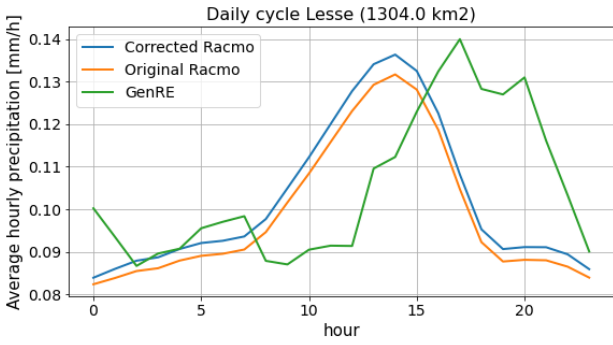
6.2.1. Calendar year





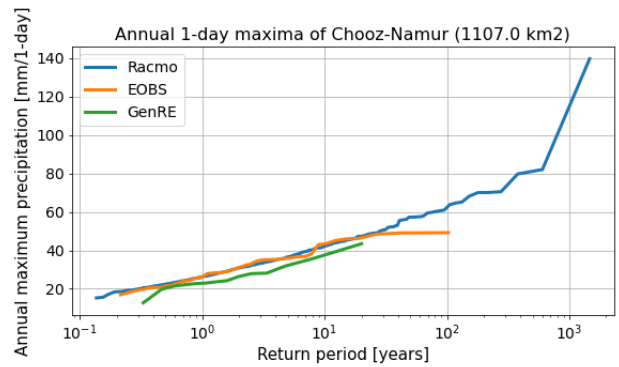
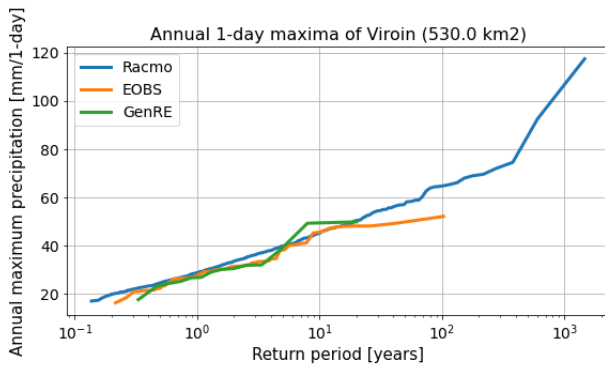
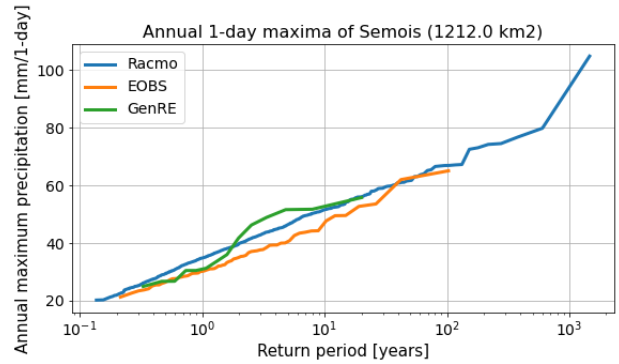
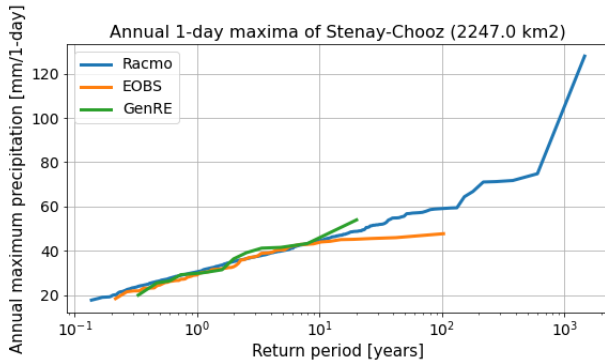
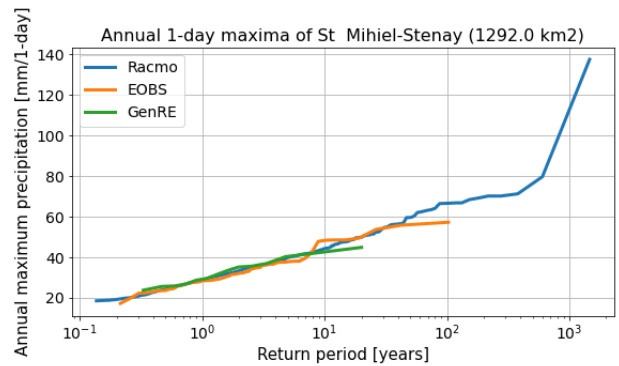
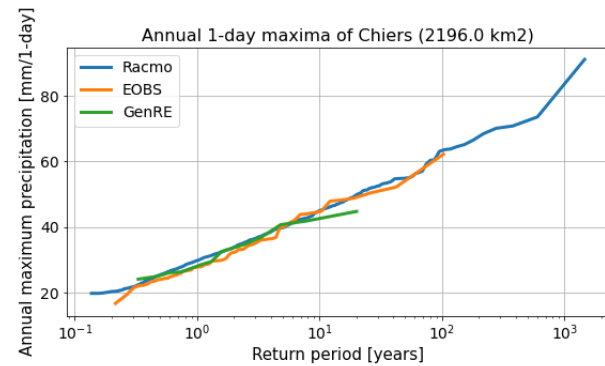
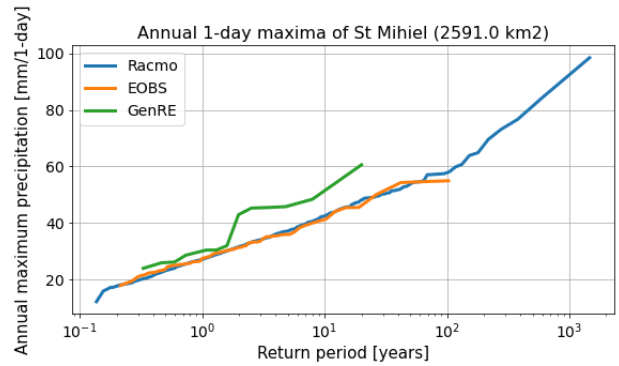
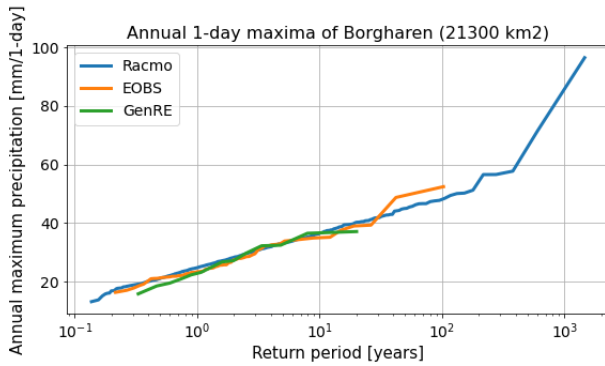
6.2.2. Summer half year

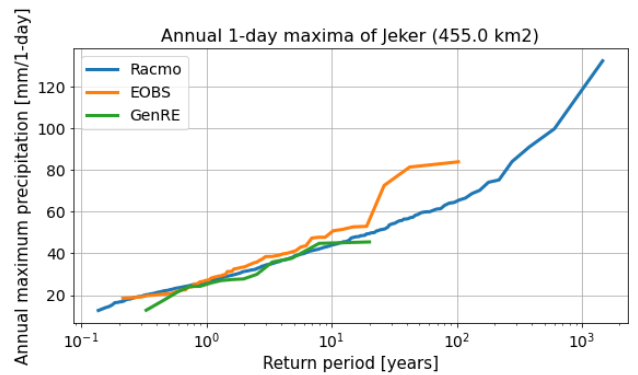
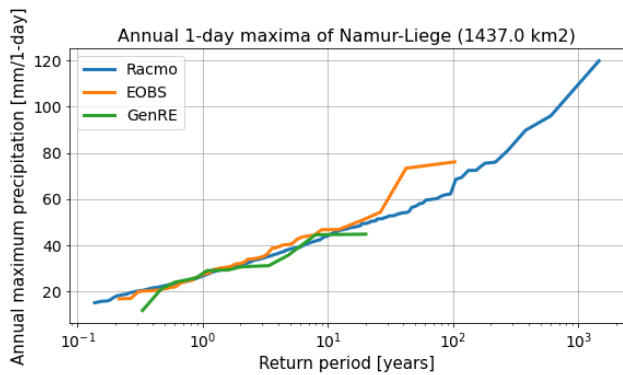
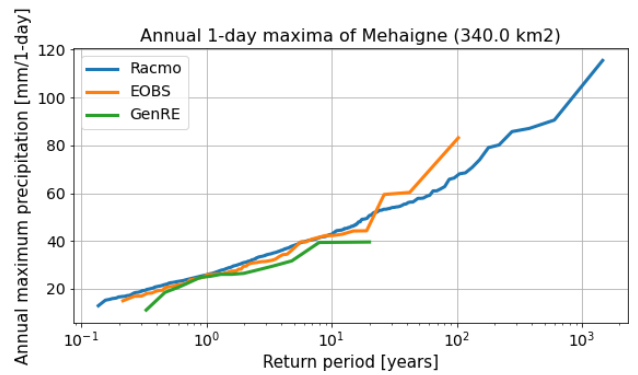
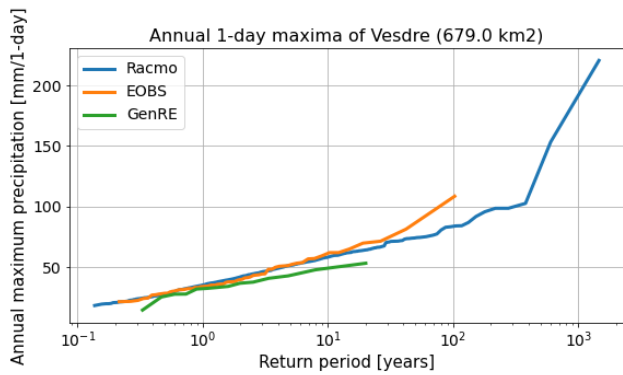
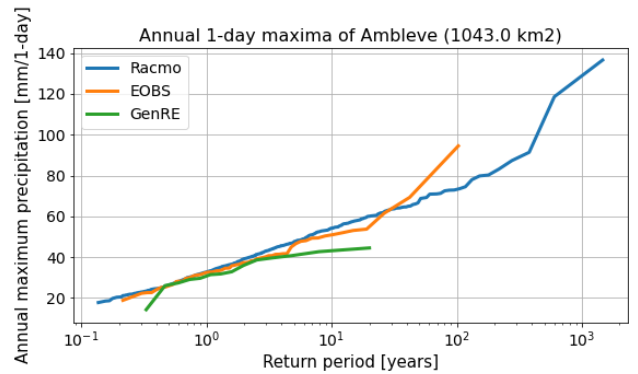
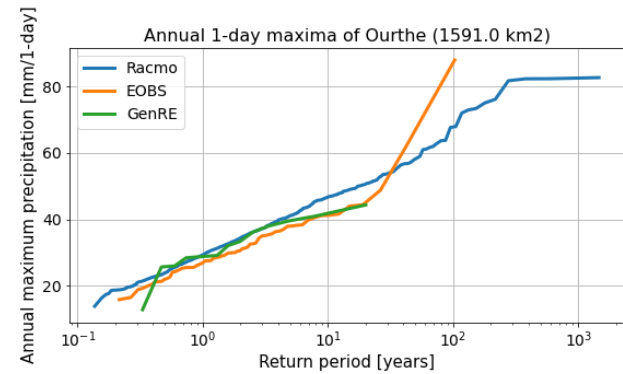
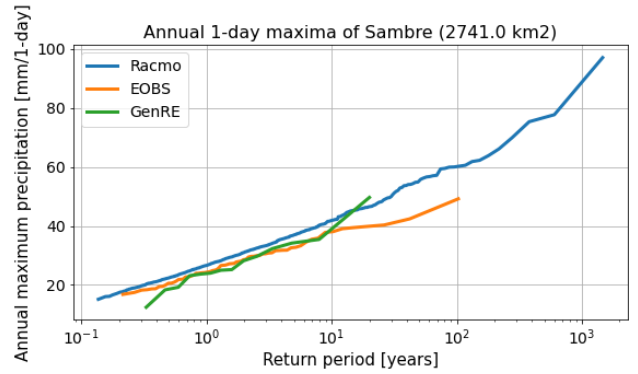
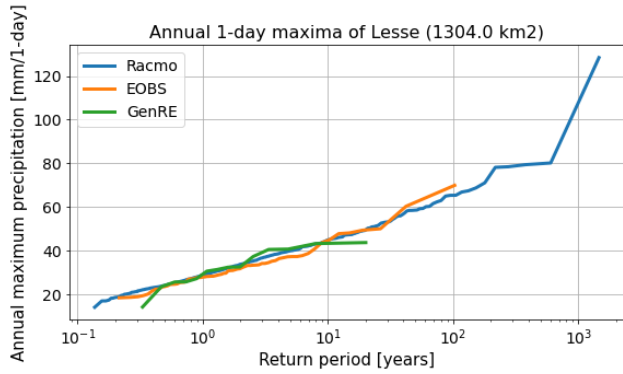




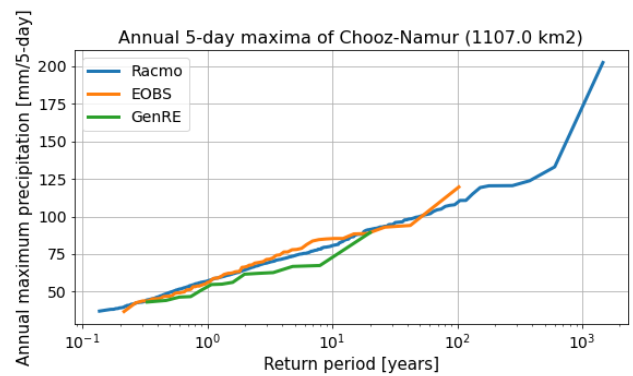
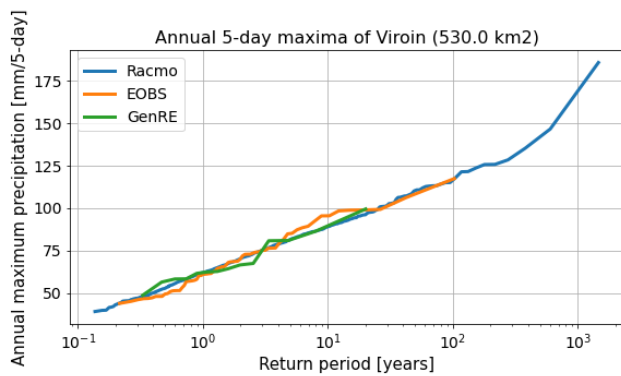
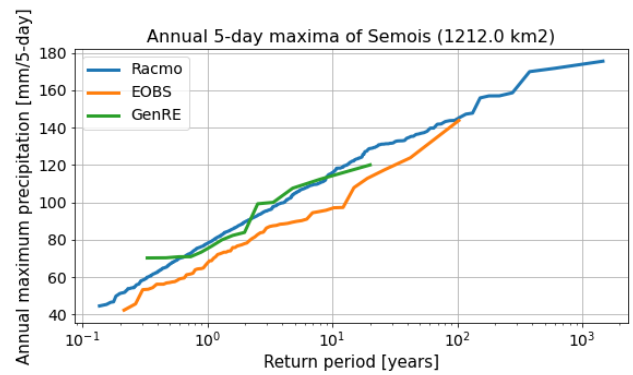
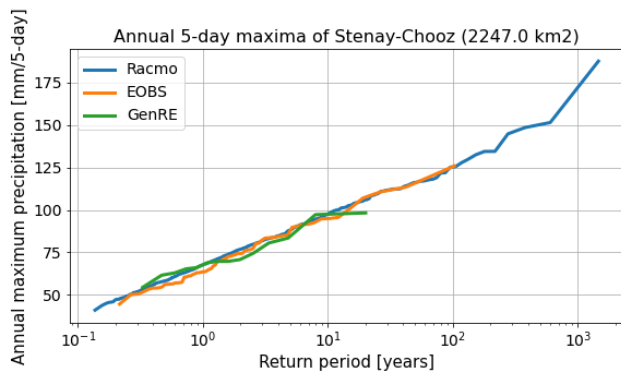
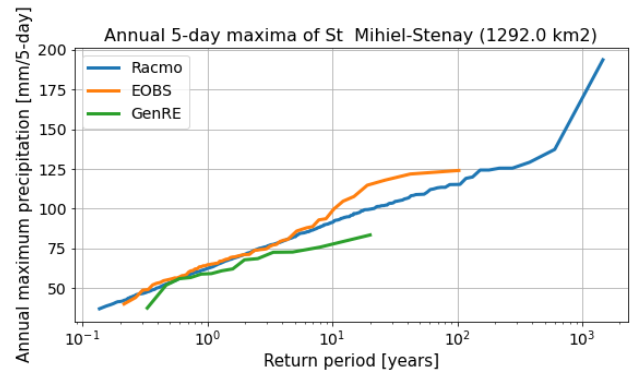
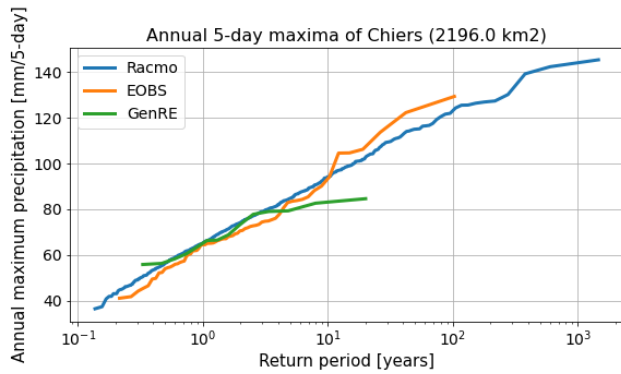
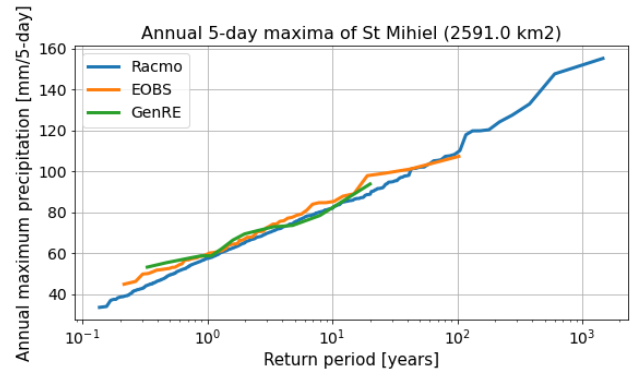
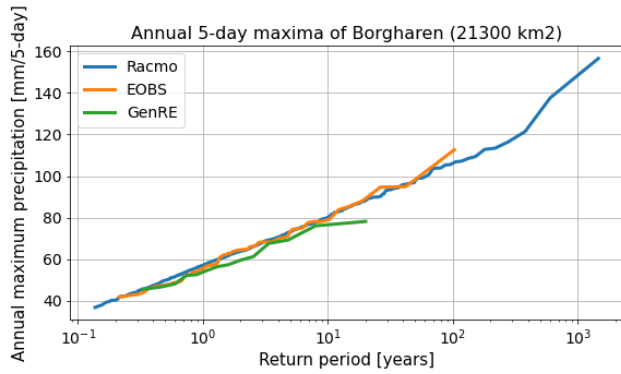
6.3. Annual extremes

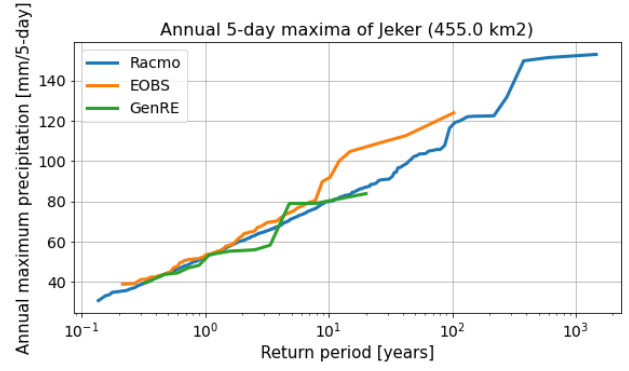
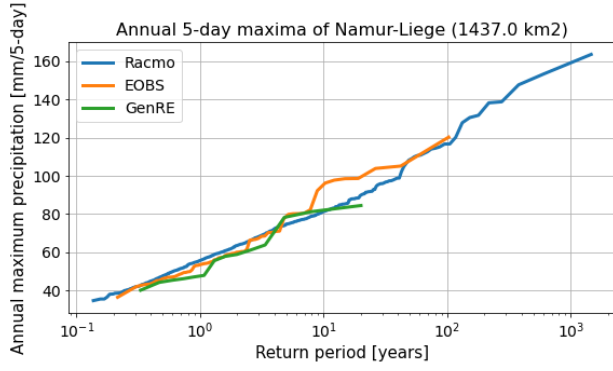
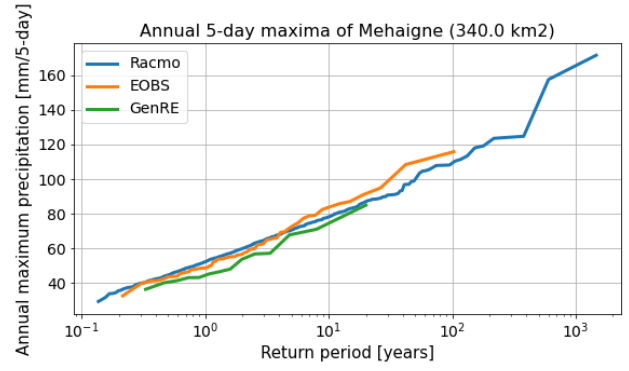
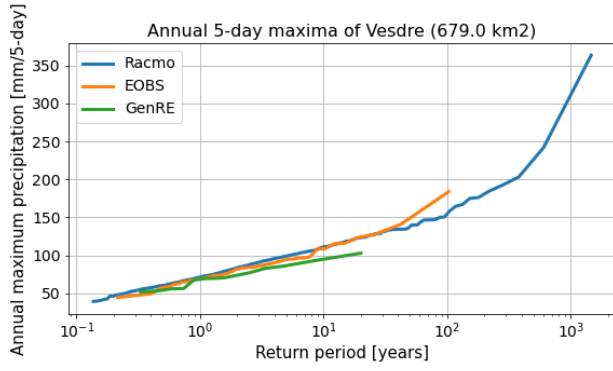
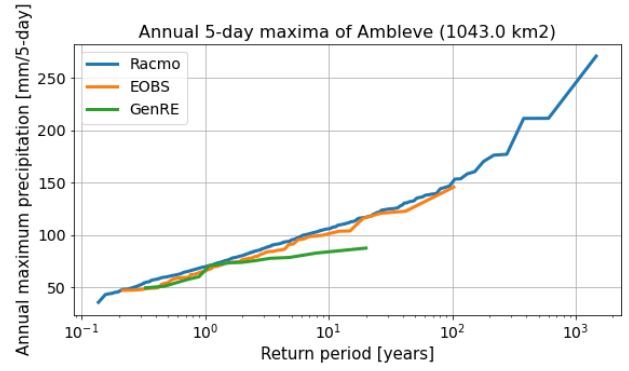
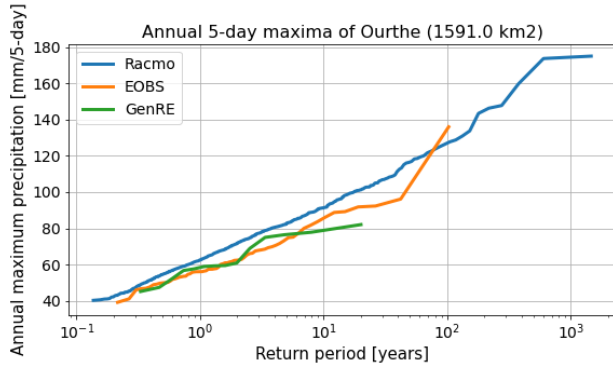
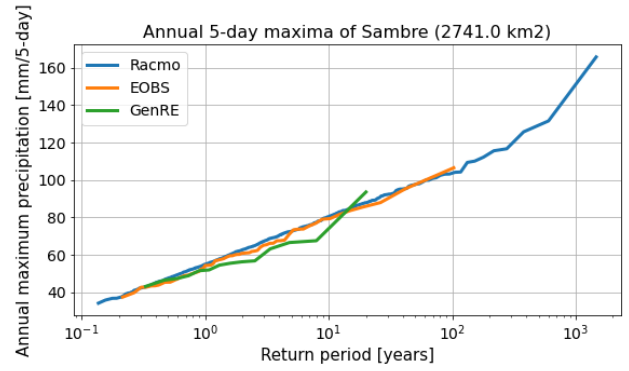
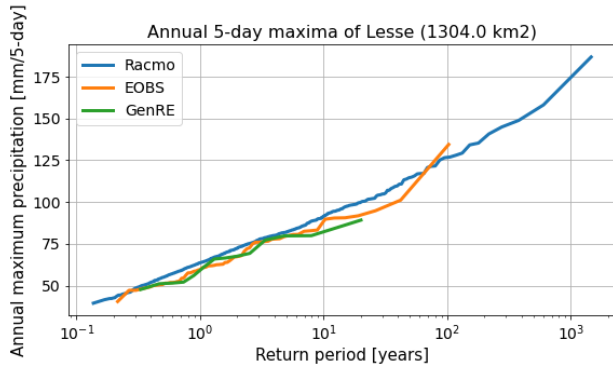
6.3.1. Daily



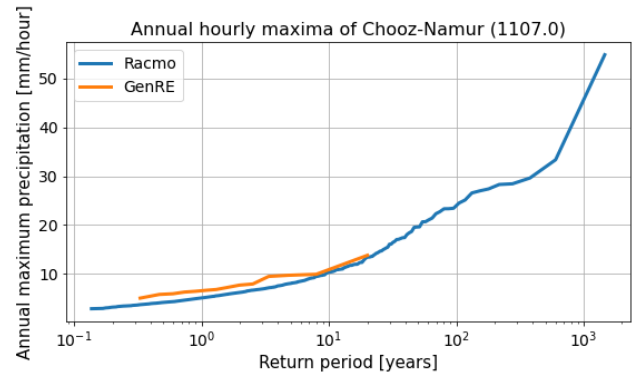
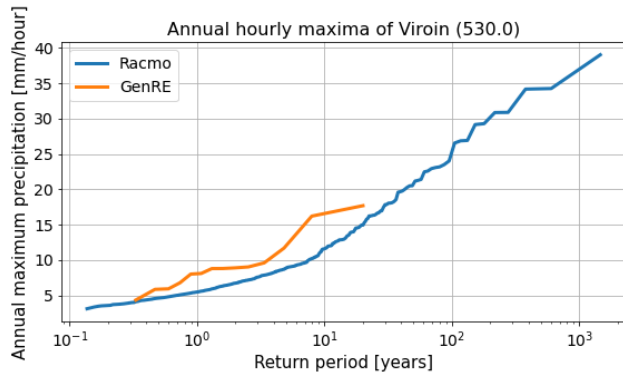
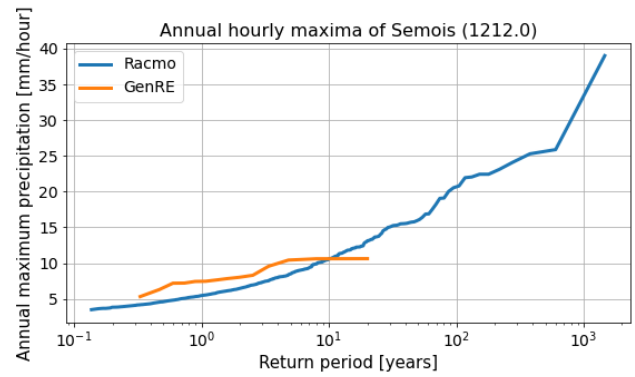
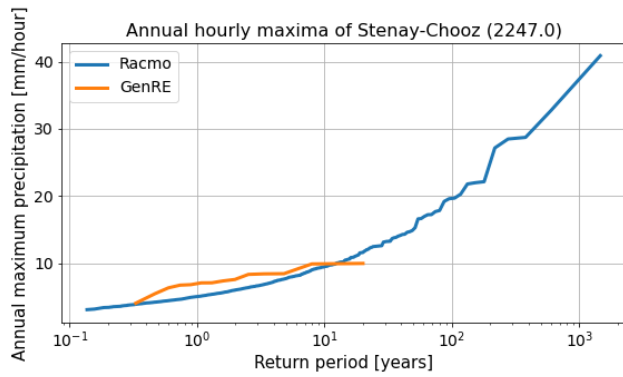
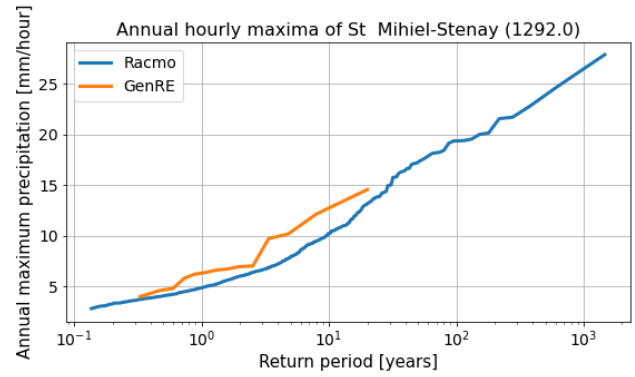
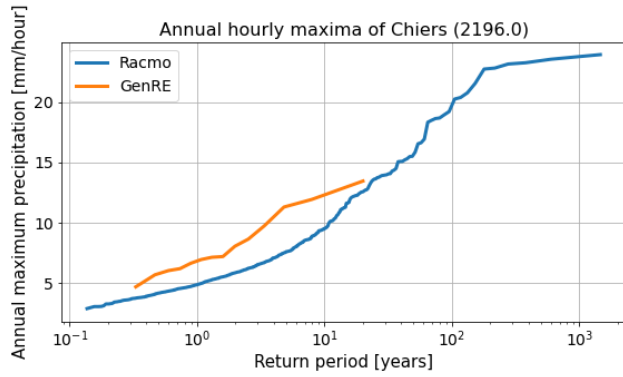
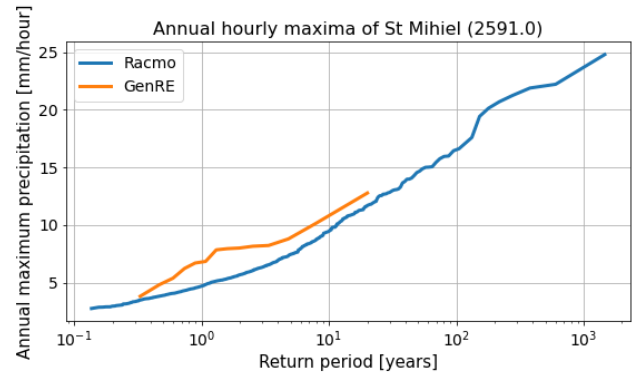
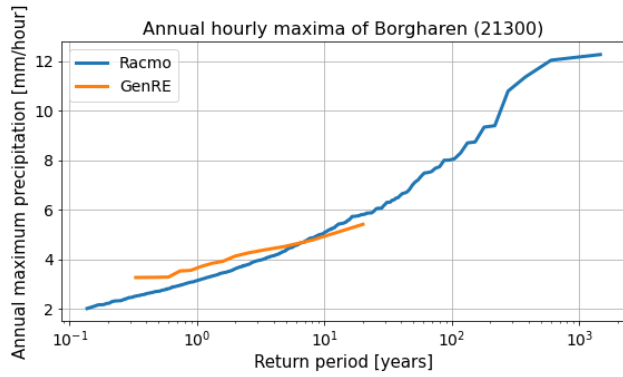


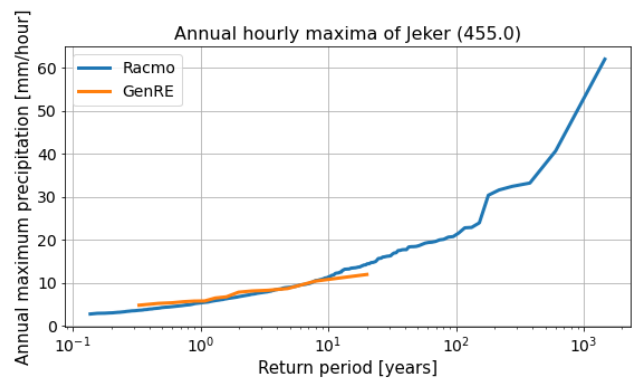
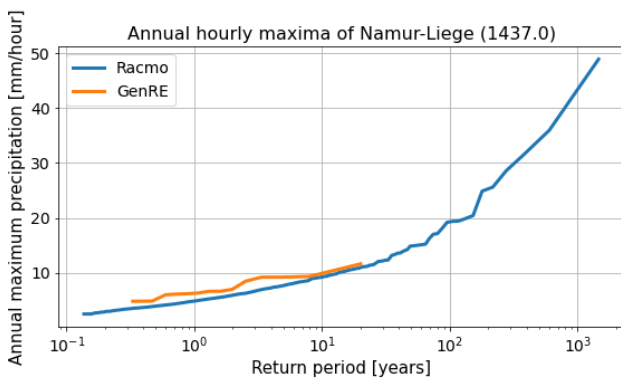
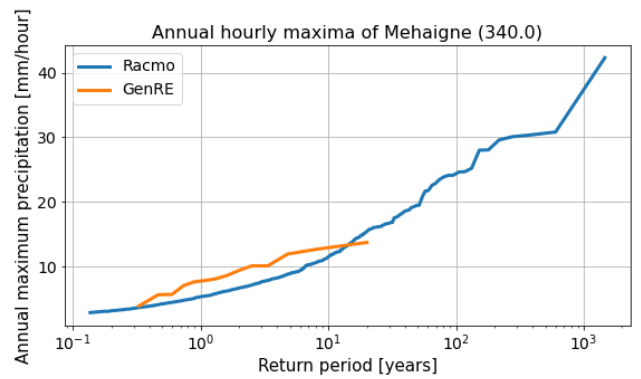
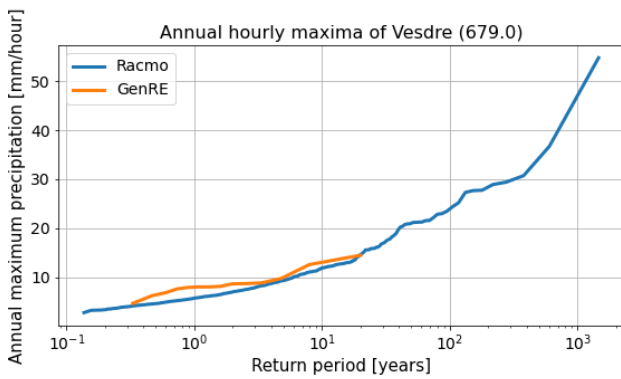
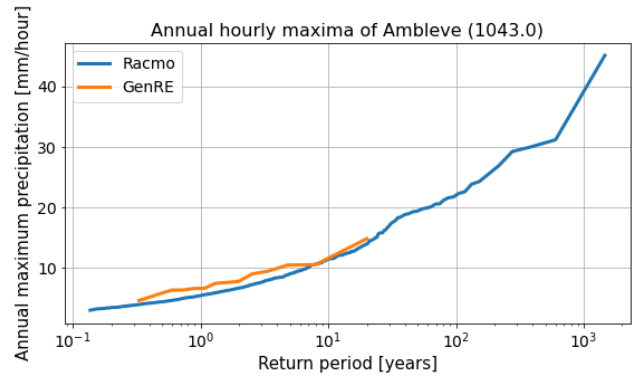
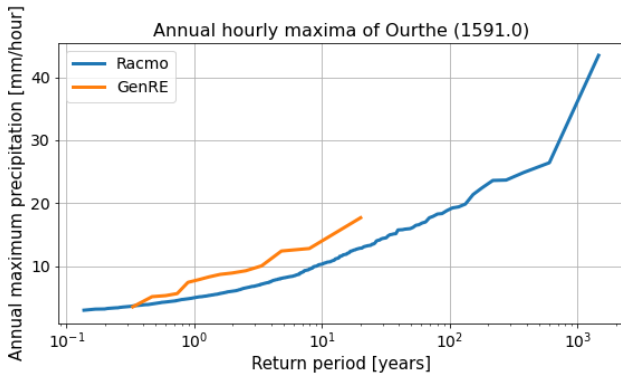
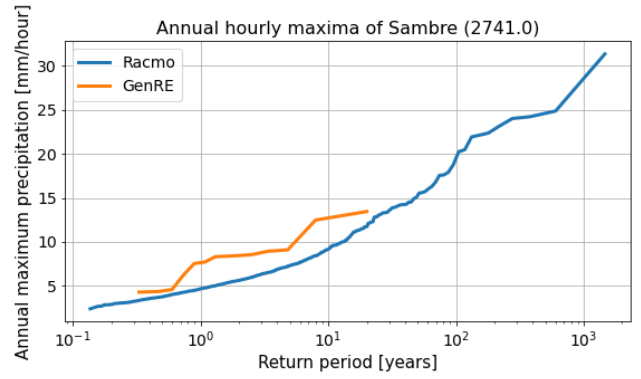
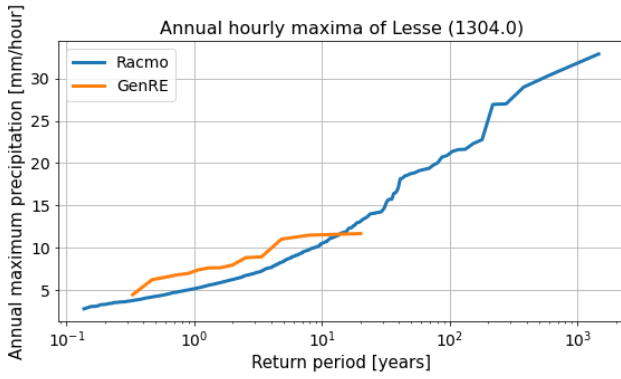
6.3.2. 5-daily





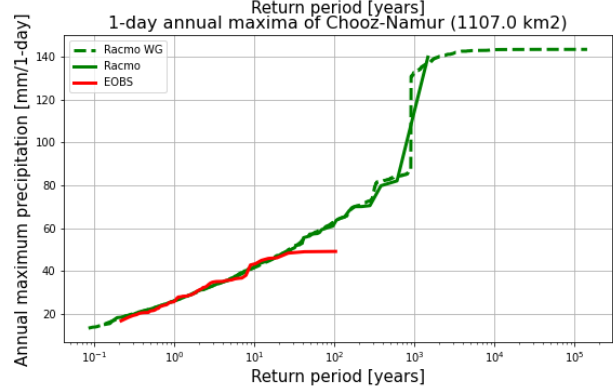
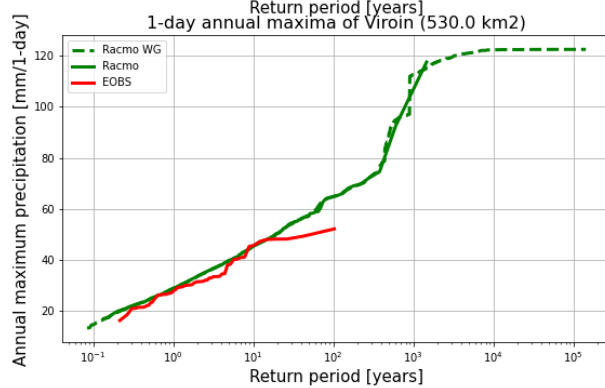
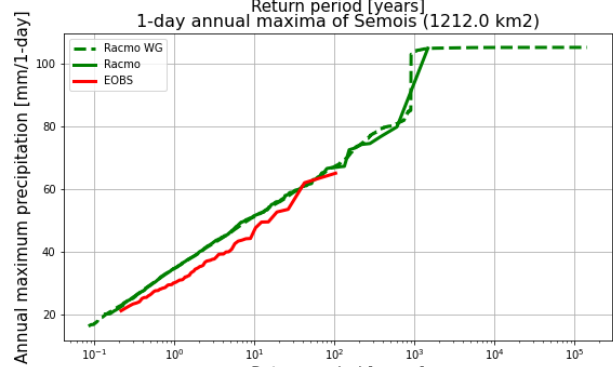
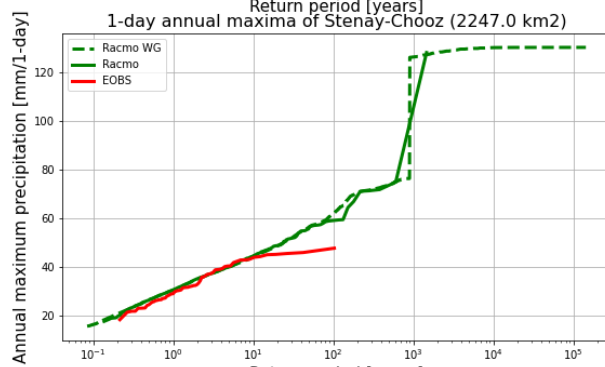
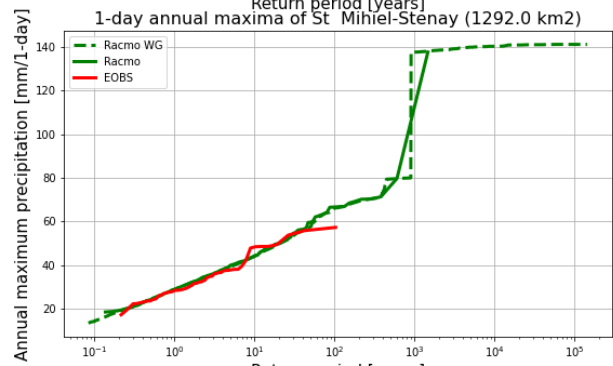
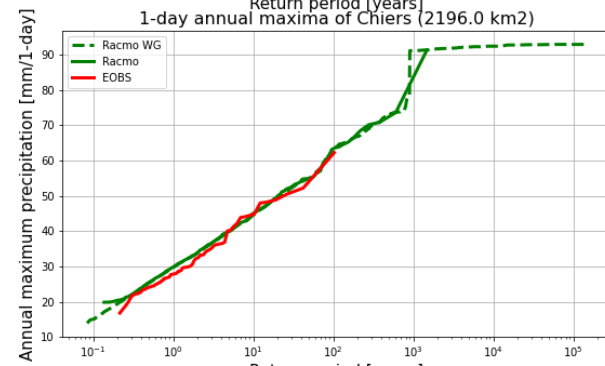
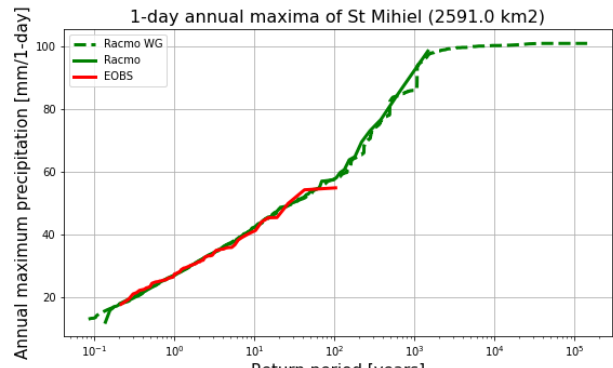
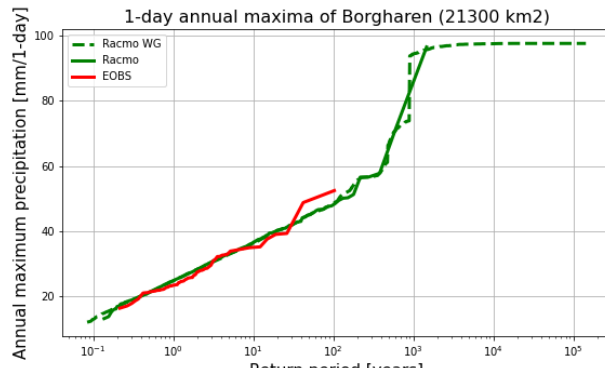
6.3.3. Hourly

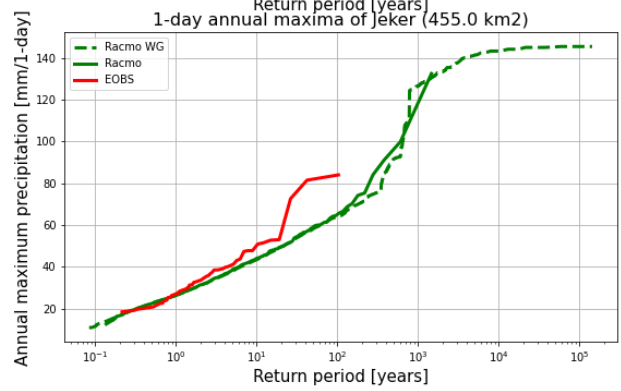
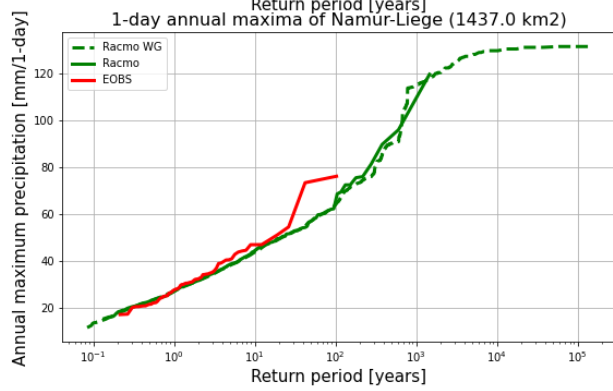
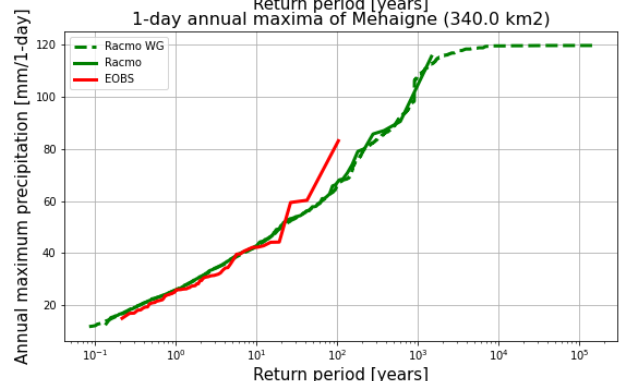
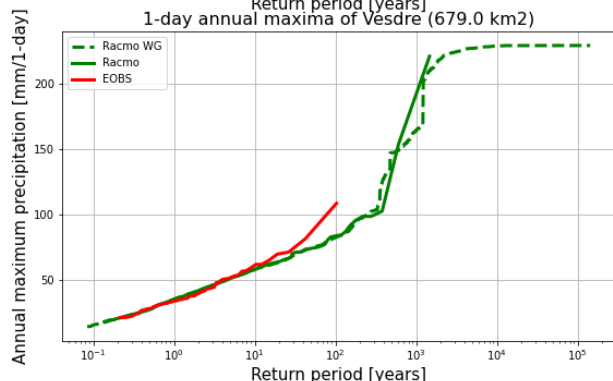
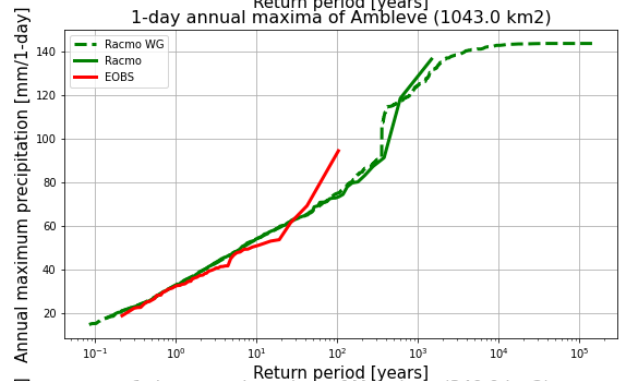
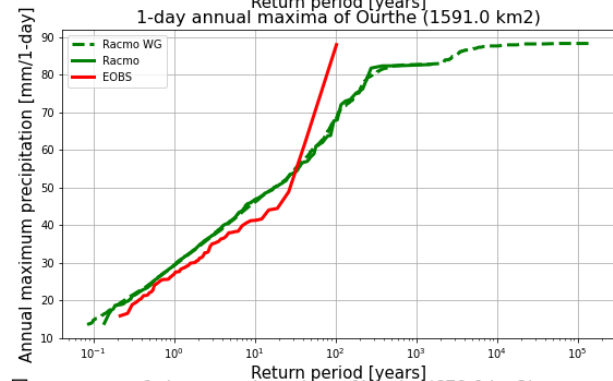
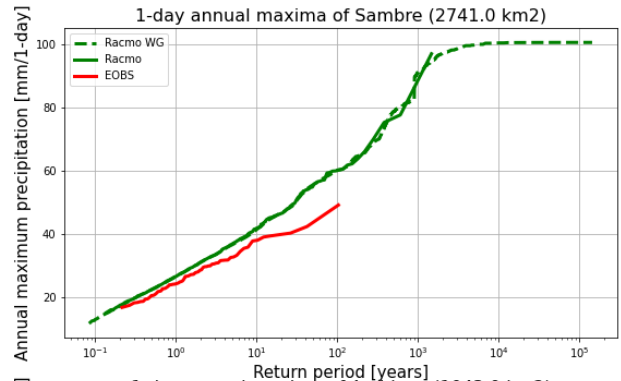
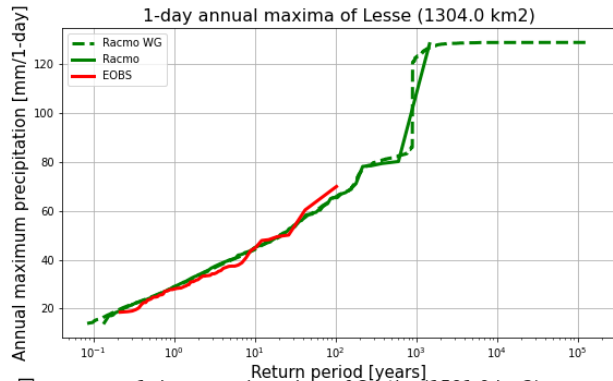




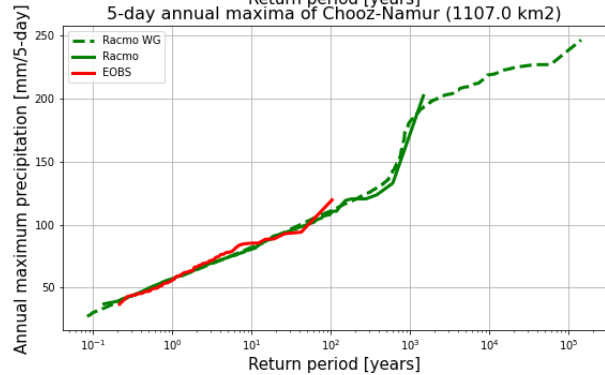
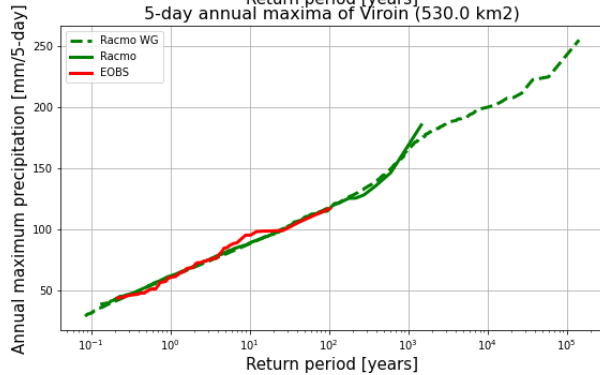
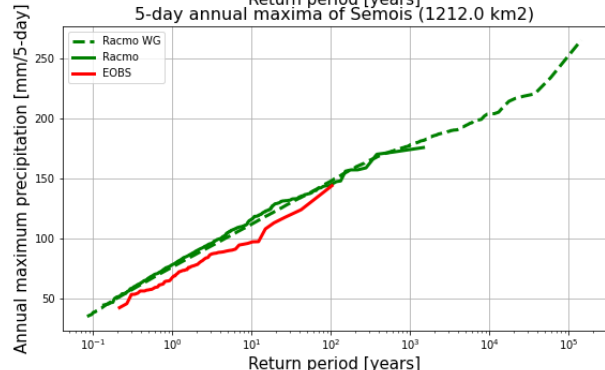
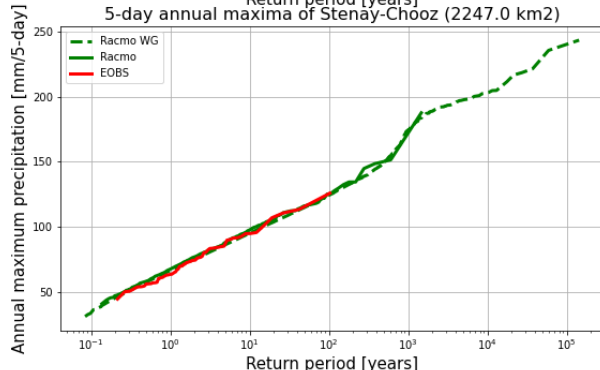
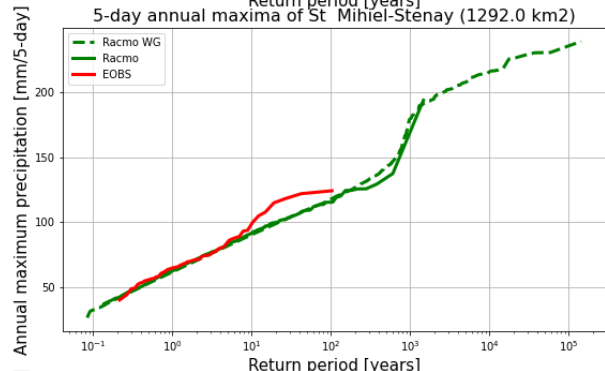
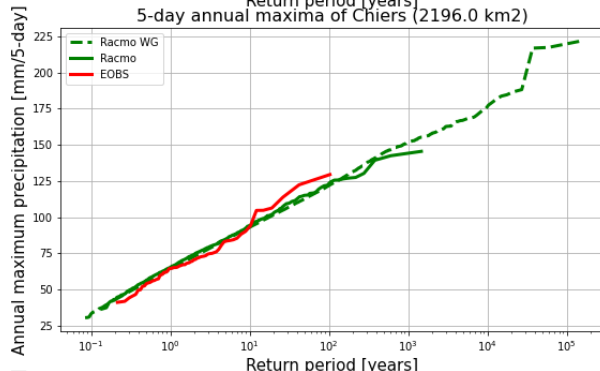
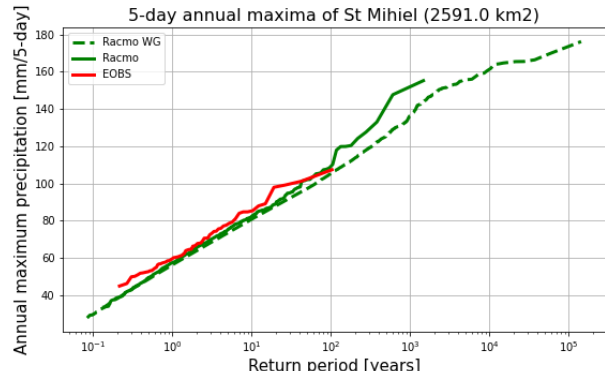
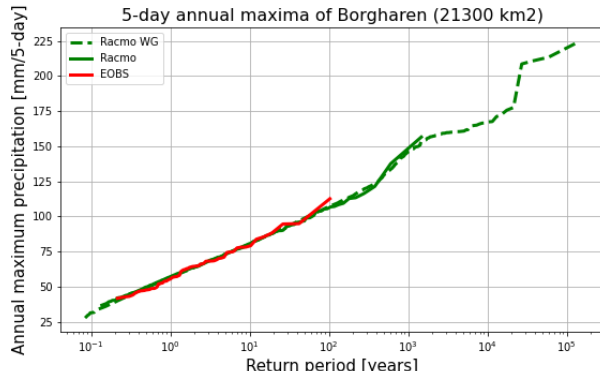
6.4. Weather generator

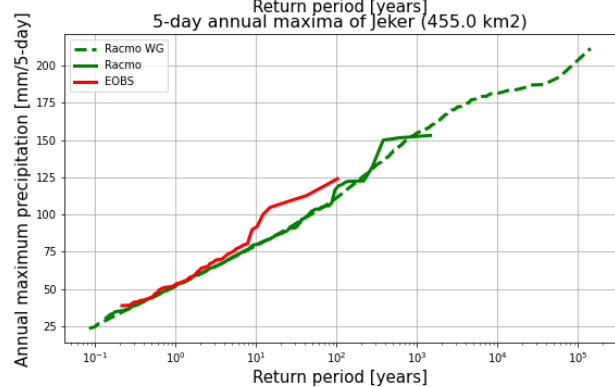
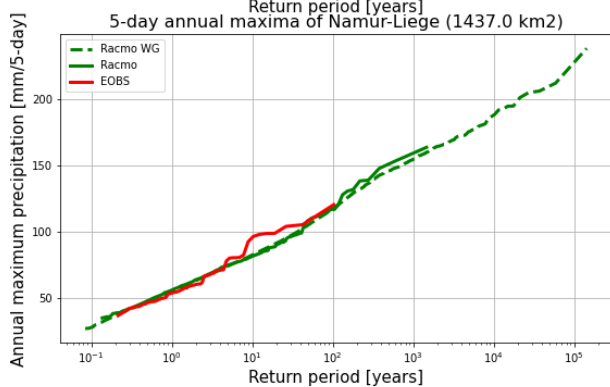
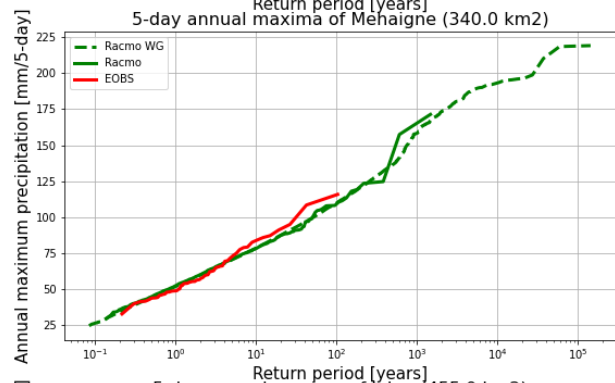
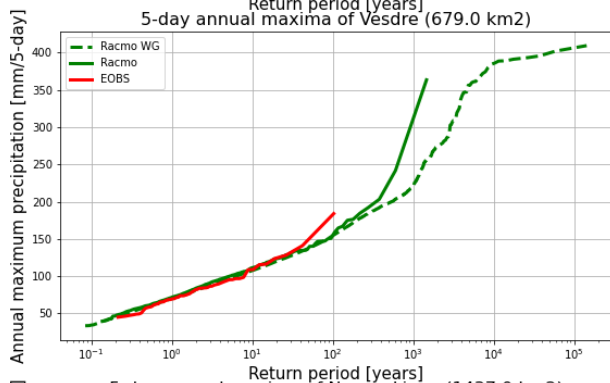
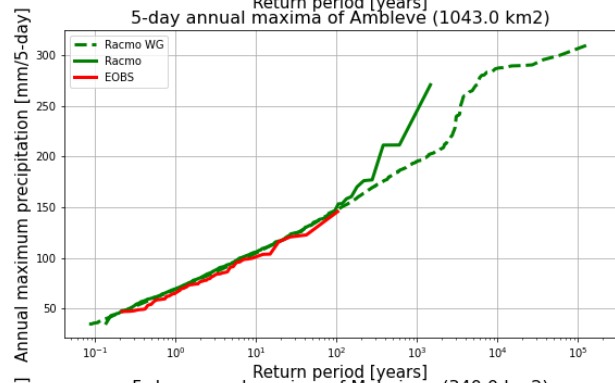
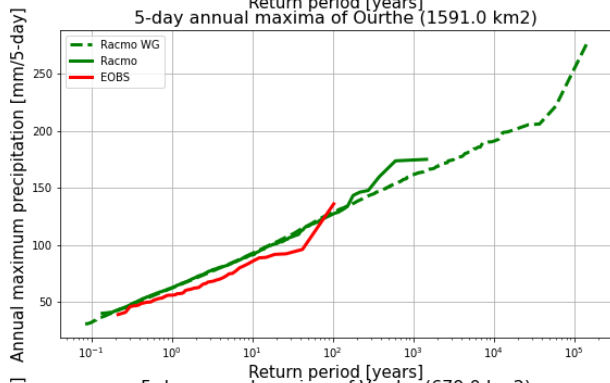
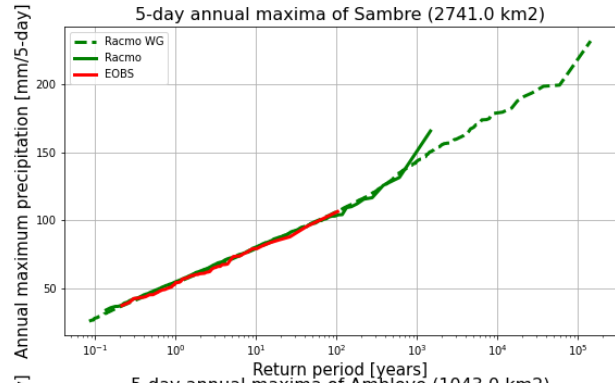
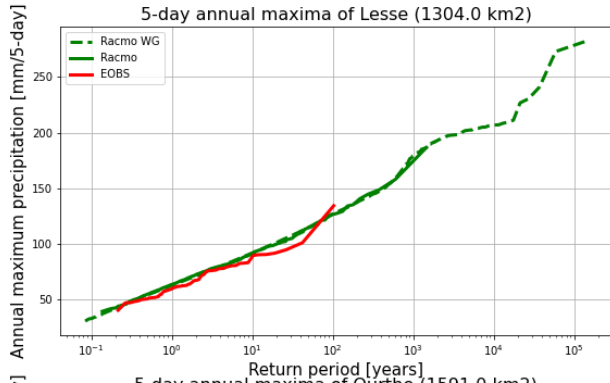
6.4.1. Daily





6.4.2. 5-daily





6.5. Return period tables

6.5.1. 2-day sum

RP (years)	1	10	100	1000	10000	100000	~1400
Meuse	36.0	53.3	71.9	91.9	113.8	137.6	124.4
St. Mihiel	38.0	58.9	81.1	105.0	121.0	145.8	136.7
Chiers	42.1	62.9	83.6	104.2	126.5	148.9	114.7
Stenay	40.7	62.3	85.6	110.7	138.0	168.5	159.5
Chooz	43.7	64.2	85.1	106.3	131.7	157.4	156.7
Semois	49.8	74.5	99.4	124.5	146.8	171.7	134.4
Viroin	41.0	62.3	85.0	109.3	141.9	175.8	156.6
Namur	37.7	57.8	80.5	106.2	145.0	186.5	175.4
Lesse	41.6	63.5	87.3	113.1	149.4	187.5	160.4
Sambre	37.0	57.2	79.6	104.5	134.3	168.2	127.7
Ourthe	41.3	64.6	91.0	120.9	155.7	196.4	143.0
Ambleve	46.2	75.4	110.4	152.5	193.8	251.4	250.4
Vesdre	48.1	80.9	121.4	171.7	212.2	276.7	349.9
Mehaigne	35.8	57.9	85.5	119.8	157.8	207.8	134.9
Liege	37.3	59.8	87.7	122.4	156.6	204.0	141.1
Jeker	36.0	58.5	86.0	119.5	154.3	200.3	141.1

6.5.2. 3-day sum

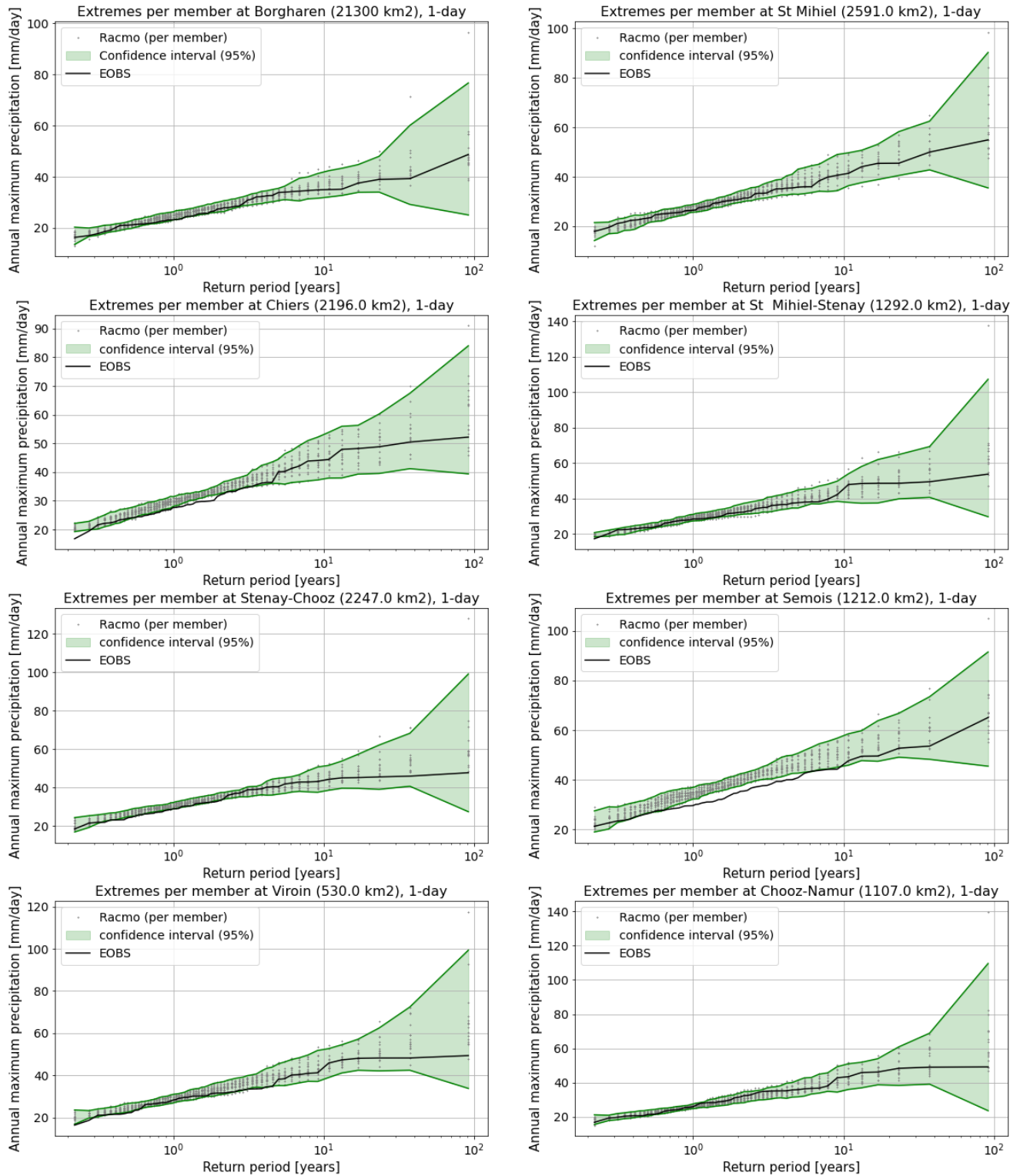
RP (years)	1	10	100	1000	10000	100000	~1400
Meuse	43.7	63.5	84.3	106.4	133.2	159.5	139.9
St. Mihiel	45.1	68.8	94.3	122.0	133.1	156.6	144.8
Chiers	50.6	74.4	97.5	119.9	146.9	171.3	128.6
Stenay	48.7	73.7	100.4	128.8	155.4	186.2	180.7
Chooz	52.6	75.8	98.8	121.8	151.9	179.0	171.0
Semois	60.5	89.2	117.3	144.9	175.0	203.7	146.8
Viroin	48.7	72.2	96.8	122.4	156.2	189.0	168.8
Namur	44.8	66.9	91.4	118.5	158.1	197.7	187.1
Lesse	49.7	74.2	100.5	128.6	169.8	209.8	173.1
Sambre	43.7	65.9	90.5	117.9	147.0	180.1	147.2
Ourthe	49.4	75.5	104.8	137.7	177.5	221.7	160.5
Ambleve	55.3	87.6	126.3	172.4	215.2	274.4	262.0
Vesdre	57.1	93.0	137.3	192.0	236.0	304.6	357.9
Mehaigne	42.1	66.0	94.3	128.1	167.7	214.6	149.2
Liege	43.9	68.7	99.6	138.0	171.0	218.0	153.3
Jeker	41.9	66.9	96.7	132.2	166.9	211.9	142.2

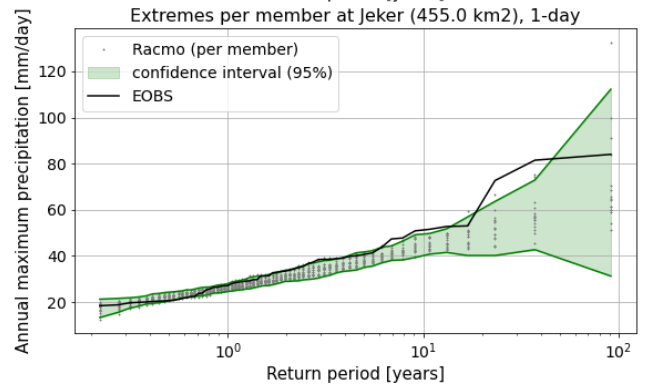
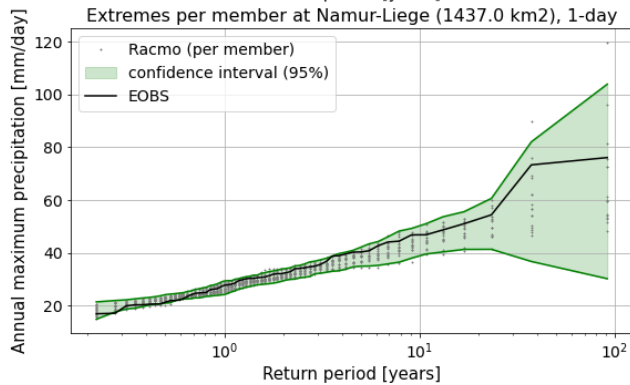
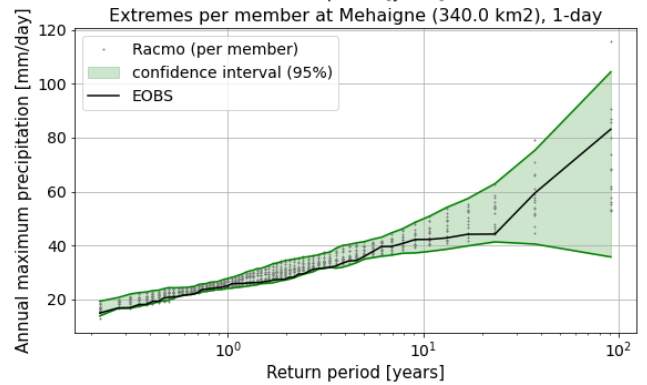
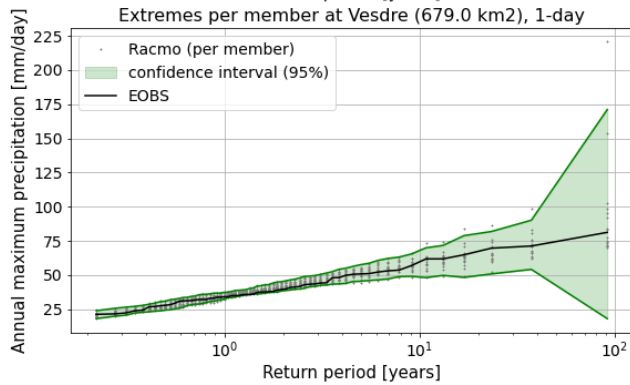
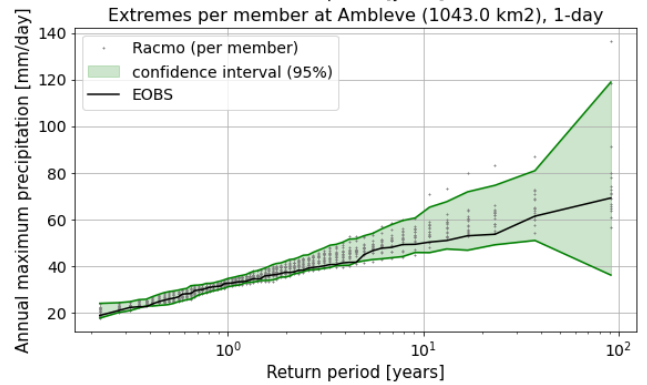
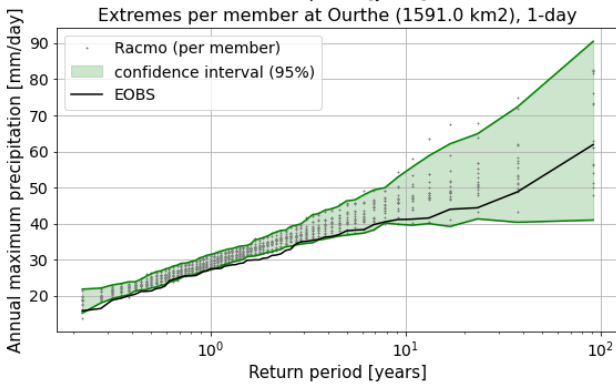
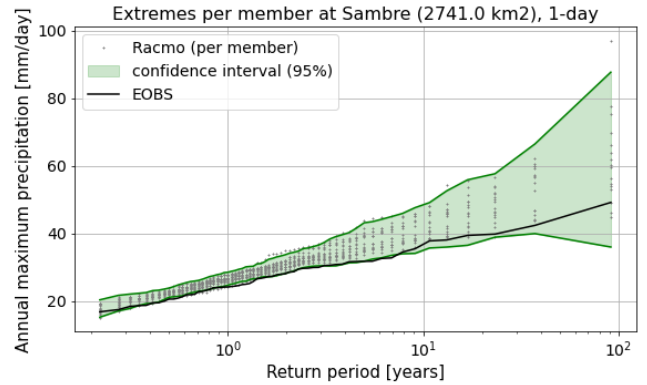
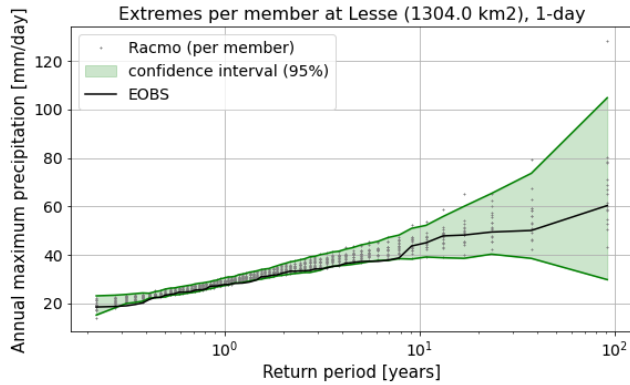
6.5.3. 5-day sum

RP (years)	1	10	100	1000	10000	100000	~1400
Meuse	56.9	80.7	105.7	131.6	158.1	184.7	156.6
St. Mihiel	57.1	83.4	109.2	134.5	150.8	172.5	155.2
Chiers	65.3	94.1	120.4	144.5	175.4	201.1	145.5
Stenay	62.4	91.4	119.3	146.2	178.6	208.2	193.8
Chooz	67.6	97.3	127.1	156.9	180.9	208.6	187.6
Semois	78.3	114.7	148.0	178.5	211.7	242.6	175.5
Viroin	61.8	89.8	118.2	147.1	177.9	209.0	185.8
Namur	56.9	82.5	109.3	137.2	174.2	208.9	202.3
Lesse	63.4	92.5	122.2	152.7	194.0	232.2	186.8
Sambre	54.9	80.4	106.7	134.0	163.5	193.8	165.8
Ourthe	62.7	92.8	124.9	159.4	200.9	243.0	175.2
Ambleve	70.0	106.9	148.8	196.3	242.3	299.6	270.8
Vesdre	71.6	111.9	159.5	215.6	261.9	328.5	363.5
Mehaigne	52.3	78.9	108.8	142.3	179.3	220.2	171.4
Liege	55.4	83.0	113.8	148.0	185.3	226.4	163.6
Jeker	52.2	79.9	110.9	145.6	180.5	220.9	153.1

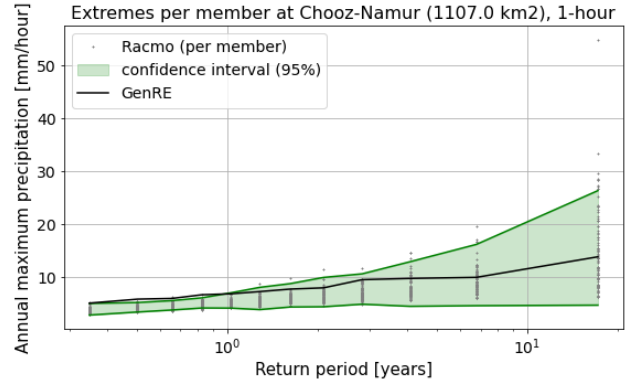
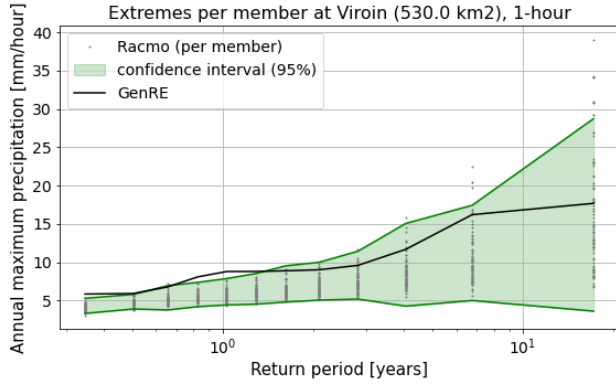
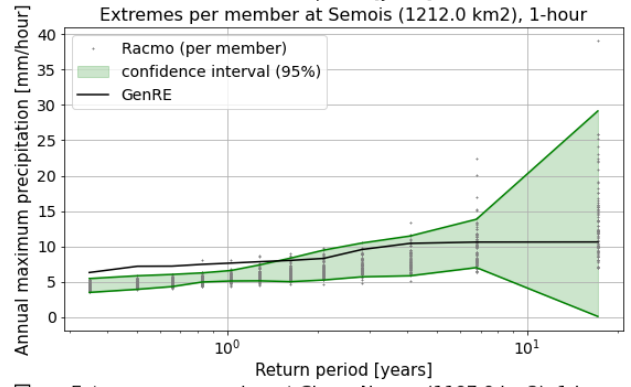
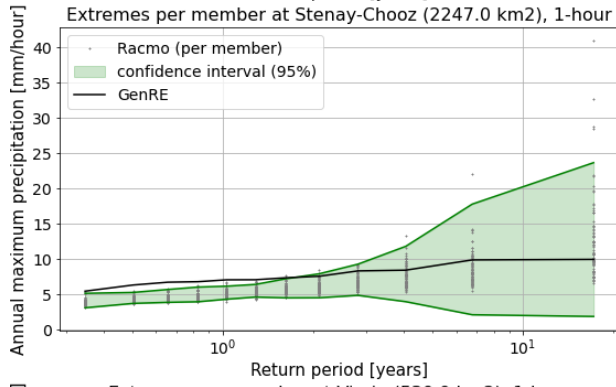
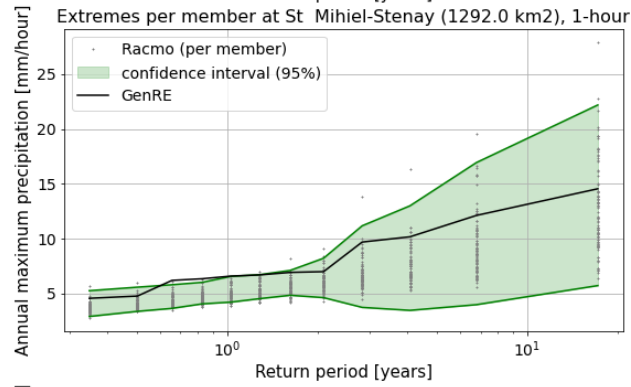
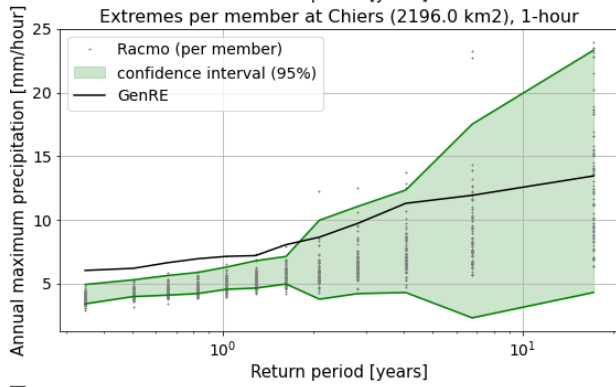
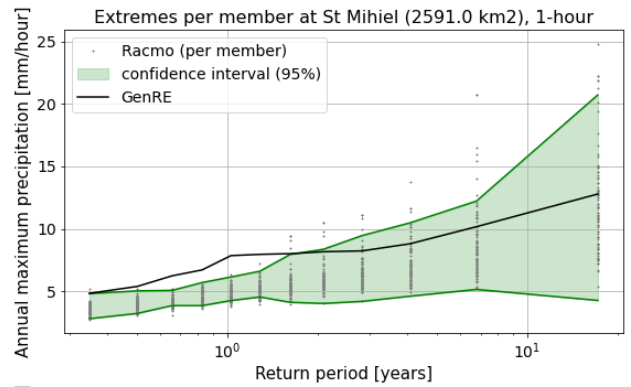
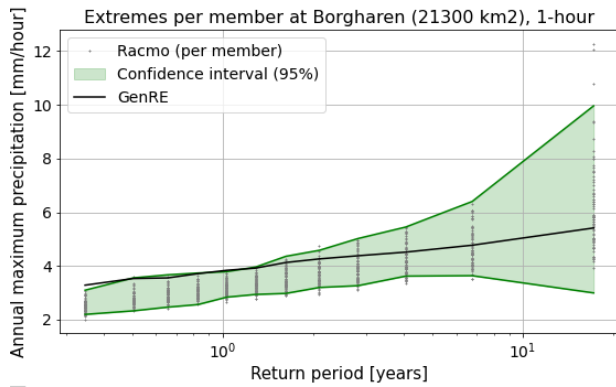
6.6. RACMO ensembles & confidence intervals

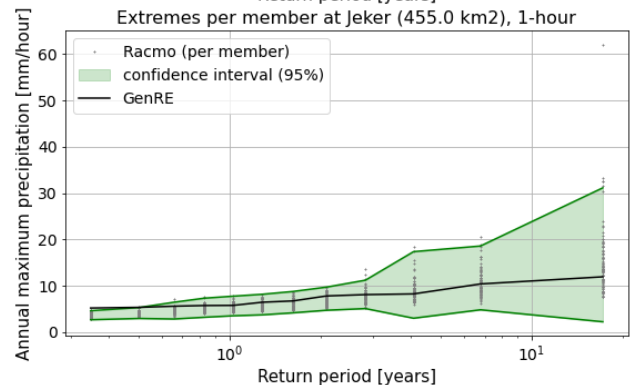
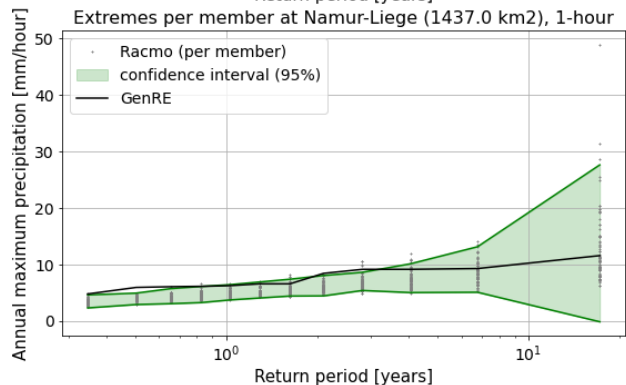
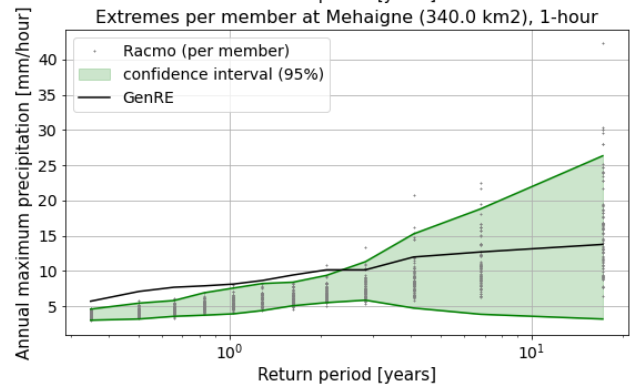
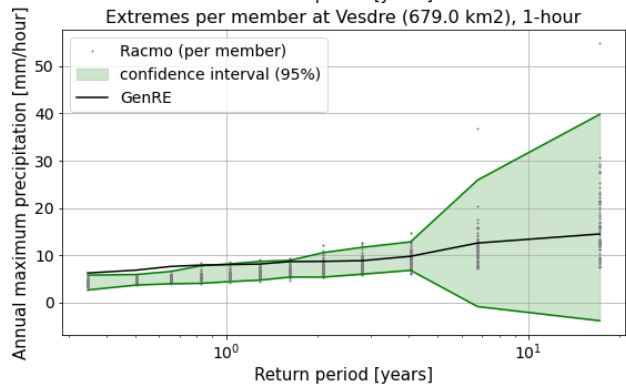
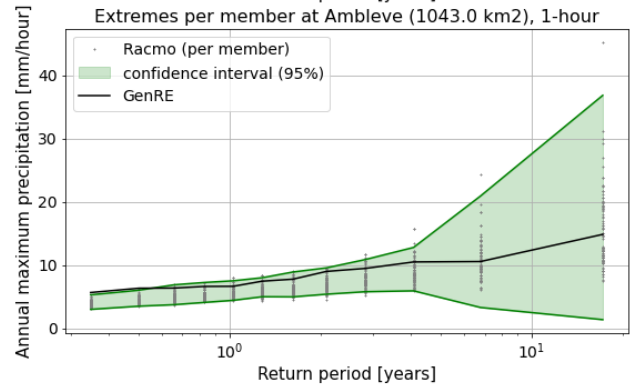
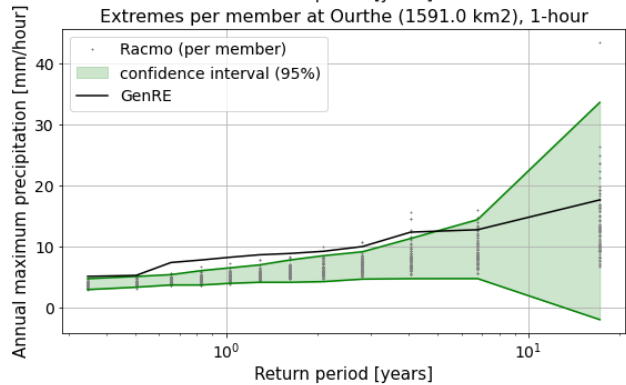
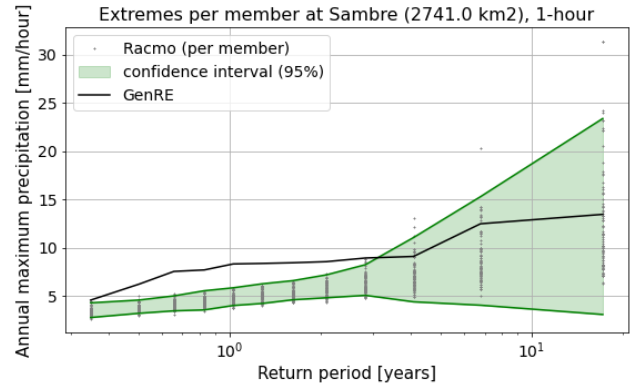
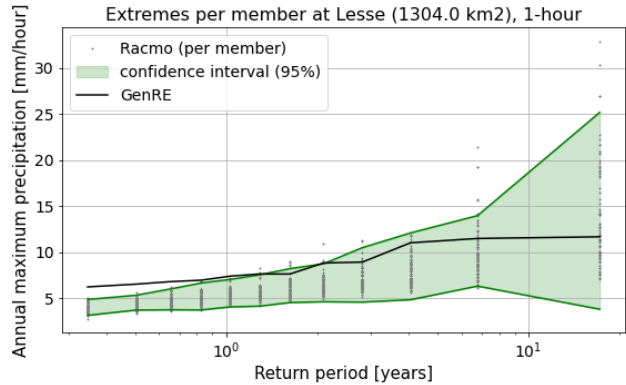
6.6.1. Daily



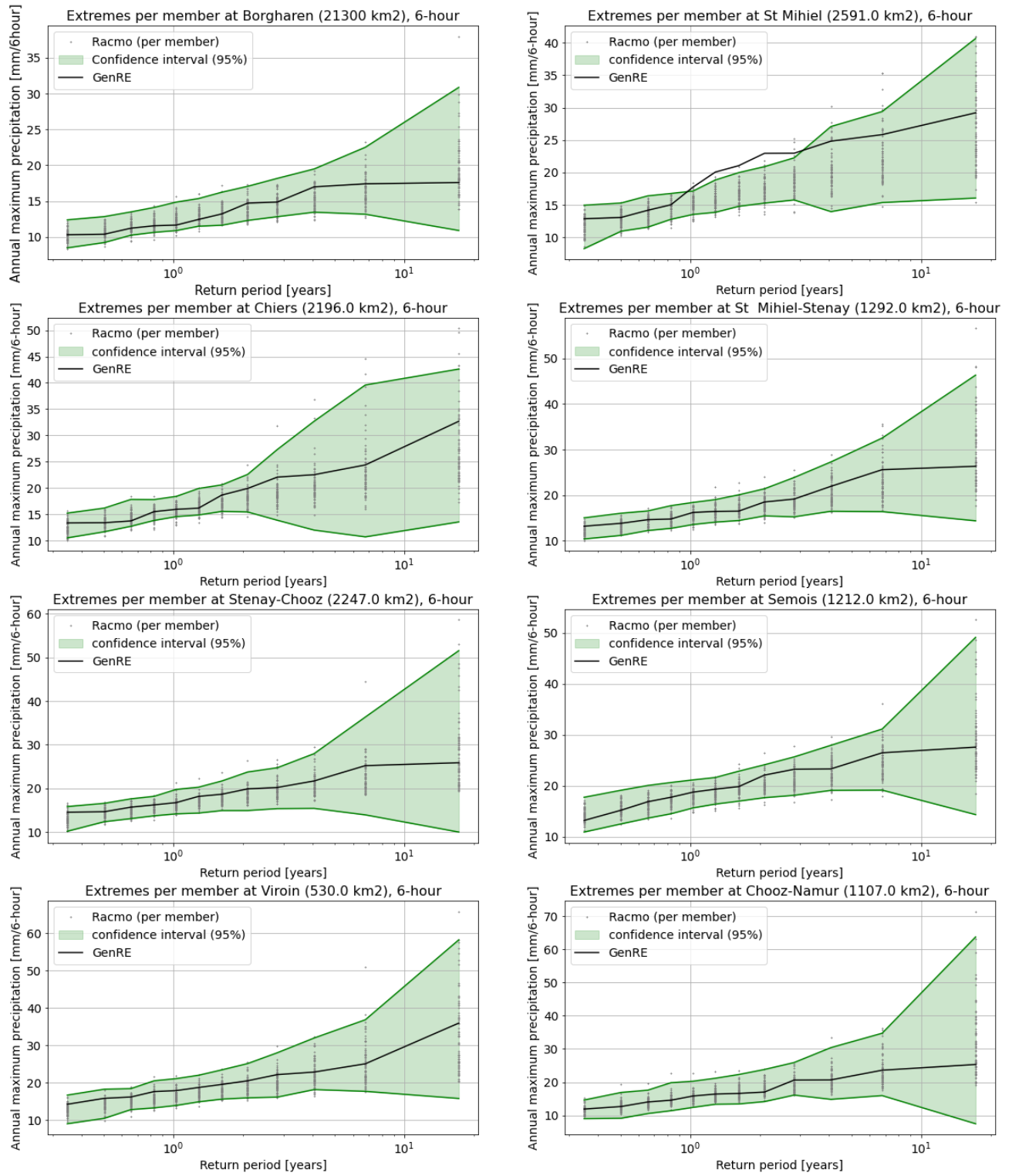


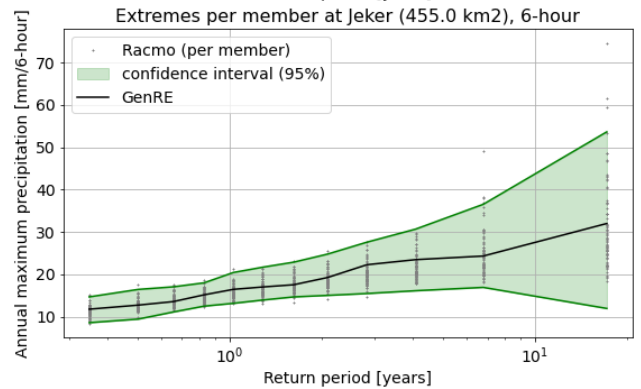
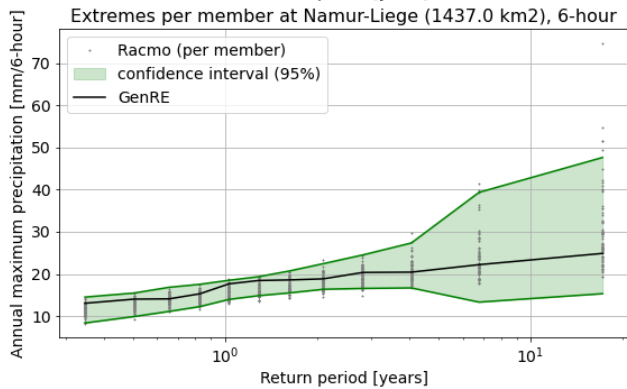
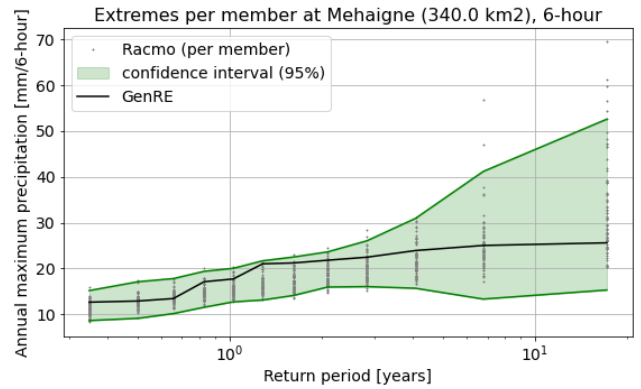
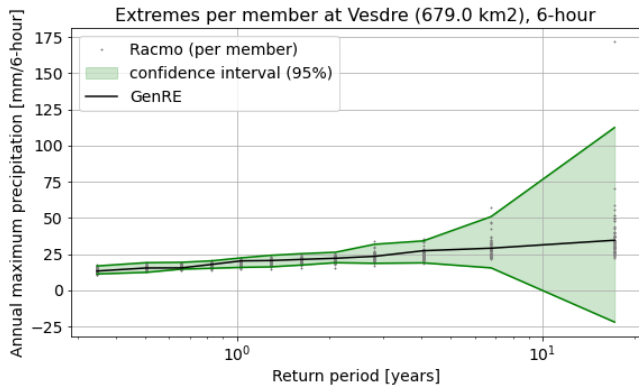
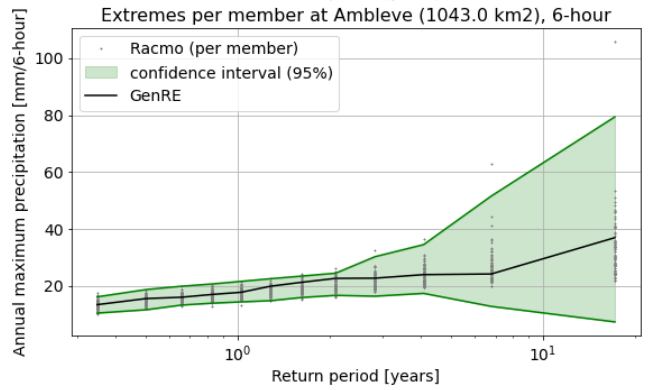
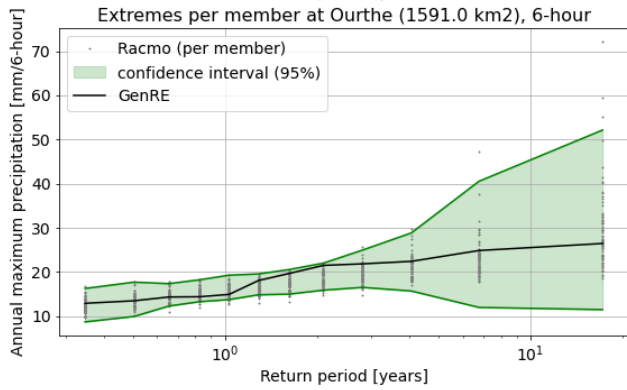
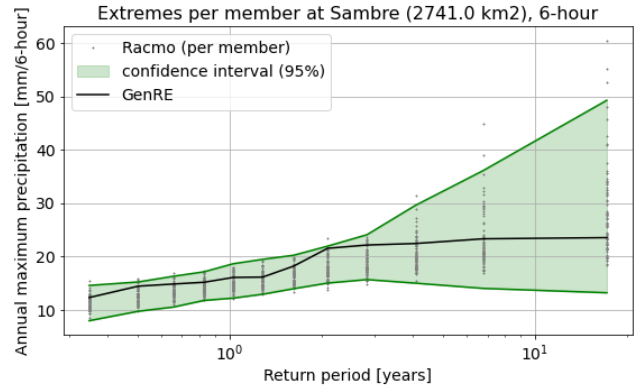
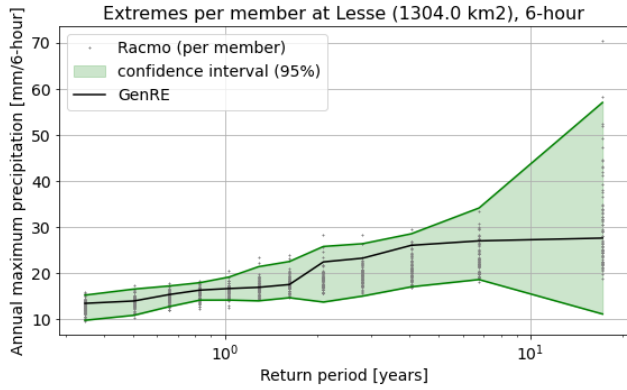
6.6.2. Hourly





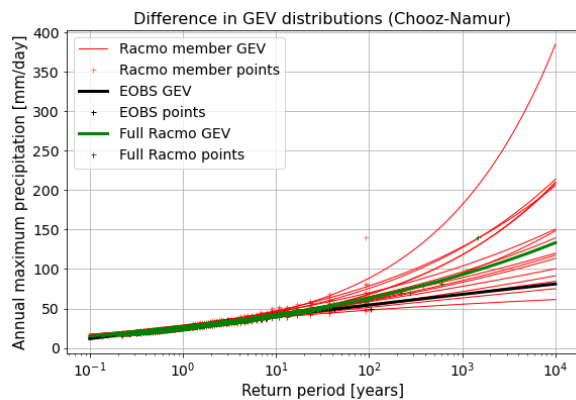
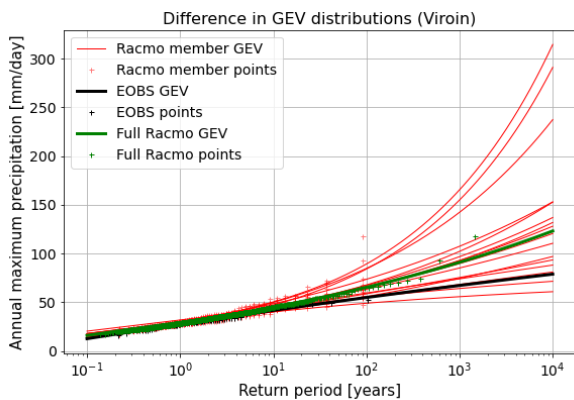
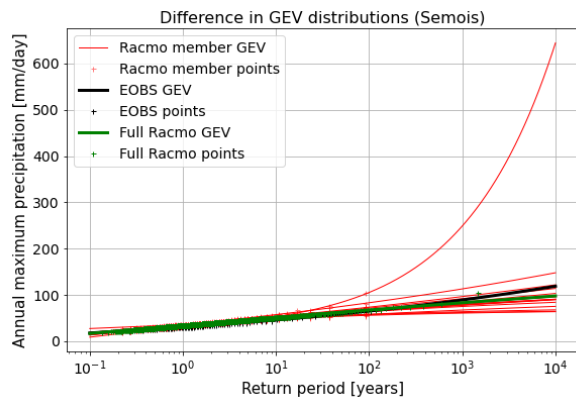
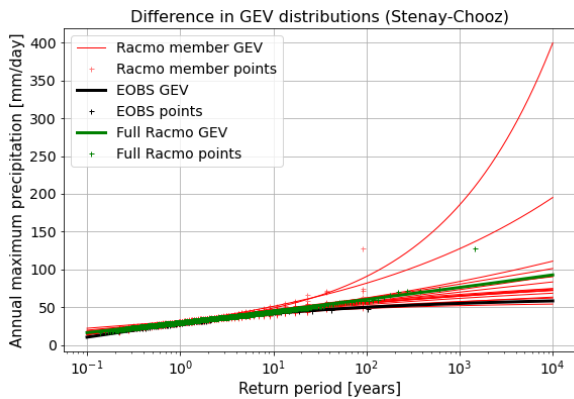
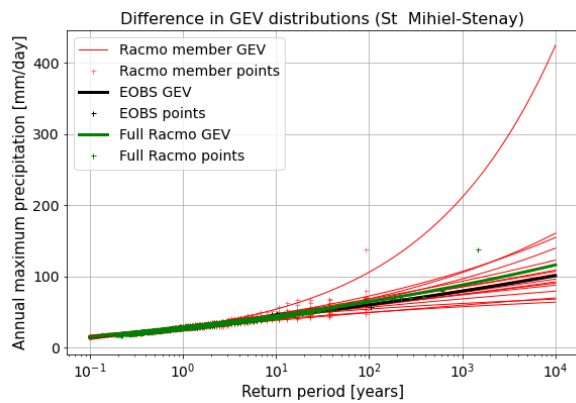
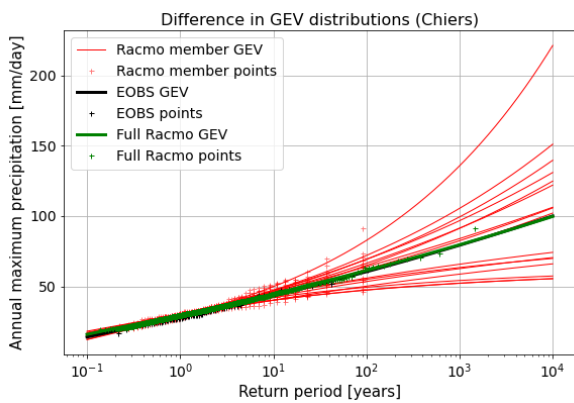
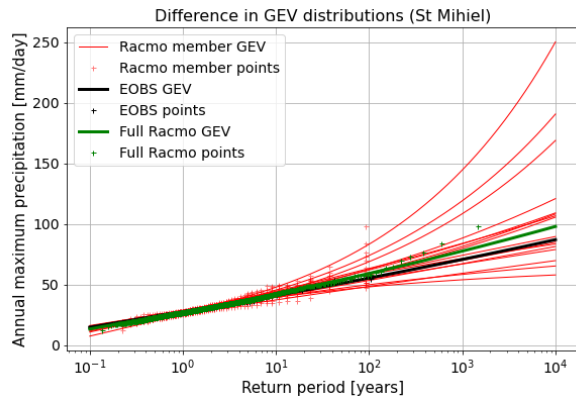
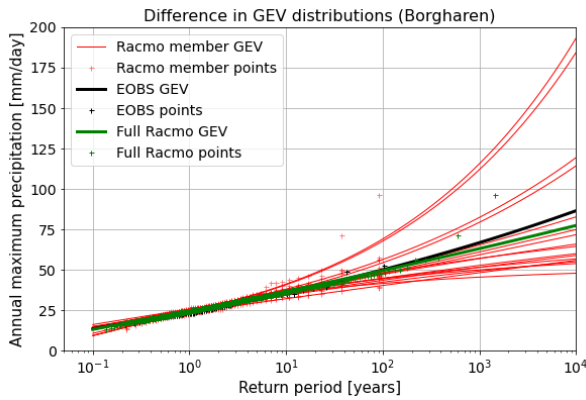
6.6.3. 6-Hourly

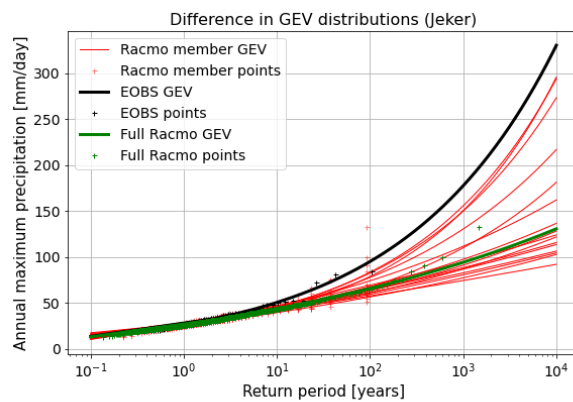
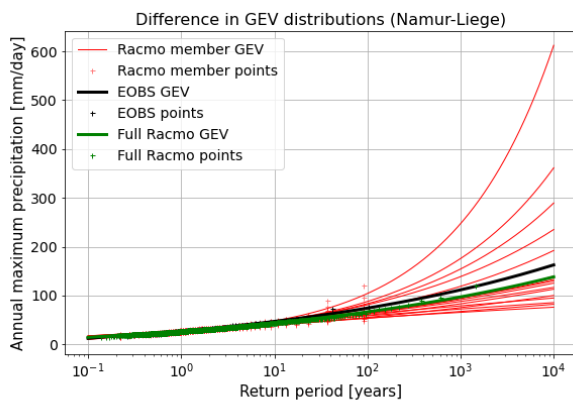
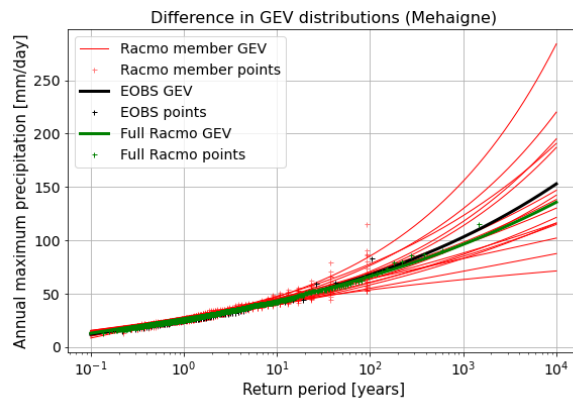
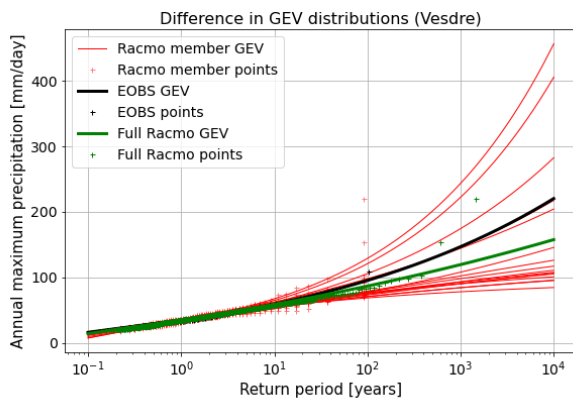
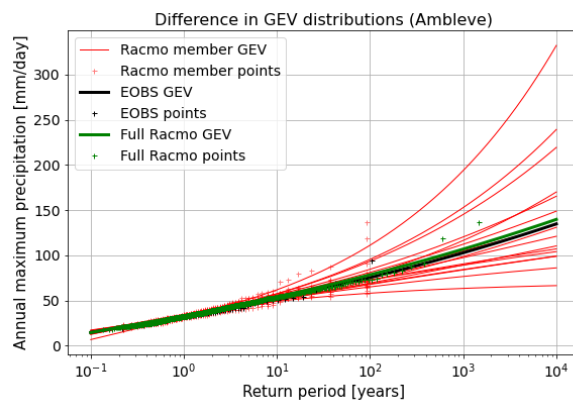
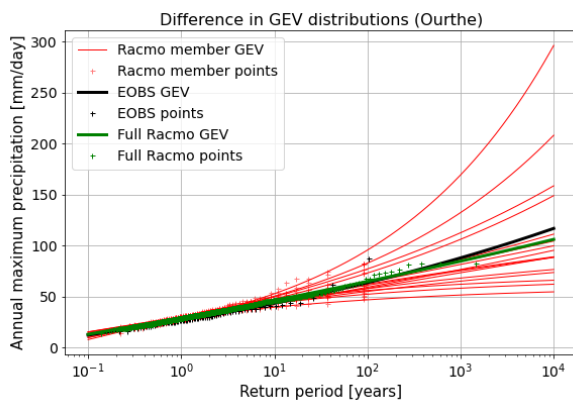
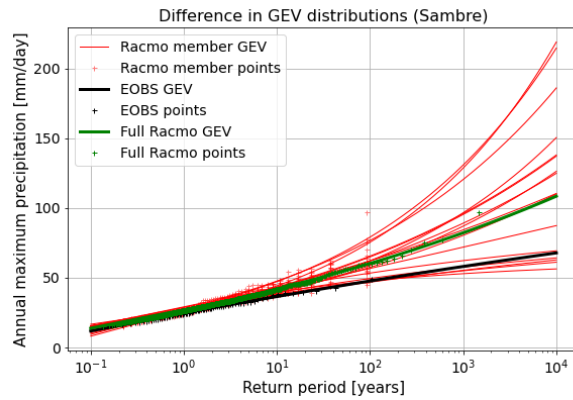
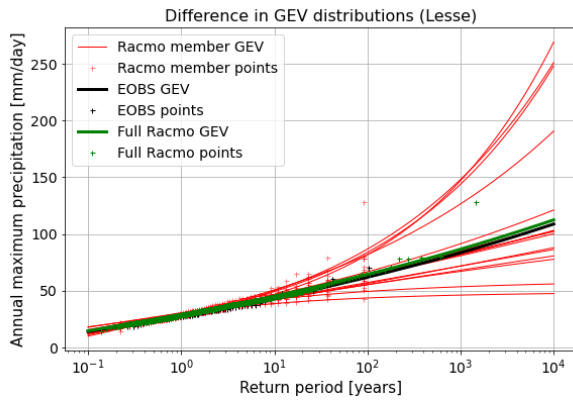




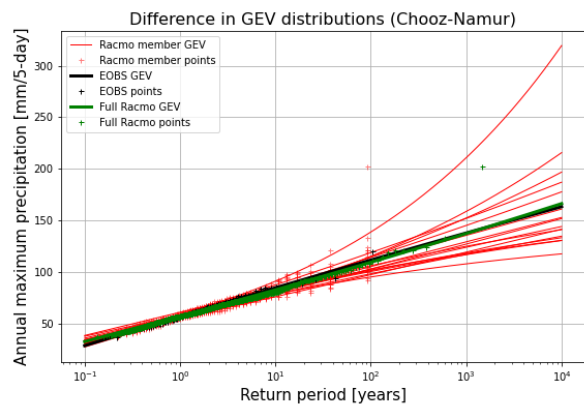
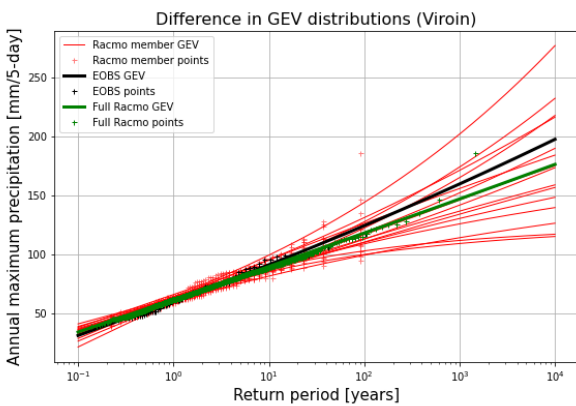
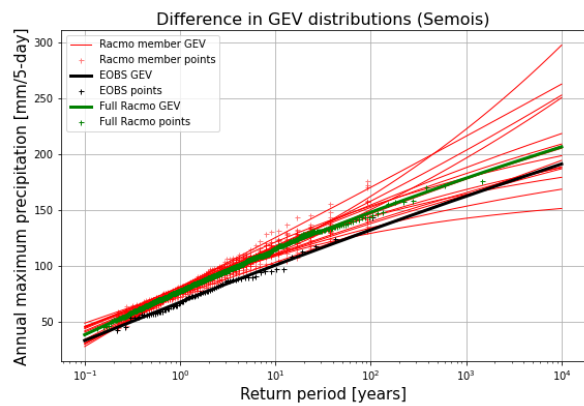
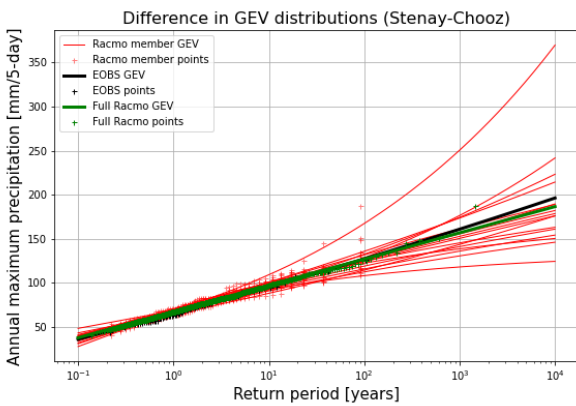
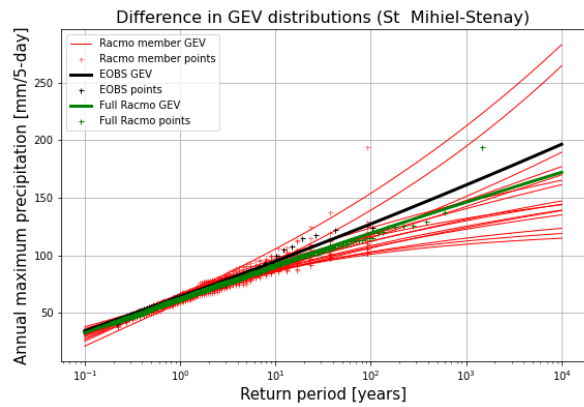
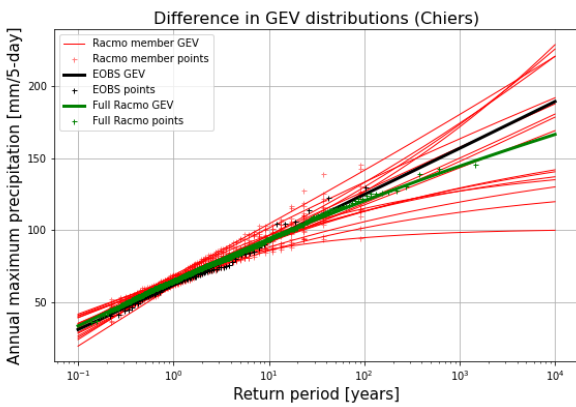
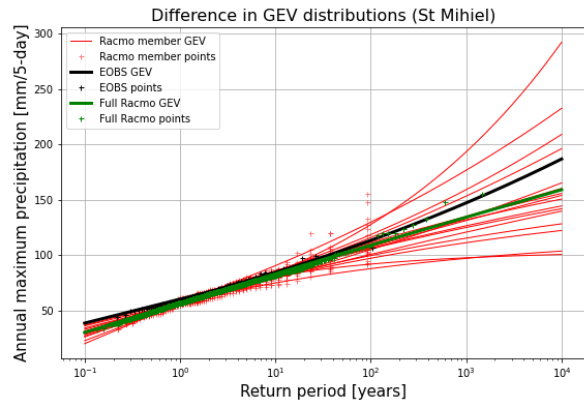
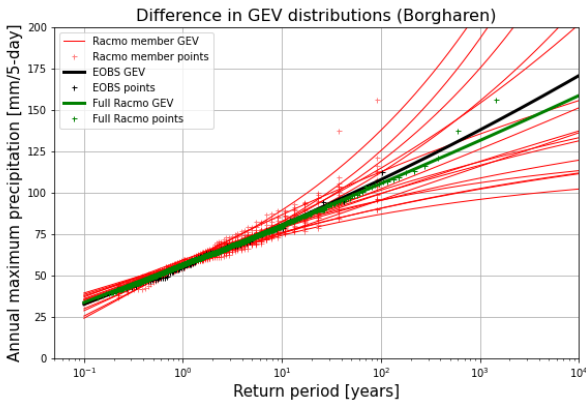
6.7. GEV distributions

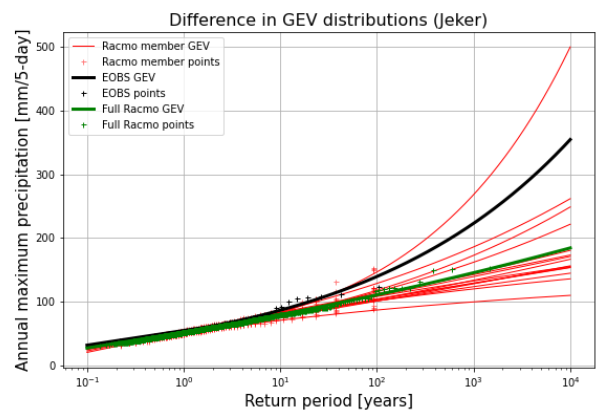
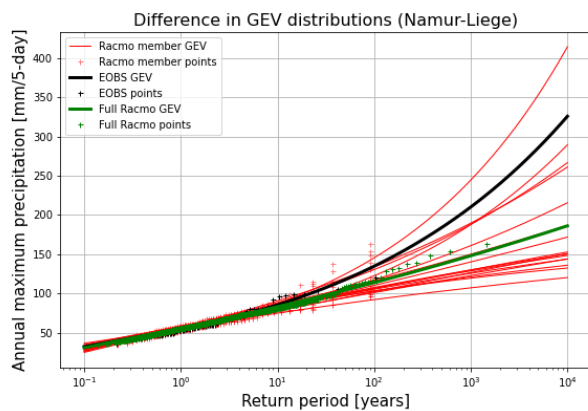
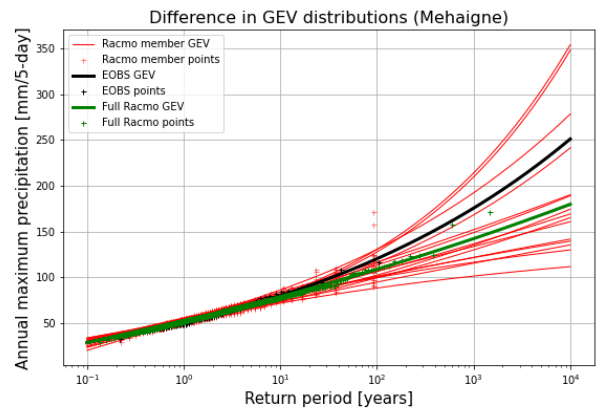
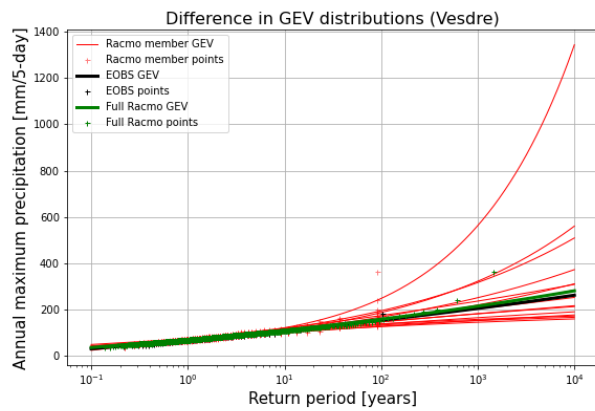
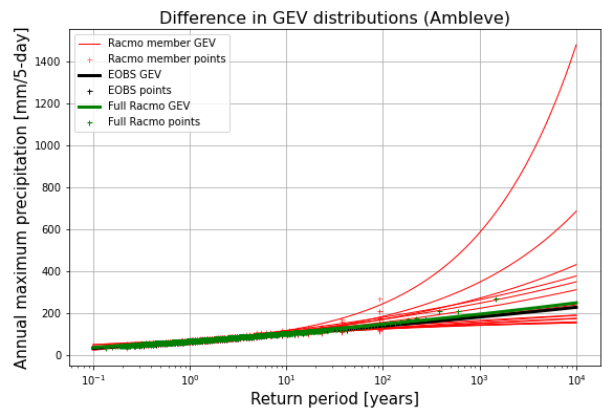
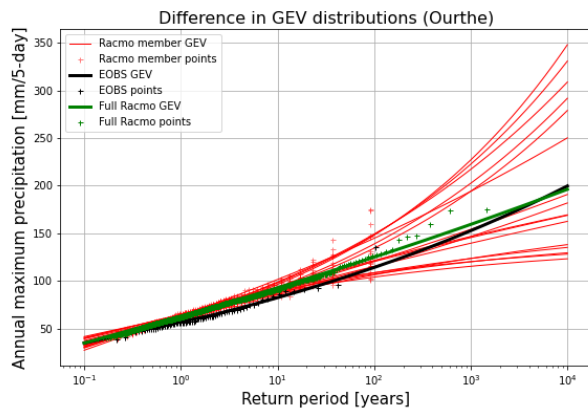
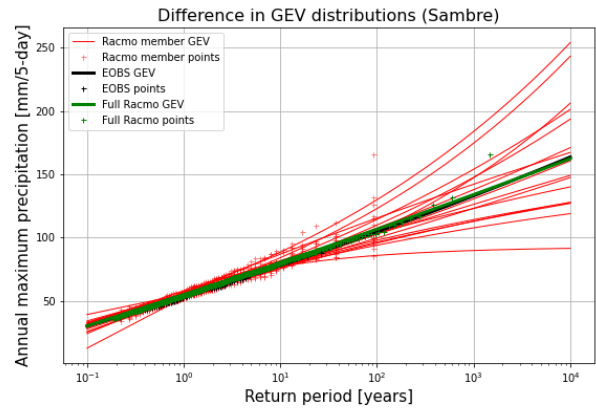
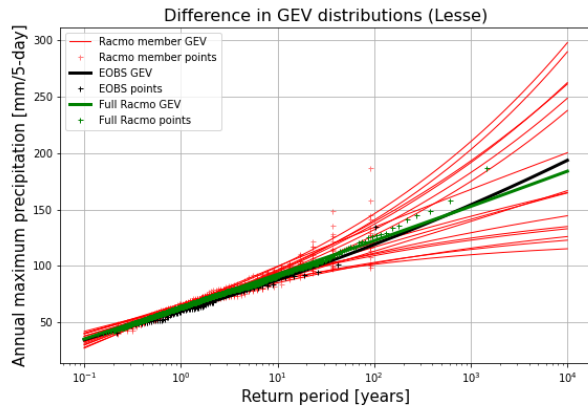
6.7.1. Daily



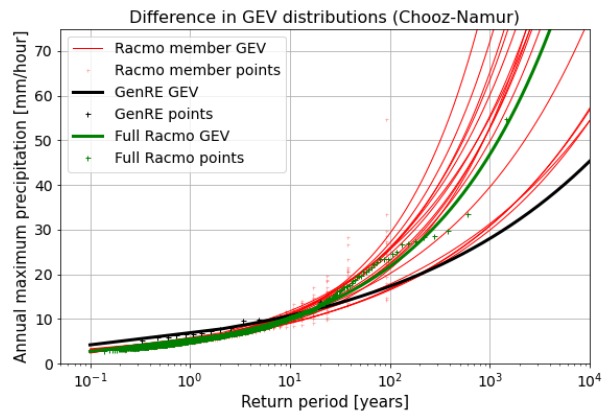
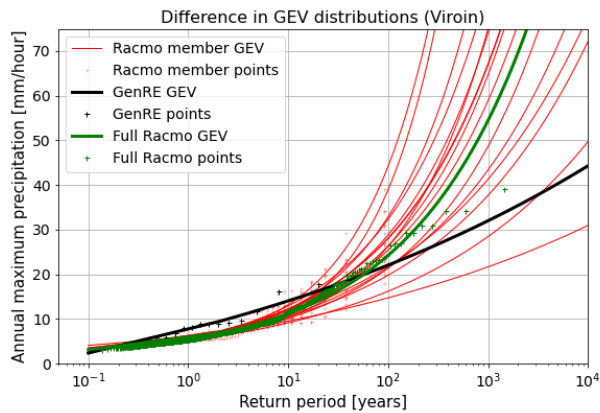
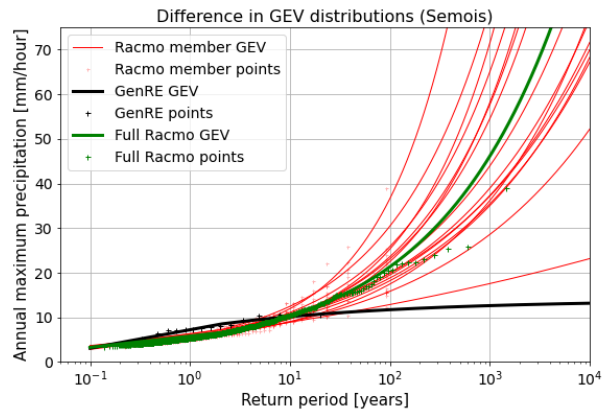
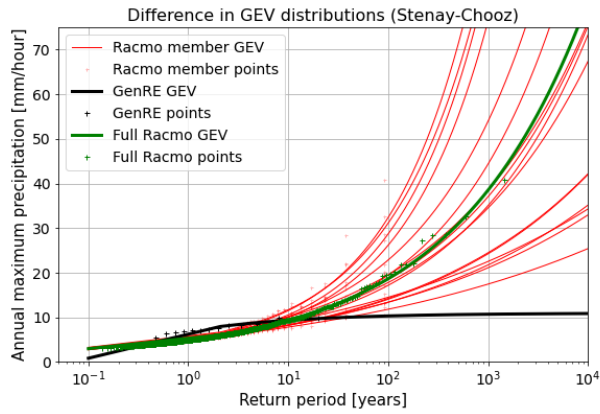
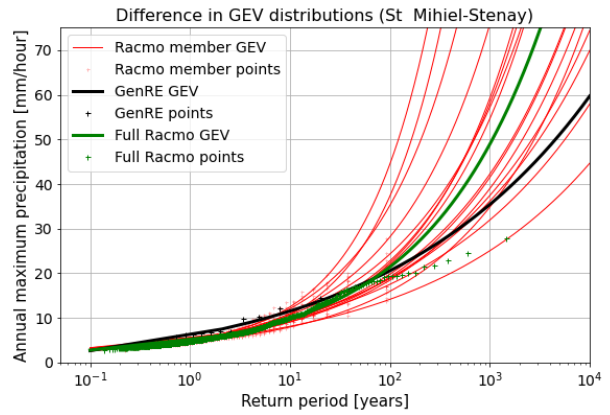
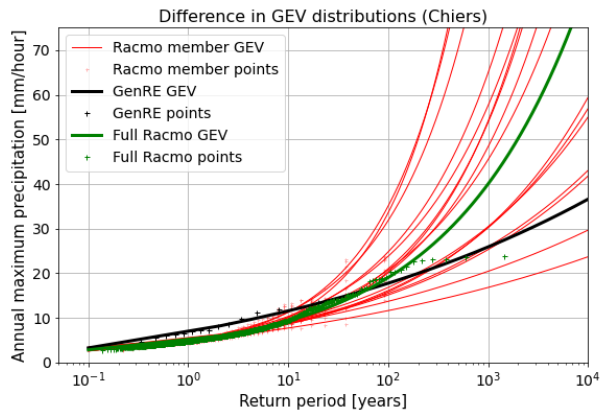
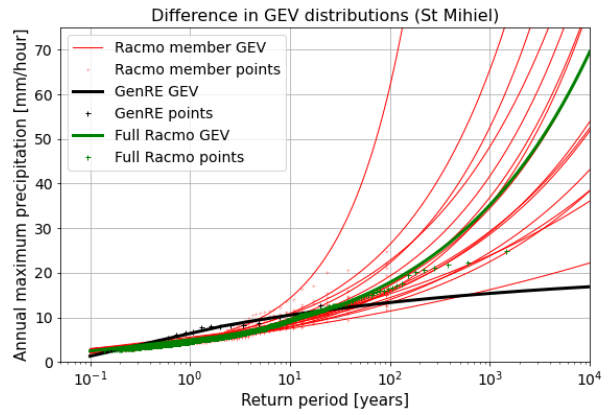
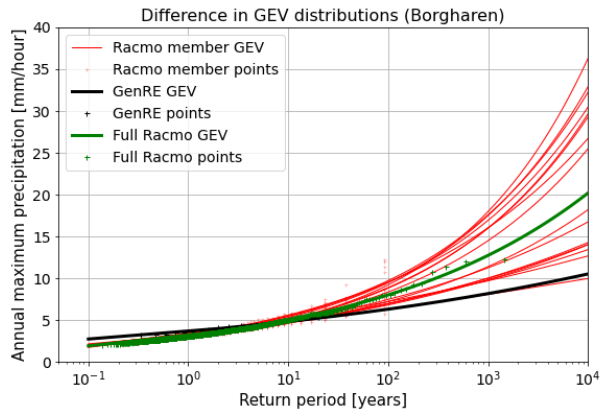


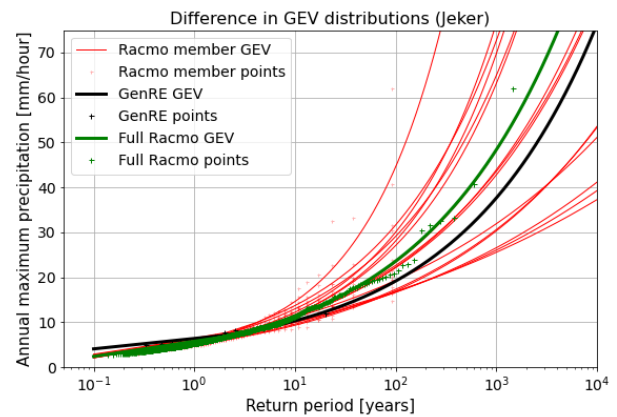
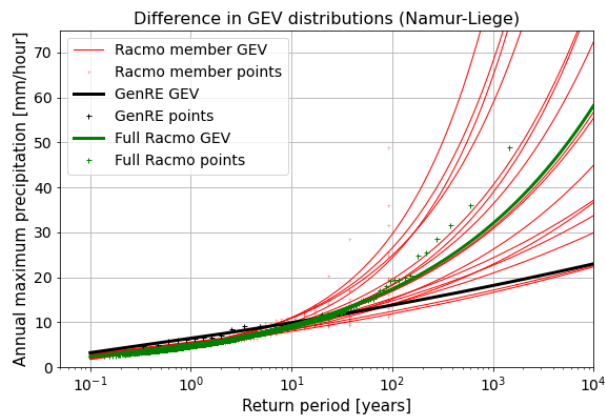
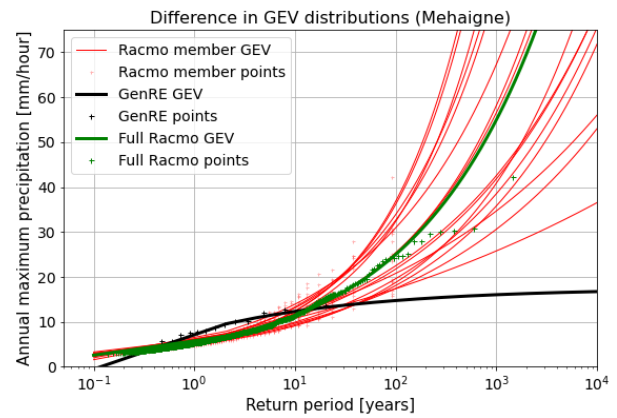
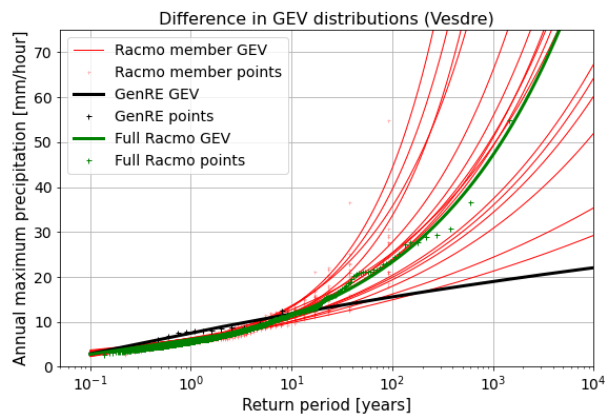
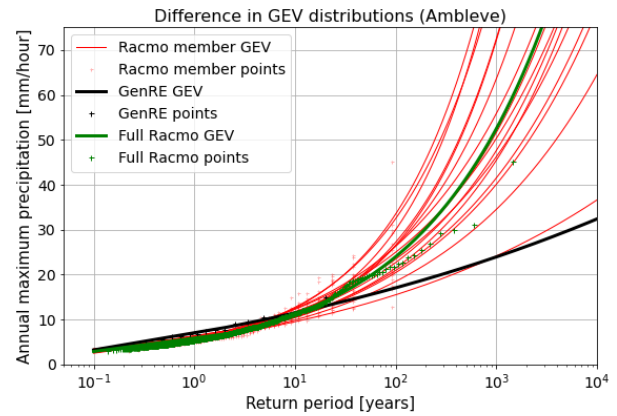
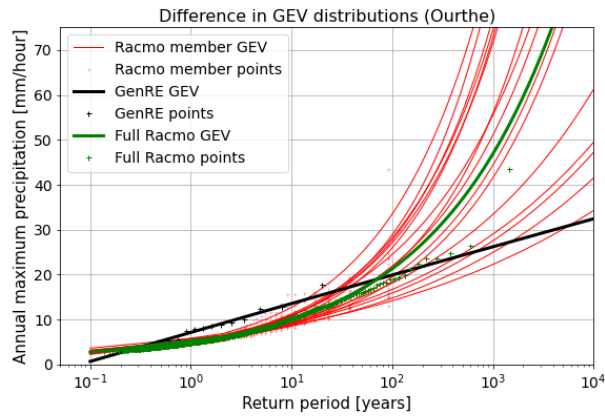
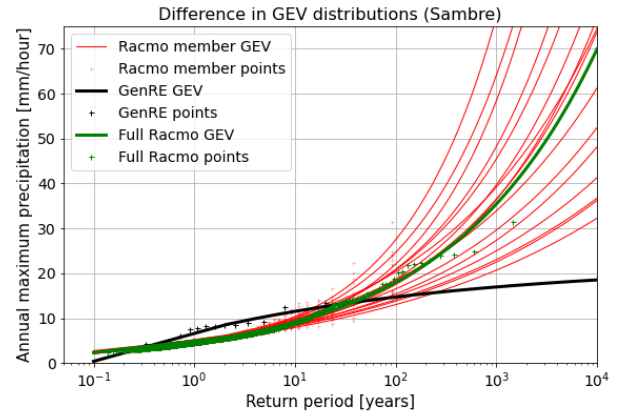
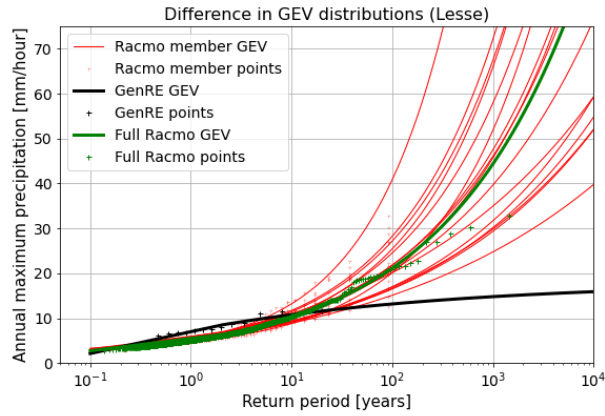
6.7.2. 5-daily





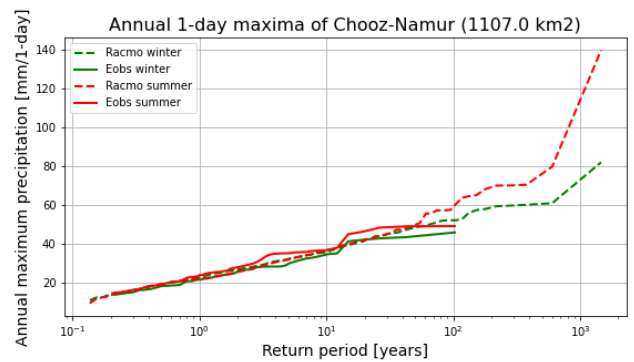
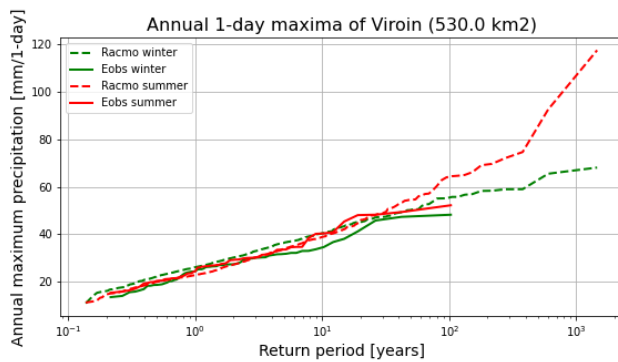
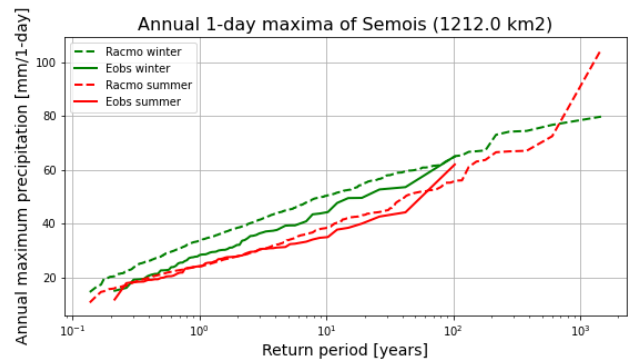
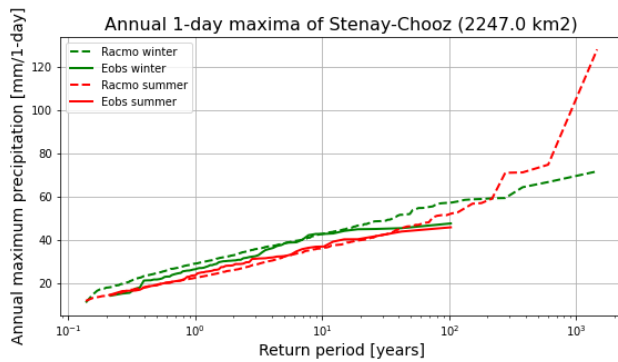
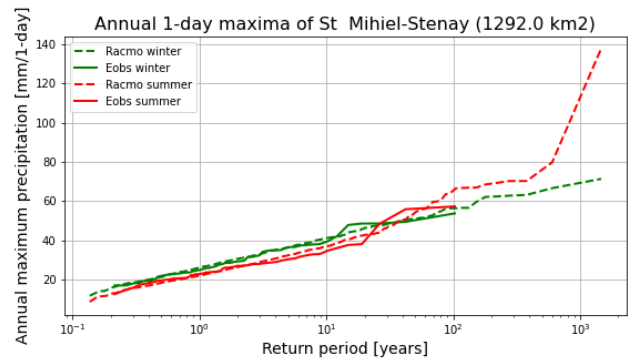
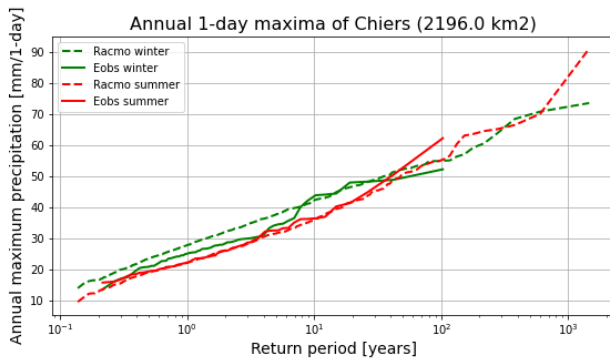
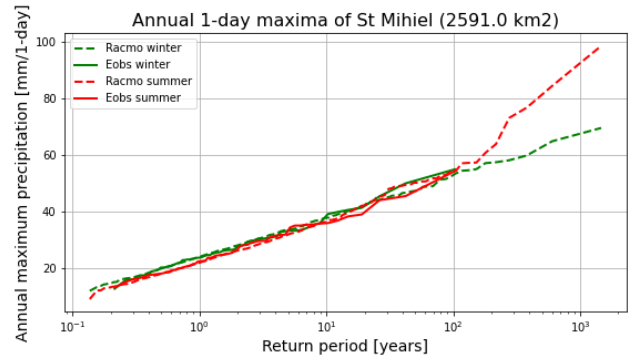
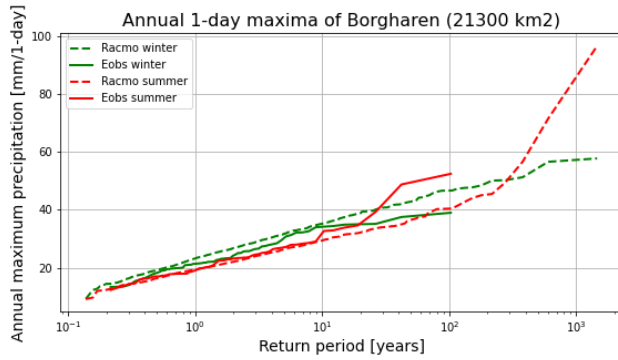
6.7.3. Hourly

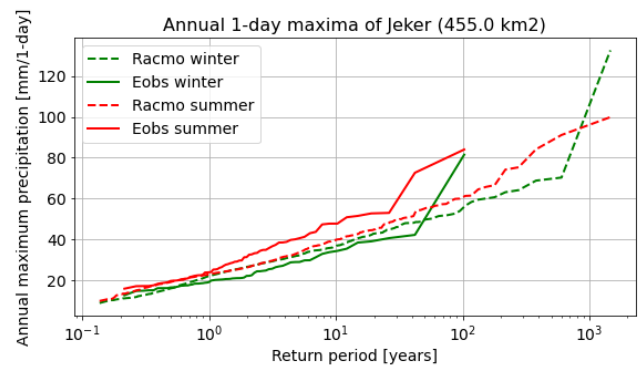
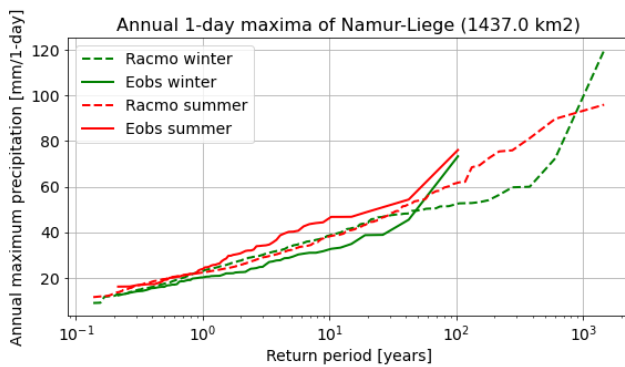
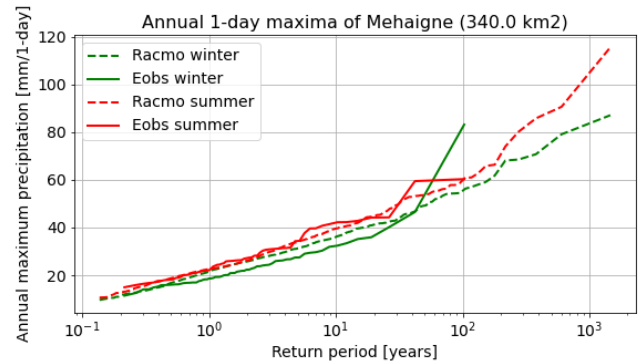
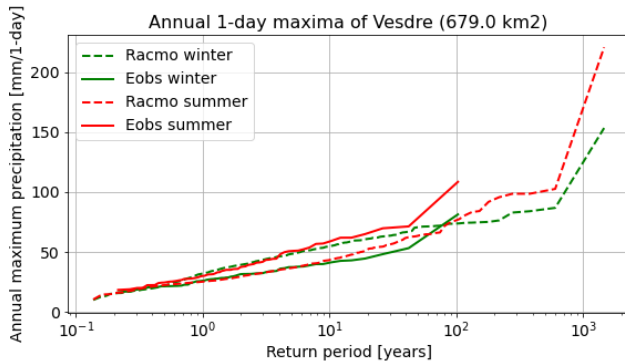
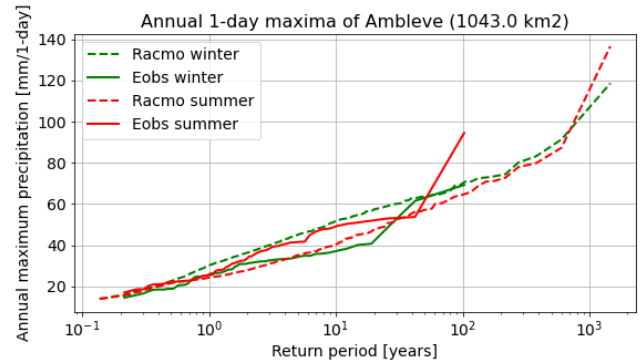
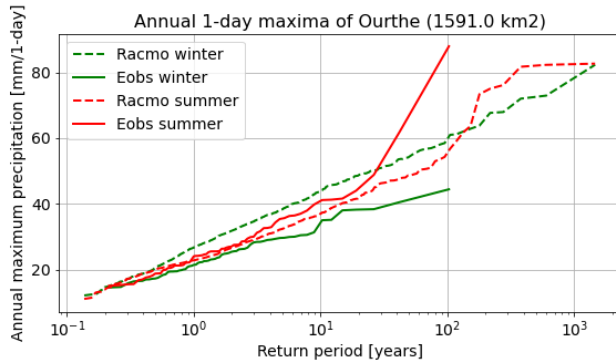
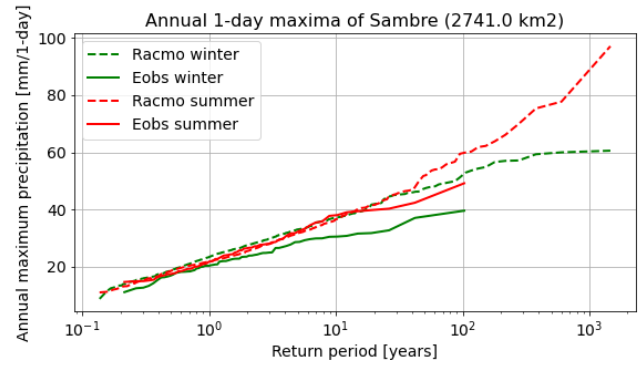
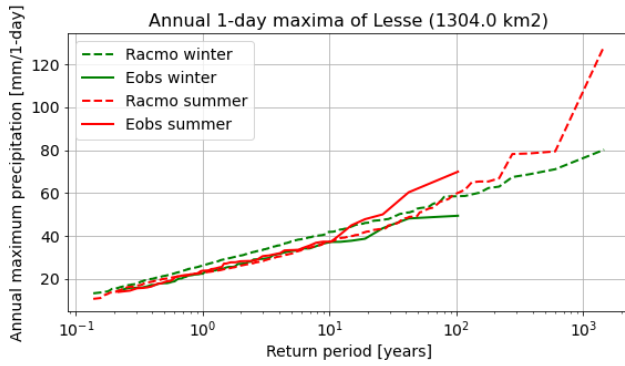




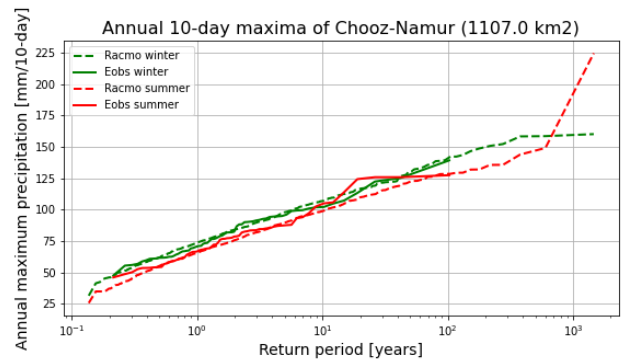
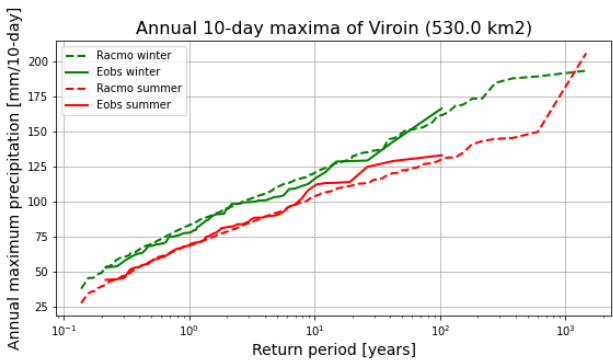
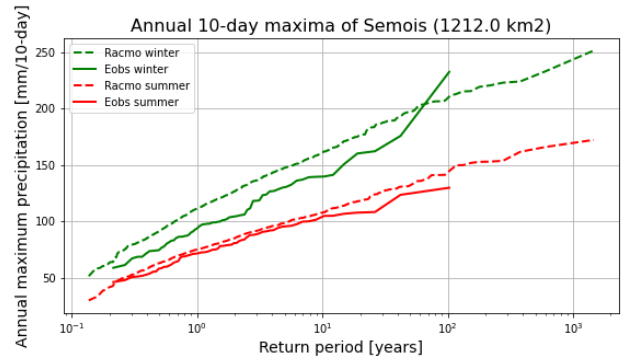
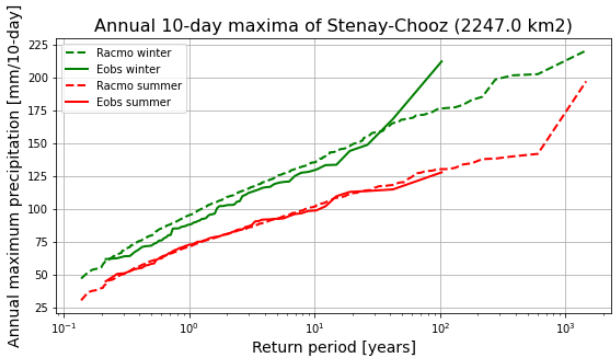
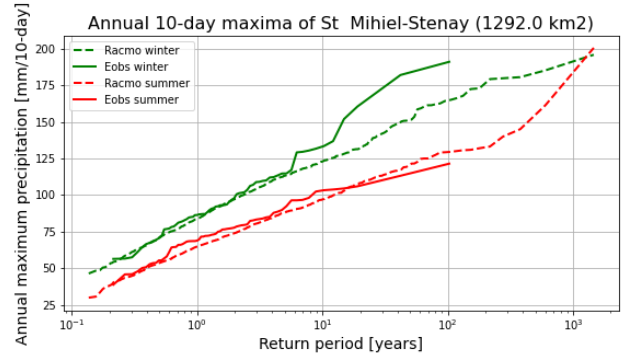
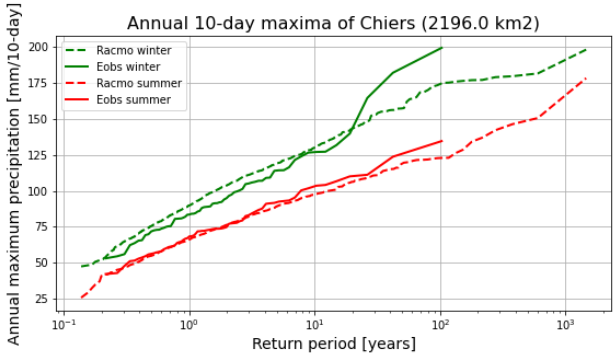
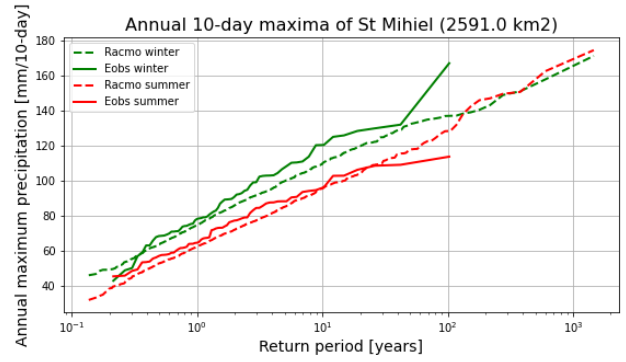
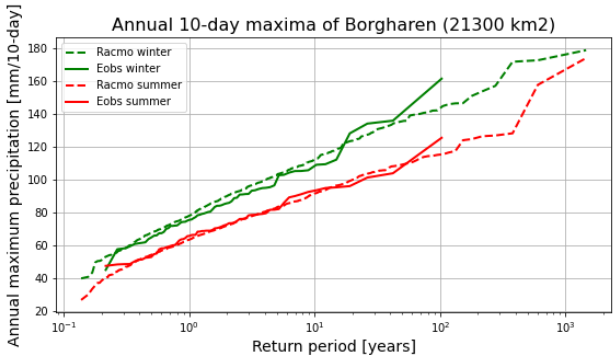
6.8. Seasonal influence

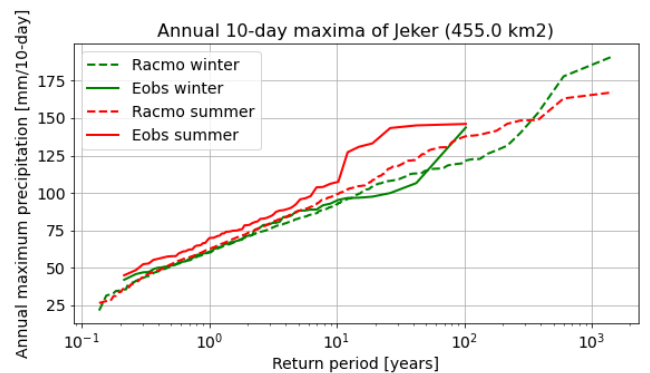
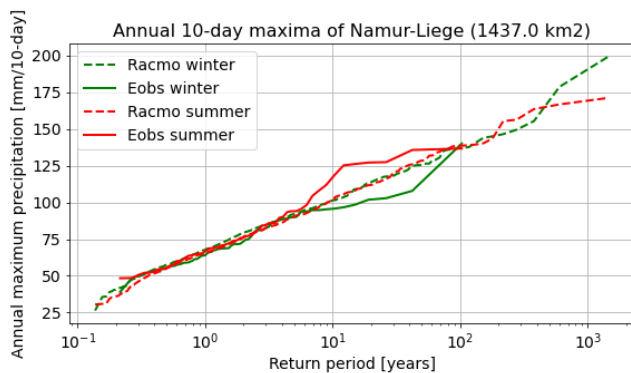
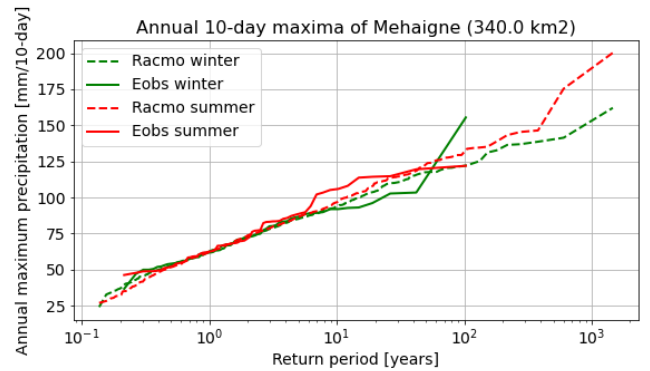
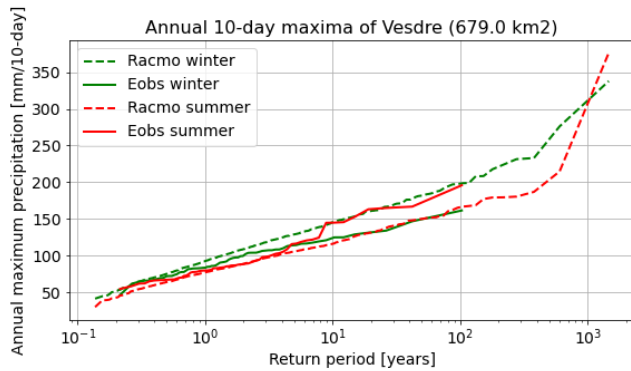
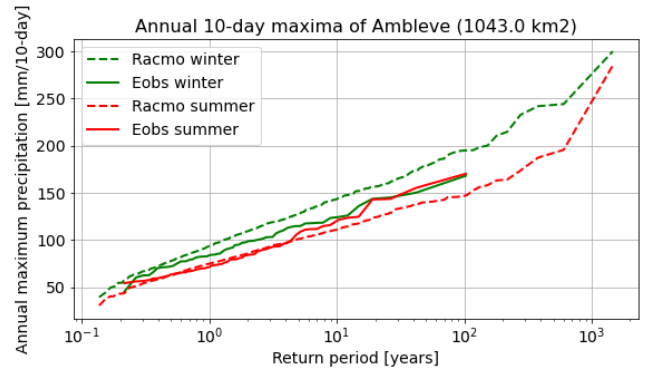
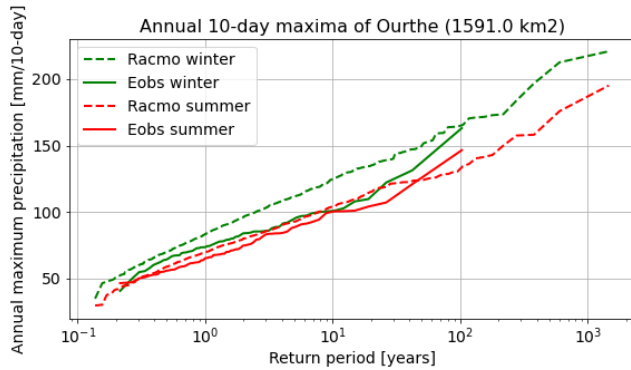
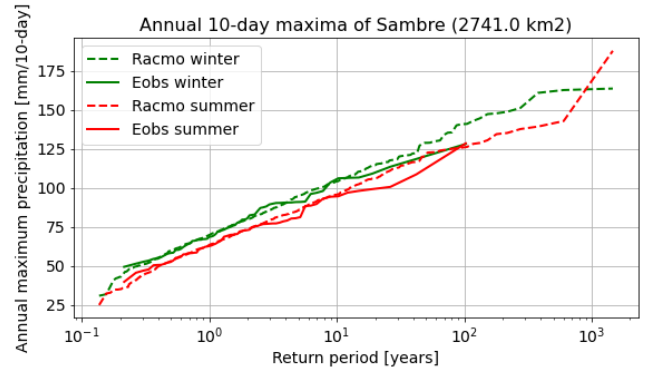
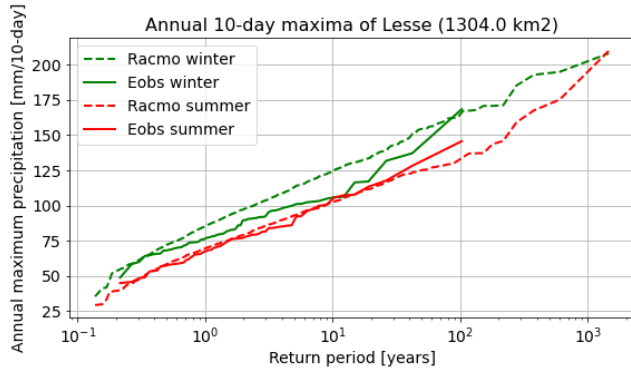
6.8.1. Daily



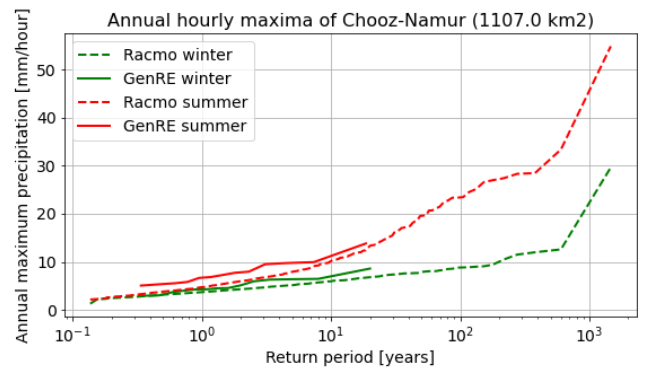
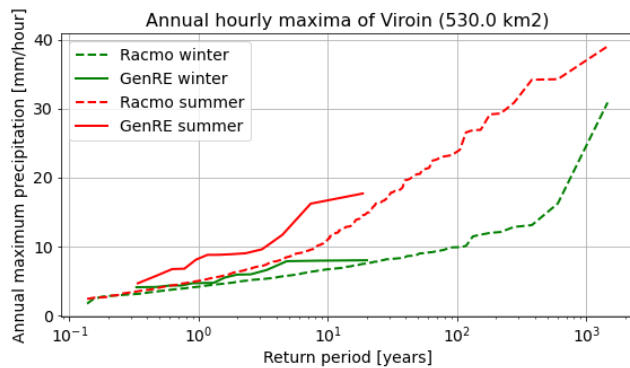
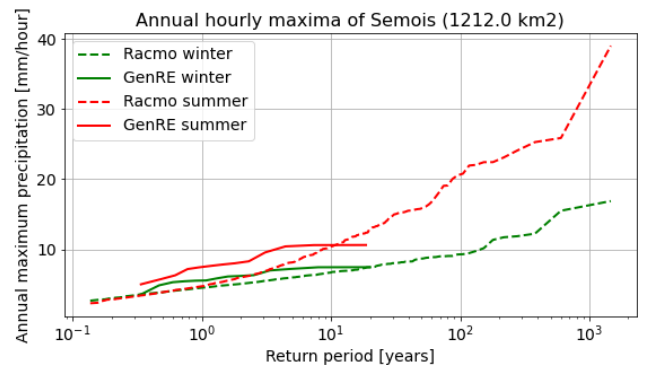
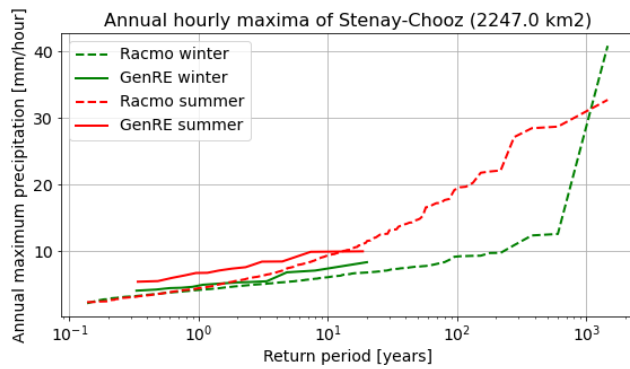
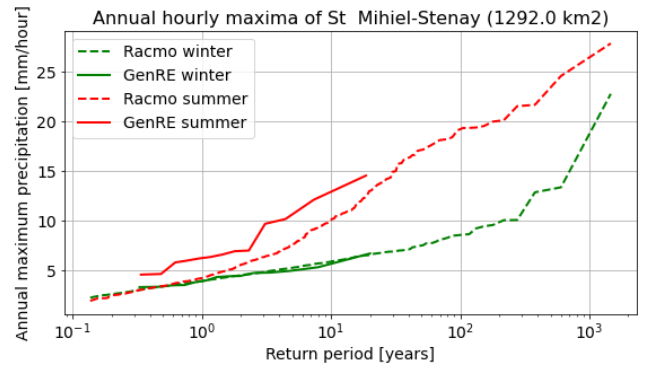
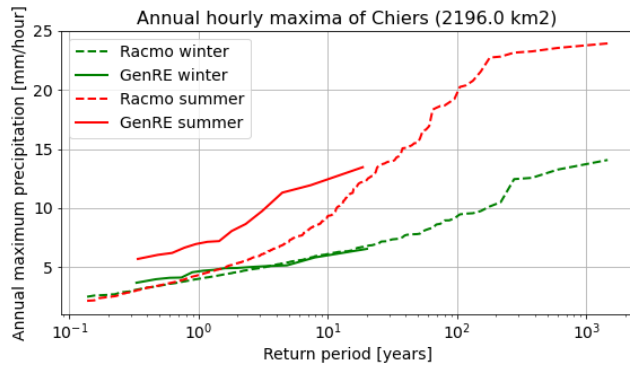
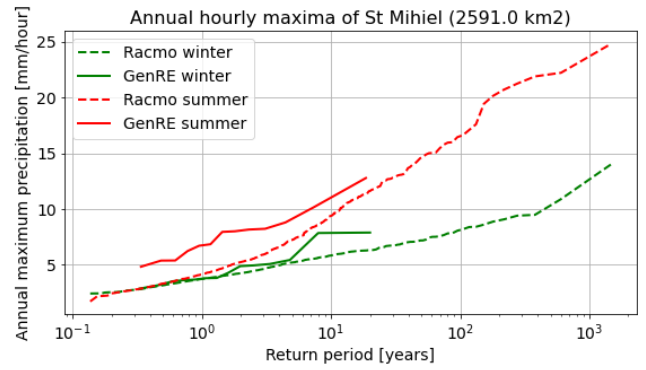
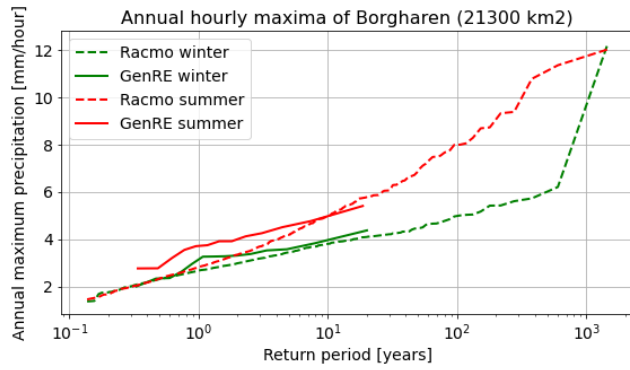


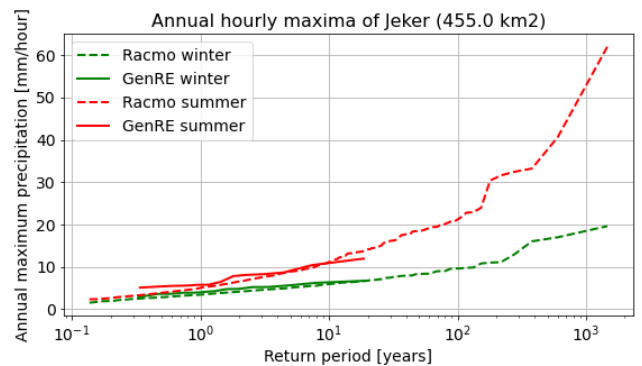
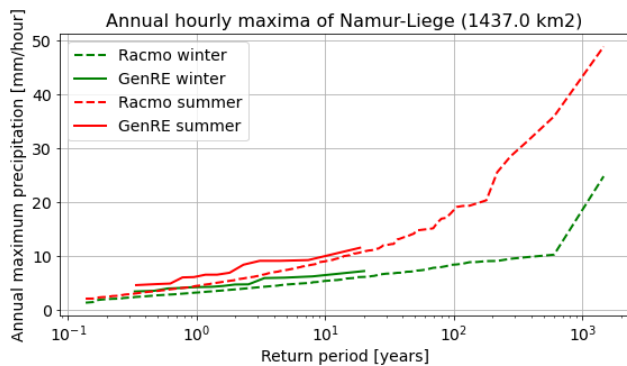
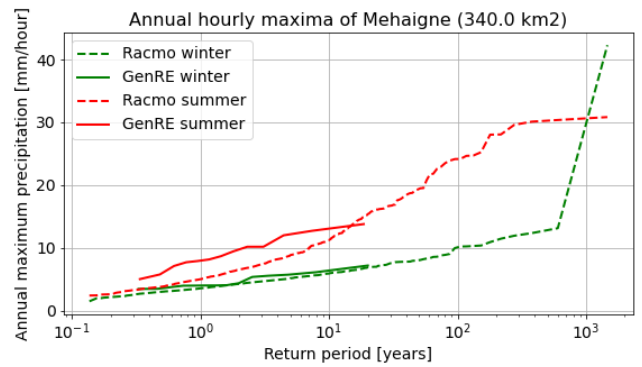
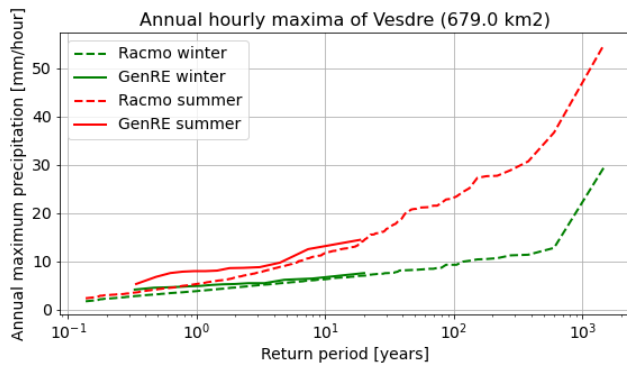
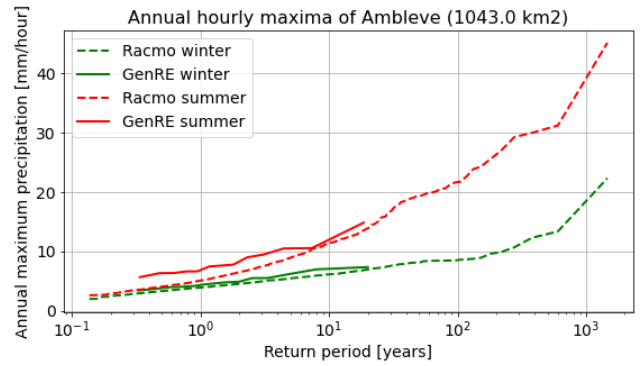
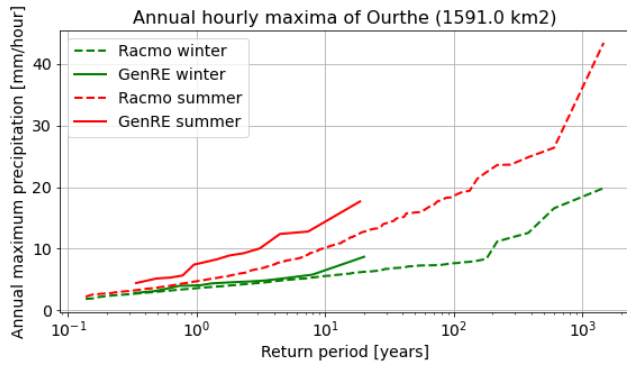
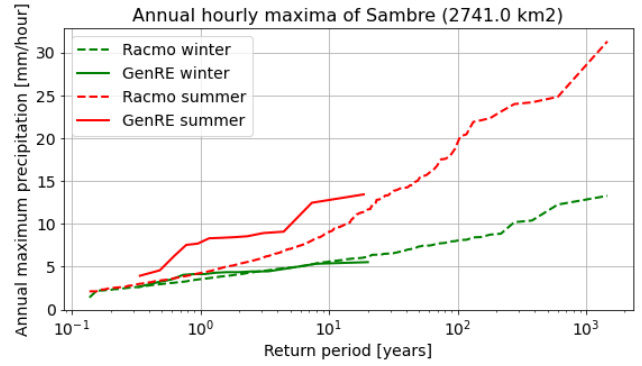
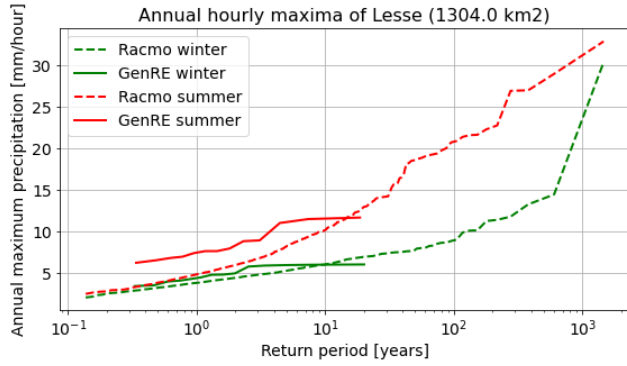
6.8.2. 10-daily





6.8.3. Hourly





Royal Netherlands Meteorological Institute

PO Box 201 | NL-3730 AE De Bilt
Netherlands | www.knmi.nl